

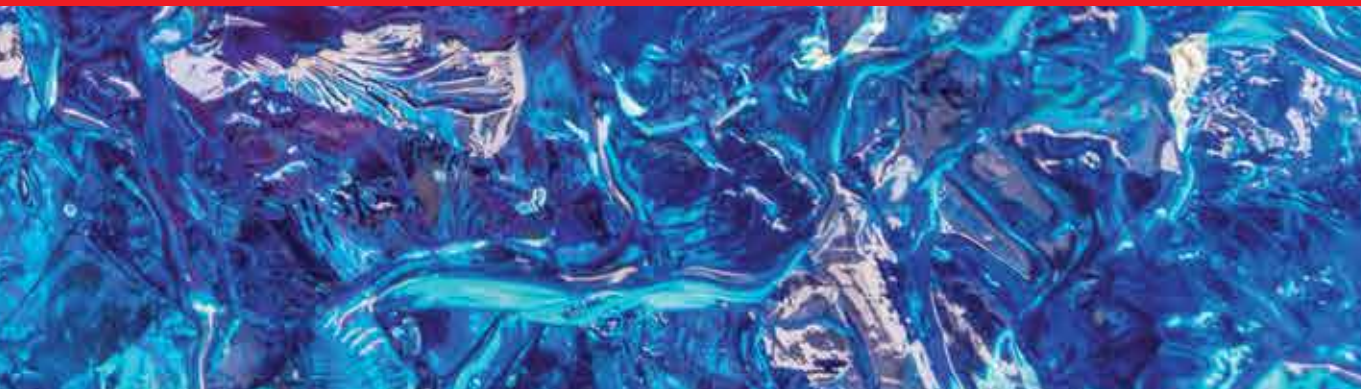


IntechOpen

Liquid Crystals

Self-Organized Soft Functional Materials
for Advanced Applications

Edited by Irina Carlescu



Liquid Crystals - Self-
Organized Soft Functional
Materials for Advanced
Applications

Edited by Irina Carlescu

Published in London, United Kingdom



IntechOpen





Supporting open minds since 2005



Liquid Crystals – Self-Organized Soft Functional Materials for Advanced Applications
<http://dx.doi.org/10.5772/intechopen.74875>
Edited by Irina Carlescu

Contributors

Akihiro Mochizuki, Vlad Popa-Nita, Robert Repnik, Takeo Sasaki, Khoa Le, Yumiko Naka, Takafumi Sassa, Dan Scutaru, Irina Carlescu, Elena-Raluca Bulai (Cioanca), Catalina Ionica Ciobanu, Gabriela Lisa, Nicolae Hurduc

© The Editor(s) and the Author(s) 2019

The rights of the editor(s) and the author(s) have been asserted in accordance with the Copyright, Designs and Patents Act 1988. All rights to the book as a whole are reserved by INTECHOPEN LIMITED. The book as a whole (compilation) cannot be reproduced, distributed or used for commercial or non-commercial purposes without INTECHOPEN LIMITED's written permission. Enquiries concerning the use of the book should be directed to INTECHOPEN LIMITED rights and permissions department (permissions@intechopen.com).

Violations are liable to prosecution under the governing Copyright Law.



Individual chapters of this publication are distributed under the terms of the Creative Commons Attribution 3.0 Unported License which permits commercial use, distribution and reproduction of the individual chapters, provided the original author(s) and source publication are appropriately acknowledged. If so indicated, certain images may not be included under the Creative Commons license. In such cases users will need to obtain permission from the license holder to reproduce the material. More details and guidelines concerning content reuse and adaptation can be found at <http://www.intechopen.com/copyright-policy.html>.

Notice

Statements and opinions expressed in the chapters are those of the individual contributors and not necessarily those of the editors or publisher. No responsibility is accepted for the accuracy of information contained in the published chapters. The publisher assumes no responsibility for any damage or injury to persons or property arising out of the use of any materials, instructions, methods or ideas contained in the book.

First published in London, United Kingdom, 2019 by IntechOpen
eBook (PDF) Published by IntechOpen, 2019

IntechOpen is the global imprint of INTECHOPEN LIMITED, registered in England and Wales, registration number: 11086078, The Shard, 25th floor, 32 London Bridge Street
London, SE19SG – United Kingdom
Printed in Croatia

British Library Cataloguing-in-Publication Data

A catalogue record for this book is available from the British Library

Additional hard and PDF copies can be obtained from orders@intechopen.com

Liquid Crystals – Self-Organized Soft Functional Materials for Advanced Applications
Edited by Irina Carlescu

p. cm.

Print ISBN 978-1-78984-884-7

Online ISBN 978-1-78984-885-4

eBook (PDF) ISBN 978-1-83881-810-4

We are IntechOpen, the world's leading publisher of Open Access books Built by scientists, for scientists

3,900+

Open access books available

116,000+

International authors and editors

120M+

Downloads

151

Countries delivered to

Our authors are among the
Top 1%

most cited scientists

12.2%

Contributors from top 500 universities



WEB OF SCIENCE™

Selection of our books indexed in the Book Citation Index
in Web of Science™ Core Collection (BKCI)

Interested in publishing with us?
Contact book.department@intechopen.com

Numbers displayed above are based on latest data collected.
For more information visit www.intechopen.com



Meet the editor



Dr. Irina Cârlescu holds a PhD degree (2005) in Organic Chemistry from “Gheorghe Asachi” Technical University of Iași, Romania. She has also completed postdoctoral studies at “Politehnica” University of Timișoara and “Gheorghe Asachi” Technical University of Iași, Romania. In 2009 she became an assistant professor and since 2016 an associate professor. Her teaching activity covers organic chemistry, biochemistry, and research strategy courses. Dr. Cârlescu was involved in research projects sponsored by the Ministry of Research and Innovation, Romania, and she is the coauthor of one book as well as the coauthor of scientific articles in peer-reviewed journals. She was a reviewer for Medicinal Chemistry Research and Applied Sciences. Her research interests include synthesis and characterization of liquid crystals with applications in optoelectronics, synthesis of azo materials for biological applications, synthesis of glycoconjugates drug release, and ferrocene derivatives.

Contents

Preface	XIII
Section 1 Introduction	1
Chapter 1 Introductory Chapter: Liquid Crystals <i>by Irina Carlescu</i>	3
Section 2 Self-Assembling Soft Functional Materials: Structure and Phase Behavior	11
Chapter 2 Bent-Core Liquid Crystals: Structures and Mesomorphic Properties <i>by Dan Scutaru, Irina Carlescu, Elena-Raluca Bulai (Cioanca), Catalina Ionica Ciobanu, Gabriela Lisa and Nicolae Hurduc</i>	13
Chapter 3 Binary Mixture Composed of Nematic Liquid Crystal and Carbon Nanotubes: A Theoretical Description <i>by Vlad Popa-Nita and Robert Repnik</i>	33
Section 3 Electro-Optic Switching Behavior and Photorefractive Effect in Ferroelectric Liquid Crystals	47
Chapter 4 In-Plane Retardation Switching Behavior at Certain Types of Smectic Liquid Crystals <i>by Akihiro Mochizuki</i>	49
Chapter 5 The Photorefractive Effect in Liquid Crystals <i>by Takeo Sasaki, Khoa Van Le, Yumiko Naka and Takafumi Sassa</i>	71

Preface

Liquid crystals (LCs) are amazing compounds that self-organize into ordered soft states, being presently indispensable for nanotechnological applications. Molecular shape and intermolecular interactions, together with nanosegregation of the molecular structure, contribute thereby to their self-assembly into thermodynamically stable functional materials. *Liquid Crystals - Self-Organized Soft Functional Materials for Advanced Applications* is focused on both theoretical models and experimental results, pointing out the chemical and physical properties (thermodynamics, electro-optic switching behavior, and non-linear optic phenomena) of LCs that could be applicable to a wide range of devices. In this respect, the chapters cover the following topics:

- chemical structure and phase transitions in bent-core LCs,
- phase and structural behavior of thermotropic LCs used to align carbon nanotubes (CNTs),
- molecular alignment of smectic layers and photorefractive effect in the ferroelectric phase, which have the potential to be used as transistors in electrical circuits or could be exploited for image storage and optical signal processing.

The chapter by Scutaru et al. presents the structure and supramolecular ordering behavior of symmetrical and asymmetrical bent-core LCs. The purpose was to design LCs with large mesophase intervals on low transition temperatures, which might expand the field of electro-optical applications. The chapter by Popa-Nita and Repnik shows the theoretical model for the phase behavior and orientational properties of a binary mixture composed of CNTs into thermotropic nematic LCs. The chapter by Mochizuki describes the relationship between tilted smectic layer structure and electro-optic properties, considering in-plane and out-of-plane retardation switching behavior. The last chapter by Sasaki et al. reviews the effect of LC mixtures on response time and gain coefficient, required for the formation of a refractive index grating in a photorefractive device.

Because of the possibility of using such materials for a wide range of applications, the study of LCs presents both theoretical and practical importance. It is expected that the book will be of interest for researchers in academia and industries, as well as advanced students.

I would like to express my gratitude to all authors for their contributions to this book.

Assoc. Prof. Irina Carlescu
“Gheorghe Asachi” Technical University of Iasi,
Romania

Section 1

Introduction

Introductory Chapter: Liquid Crystals

Irina Carlescu

1. Introduction

The domain of liquid crystals represents an actual and dynamic scientific area, directly implied in top technologies as nanotechnologies, aerospace domain, microelectronics, and molecular biology [1]. For about 130 years, liquid crystals have been the subject of study for fundamental science and in many fields of research such as chemistry, physics, medicine, and engineering as well, which contributed to the progress in materials science and to innovative applications. In addition, as a result of the recent development of advanced synthetic methods and characterization techniques, the nanostructured liquid crystalline compounds that display special ordering properties and assign new functions have been highlighted, such as electro-optical effects, actuation, chromism, sensing, or templating [1–4].

Compared to other solid-state materials, liquid crystals present unique attributes, because they easily respond to external stimuli such as surfaces, light, heat, mechanical force, or electric and magnetic fields and eliminate defects by self-healing [5–9]. Thus, the understanding of the relationship between chemical structures of liquid crystalline compounds and their specific functions is becoming more important.

Liquid crystals are quintessential soft matter materials that present one to several distinct phases between the crystalline solid phase (Cr) and the isotropic liquid phase (Iso) [10–13]. These intermediary phases or mesophases not only possess some typical properties of a crystalline elastic solid like positional and orientational order as well as anisotropy of optical, electrical, and magnetic properties but also have the characteristic properties of an ordinary viscous liquid such as fluidity, formation and fusion of droplets, or mechanical properties [14–19]. Consequently, the compounds that present mesophases have intermediary symmetry properties, between an isotropic liquid and a crystalline solid; hence, a viscoelastic nature can be attributed to liquid crystals. Moreover, the unique combination of order and mobility represents the basis for self-assembly and supramolecular structure formation in technical systems. Generally, liquid crystals are elongated shape molecules, which are more or less parallel to each other in mesophases, contributing to anisotropic physical properties. These properties associated with their viscoelastic nature induce in liquid crystals the ability to easily respond under external stimuli and to change their configuration [20].

Depending on particular conditions where mesophases arise, liquid crystals have been classified into two classes: lyotropic and thermotropic. Thermotropic liquid crystals can be obtained either by heating a crystalline solid or by cooling an isotropic liquid. In the case of thermotropic liquid crystals, when the crystalline state is heated, the positional ordering of molecules vanishes but not the orientational one and so the

resultant ordered dynamic phase flows like a liquid and yet possesses the anisotropic properties of a crystal [21]. Upon further heating, this intermediary structure or mesophase loses as well the orientational ordering and transforms into a liquid. Unlike thermotropic liquid crystals, lyotropic liquid crystals are obtained by dissolving amphiphilic mesogen in a suitable solvent, to a specific concentration [22].

Most liquid crystals are organic molecules composed of π -conjugated systems and flexible alkyl chains attached to these. Although the functional conjugated units maintain the order, they have poor solubility in organic solvents, which limits the processing in optoelectronic devices [23]. Attachment of alkyl chains reduces the melting points and increases the solubility, while protecting the conjugated units from oxygen aggression. Hence, the optimum ratio between van der Waals interactions of the alkyl chains and π - π interactions of the conjugated units results in modulation of physical states and optoelectronic properties of liquid crystals [24].

Based on different geometry of the constituents, liquid crystalline molecules have been classified into calamitic or rod-like (elongated molecules), discotic (disc-shaped molecules), and bent-core or banana-shaped molecules. Another classification was based on symmetry of phases, which changes during the phase transitions. Besides, the phase symmetry targets the molecular organization in the phases and determines the physical properties of liquid crystals.

While the small calamitic liquid crystal organic molecules have been used in LCD devices [25] and π -conjugated discotic liquid crystalline molecules proved to be adequate for electron transport [26] and photoluminescence [27], the supra-molecular unconventional liquid crystals based on non-covalent interactions and polymeric systems are used for high strength fibers, encapsulation of microelectronic circuits, actuators, and organic photovoltaic or renewable energy [28–30]. Additionally, the combination between nanoparticles (e.g. CNTs) and liquid crystals that promote the self-assembly into well-defined periodic structures represents another research domain that is dealing with the improvement of electro-optic characteristics in devices or obtaining metamaterials [31–36].

Between mesophases, the nematic phase (N) is the least ordered (since it exhibits only long-range orientational order) and more fluid (less viscous) and easily responds to electric fields or formation of a mono-domain liquid crystal phase, successfully applied to flat-panel displays [37]. When chiral mesogens are introduced into a liquid crystalline structure or chiral molecules are added to a liquid crystal phase, a chiral phase is generated. In a cholesteric mesophase or chiral nematic phase (N*), the molecular orientation twists through the medium with a certain periodicity, while the positions of molecules are not correlated. Smectic phases (Sm) are distinguished from nematic ones by their stratification or ordering in the layers. Hence, in a smectic A mesophase, molecules may be on the average perpendicular to the layers; while in smectic C, the molecules adopt a uniformly tilted configuration, being inclined with a certain angle. The increase of molecular order leads to higher ordered smectic phases (Sm B, SmE, and SmG) [38]. The chiral smectic A phase (SmA*) presents about the same structure as the achiral SmA phase, except the physical properties. On the other hand, the chiral smectic C phase (SmC*) is different from any liquid crystalline phase and exhibits ferroelectric (FE) switching behavior.

Ferroelectricity appears in the case of molecules that present spontaneous and reversible electric polarization (P) that can be switched by using an external electric field [39, 40]. This physical phenomenon may be successfully accomplished by organic ferroelectric materials and used in devices like computer memories, sensors, and optics. In self-ordered liquid crystalline systems, ferroelectricity appears because of organization of chiral mesogens or the intrinsic dipole within achiral molecules,

which allows the facile switching of molecular dipoles. In mostly ordinary liquid crystalline phases (N, SmA, and SmC), the high rotational symmetry around the long molecular axis prevents the appearance of ferroelectricity. For chiral SmC* phase, electro-optical effects with speeds below microsecond order have been registered, so that SmC* liquid crystalline phase can be switched ON or OFF about 10^3 times more rapidly than nematic liquid crystals [41].

In liquid crystalline systems, chirality induces a one-dimensional helical structure, where the helical axis is perpendicular to the local director (for cholesteric mesophases) or is tilted from the normal layer so that the director precesses around the helix axis with a particular periodicity (for SmC* phases) [42]. The remarkable behavior of SmC* phases induced unique optical properties such as electro-optical effects, low-threshold laser emission, circular dichroism, or Bragg reflection [11, 43].

Similar to the SmC* phase, the discotic phase containing pendant chiral side chains forms ferroelectric columnar phases, though the switching phenomenon is not very clear. However, two possibilities have been suggested: the entire column rotates 180° around the columnar axis or the molecules reorient independently [44].

Although bent-core (BC) molecules are non-chiral mesogens, polar properties were reported for this unconventional liquid crystalline class [45]. The novelty of BC structures arises from simple bending by approximately 120° of the mesogenic core, resulting in a compact packing arrangement of molecules, which restricts rotational freedom with high impact on the structure of the liquid crystalline phases. According to the polar axis direction in adjacent layers, these phases can show ferroelectric (FE) or antiferroelectric (AF) behavior. The switching process in BC compounds under an electric field influence has been associated with π - π interaction type between the aromatic cycles that result after molecular restricted rotation around a tilted cone, while the chirality in the layers remains the same (the tilting and polar direction reverses) [46–55].

In order to be useful in devices, liquid crystals need to be forced and adequately aligned. Therefore, samples are formed between a pair of surface treated glass plates with about few microns distance. Compared to other mesophases, the alignment in the SmC* phase is more difficult to obtain. By placing a ferroelectric liquid crystal sample between crossed polarizers with the director n aligned along one of the polarizers, the helix is suppressed by surface action. Hence, the sample becomes an electro-optic switch that shows spontaneous polarization and two surfaces which interact to stably unwind the spontaneous ferroelectric helix result. This is known as a surface-stabilized-ferroelectric-liquid-crystal (SSFLC) device, very attractive for display applications because of very fast switching response [56]. Thus, the SSFLCs are of great interest for electro-optic devices based on the memory effect. Moreover, another application of optically addressed SSFLC targets optical holography [57].

Author details

Irina Carlescu

“Gheorghe Asachi” Technical University of Iasi, Iasi, Romania

*Address all correspondence to: icarlescu@ch.tuiasi.ro

IntechOpen

© 2018 The Author(s). Licensee IntechOpen. This chapter is distributed under the terms of the Creative Commons Attribution License (<http://creativecommons.org/licenses/by/3.0>), which permits unrestricted use, distribution, and reproduction in any medium, provided the original work is properly cited. 

References

- [1] Lagerwall JPF, Scalia G. A new era for liquid crystal research: Applications of liquid crystals in soft matter nano-, bio- and microtechnology. *Current Applied Physics*. 2012;**12**(6):1387-1412. DOI: 10.1016/j.cap.2012.03.019
- [2] Körner H, Shiota A, Bunning TJ, Ober CK. Orientation-on-demand thin films: Curing of liquid crystalline networks in ac electric fields. *Science*. 1996;**272**(5259):252-255. DOI: 10.1126/science.272.5259.252
- [3] Hulvat JF, Stupp SI. Liquid-crystal templating of conducting polymers. *Angewandte Chemie*. 2003;**42**(7):778-781. DOI: 10.1002/anie.200390206
- [4] Hentze HP, Kaler EW. Polymerization of and within self-organized media. *Current Opinion in Colloid and Interface Science*. 2003;**8**(2):164-178. DOI: 10.1016/S1359-0294(03)00018-9
- [5] Goodby JW et al. *Handbook of Liquid Crystals*. 2nd ed. Weinheim: Wiley; 2014
- [6] Sagara Y, Kato T. Mechanically induced luminescence changes in molecular assemblies. *Nature Chemistry*. 2009;**1**:605-610. DOI: 10.1038/nchem.411
- [7] Yu Y, Nakano M, Ikeda T. Directed bending of a polymer film by light. *Nature*. 2003;**425**:145. DOI: 10.1038/425145a
- [8] Schadt M. Nematic liquid crystals and twisted nematic LCDs. *Liquid Crystals*. 2015;**42**:646-652. DOI: 10.1080/02678292.2015.1021597
- [9] Bisoyi HK, Quan L. Light-driven liquid crystalline materials: From photo-induced phase transitions and property modulations to applications. *Chemical Reviews*. 2016;**116**(24):15089-15166. DOI: 10.1021/acs.chemrev.6b00415
- [10] Li Q. *Nanoscience with Liquid Crystals: From Self-Organized Nanostructures to Applications*. Heidelberg: Springer-Verlag; 2014
- [11] de Gennes PG, Prost J. *The Physics of Liquid Crystals*. Oxford: Oxford University Press; 1993
- [12] Chandrasekhar S. *Liquid Crystals*. Cambridge, UK: Cambridge University Press; 1992
- [13] Collings PJ, Hird M. *Introduction to Liquid Crystals: Chemistry and Physics*. London: Taylor & Francis; 1997
- [14] Demus D, Goodby JW, Gray GW, Spiess HW, Vill V. *Handbook of Liquid Crystals*. Weinheim: Wiley-VCH; 1998
- [15] Collings PJ, Hird M. *Introduction to Liquid Crystals Chemistry and Physics*. London: Taylor and Francis; 1997
- [16] Kato T, Mizoshita N, Kishimoto K. Functional liquid-crystalline assemblies: Self-organized soft materials. *Angewandte Chemie, International Edition*. 2005;**45**(1):38-68. DOI: 10.1002/anie.200501384
- [17] Tschierske C. Non-conventional soft matter. *Annual Reports on the Progress of Chemistry*. 2001;**97**:191-267. DOI: 10.1039/B101114F
- [18] Goodby JW, Saez IM, Cowling SJ, Geortz V, Draper M, Hall AW, et al. Transmission and amplification of information and properties in nanostructured liquid crystals. *Angewandte Chemie, International Edition*. 2008;**47**(15):2754-2787. DOI: 10.1002/anie.200701111
- [19] Tschierske C. Liquid crystal engineering – New complex mesophase structures and their relations to polymer morphologies, nanoscale patterning and crystal engineering. *Chemical Society*

- Reviews. 2007;**36**(12):1930-1970. DOI: 10.1039/B615517K
- [20] Dunmur D, Sluckin T. Soap, Science and Flat-Screen TVs- A History of Liquid Crystals. Oxford: Oxford University Press; 2011
- [21] Sluckin TJ, Dunmur DA, Stegemeyer H. Crystals That Flow: Classic Papers from the History of Liquid Crystals. Boca Raton, FL: CRC Press; 2004
- [22] Garti N, Somasundaran P, Mezzenga R. Self-Assembled Supramolecular Architectures: Lyotropic Liquid Crystals. NJ: Wiley; 2012
- [23] Moonen PF, Yakimets I, Huskens J. Fabrication of transistors on flexible substrates: From mass-printing to high-resolution alternative lithography strategies. *Advanced Materials*. 2012;**24**(41):5526-5541. DOI: 10.1002/adma.201202949
- [24] Fengniu L, Takashi N. Alkyl- π engineering in state control toward versatile optoelectronic soft materials. *Science and Technology of Advanced Materials*. 2015;**16**(1):1468-6996. DOI: 10.1088/1468-6996/16/1/014805
- [25] Kawamoto H. The history of liquid-crystal displays. *Proceedings of the IEEE*. 2002;**90**(4):460-500. DOI: 10.1109/JPROC.2002.1002521
- [26] Kato T, Yoshio M, Ichikawa T, Soberats B, Ohno H, Funahashi M. Transport of ions and electrons in nanostructured liquid crystals. *Nature Reviews Materials*. 2017;**2**(4):1-20. DOI: 10.1038/natrevmats.2017.1
- [27] Wang YF, Shi JW, Chen JH, Zhu WG, Baranoff E. Recent progress in luminescent liquid crystal materials: Design, properties and application for linearly polarised emission. *Journal of Materials Chemistry C*. 2015;**3**(31):7993-8005. DOI: 10.1039/c5tc01565k
- [28] Bisoyi HK, Urbas AM, Li Q. Soft materials driven by photothermal effect and their applications. *Advanced Optical Materials*. 2018;**6**(15):1-21. DOI: 10.1002/adom.201800458
- [29] Iwan A. An overview of LC polyazomethines with aliphatic-aromatic moieties: Thermal, optical, electrical and photovoltaic properties. *Renewable and Sustainable Energy Reviews*. 2015;**52**:65-79. DOI: 10.1016/j.rser.2015.07.078
- [30] Dong LQ, Feng YY, Wang L, Feng W. Azobenzene-based solar thermal fuels: Design, properties, and applications. *Chemical Society Reviews*. 2018;**47**(19):7339-7368. DOI: 10.1039/c8cs00470f
- [31] Agarwal A, Lilly GD, Govorov AO, Kotov NA. Optical emission and energy transfer in nanoparticle, nanorod assemblies: Potential energy pump system for negative refractive index materials. *Journal of Physical Chemistry C*. 2008;**112**(47):18314-18320. DOI: 10.1021/jp8006238
- [32] Sanchez-Iglesias A, Grzelczak M, Rodriguez-Gonzalez B, Alvarez-Puebla RA, Liz-Marzan LM, Kotov NA. Gold colloids with unconventional angled shapes. *Langmuir*. 2009;**25**(19):11431-11435. DOI: 10.1021/la901590s
- [33] Kretzers IKJ, Parker RJ, Olkhov RV, Shaw AM. Aggregation kinetics of gold nanoparticles at the silica-water interface. *Journal of Physical Chemistry C*. 2009;**113**(14):5514-5519. DOI: 10.1021/jp809304z
- [34] Liu QK, Cui YX, Gardner D, Li X, He SL, Smalyukh II. Self-alignment of plasmonic gold nanorods in reconfigurable anisotropic fluids for tunable bulk metamaterial applications. *Nano Letters*. 2010;**10**(4):1347-1353. DOI: 10.1021/nl9042104

- [35] Lin MH, Chen HY, Gwo S. Layer-by-layer assembly of three-dimensional colloidal supercrystals with tunable plasmonic properties. *Journal of the American Chemical Society*. 2010;132(32):11259-11263. DOI: 10.1021/ja103722p
- [36] Garbovskiy Y, Glushchenko A. Ferroelectric nanoparticles in liquid crystals: Recent progress and current challenges. *Nanomaterials*. 2017;7(11):1-20. DOI: 10.3390/nano7110361
- [37] Bremer M, Kirsch P, Klasen-Memmer M, Tarumi K. The TV in your pocket: Development of liquid-crystal materials for the new millennium. *Angewandte Chemie, International Edition*. 2013;52:8880-8896. DOI: 10.1002/anie.201300903
- [38] Andrienko D. Introduction to liquid crystals. *Journal of Molecular Liquids*. 2018;267:520-541. DOI: 10.1016/j.molliq.2018.01.175
- [39] Alok ST, Kaeser A, Matsumoto M, Aida T, Stupp SI. Supramolecular ferroelectrics. *Nature Chemistry*. 2015;7(4):281-294. DOI: 10.1038/nchem.2206
- [40] Jakli A, Lischka C, Weissflog W, Pezl G, Rauch S, Heppke G. Structural transitions of smectic phases formed by achiral bent-core molecules. *Ferroelectrics*. 2000;243(1):239-247. DOI: 10.1080/00150190008008025
- [41] Lagerwall JPF, Giesselmann F. Current topics in smectic liquid crystal research. *ChemPhysChem*. 2006;16(1):20-45. DOI: 10.1002/cphc.200500472
- [42] Kitzerow HS, Bahr C. *Chirality in Liquid Crystals*. New York: Springer; 2001
- [43] Dunmur K. In: Demus DD, Goodby J, Gray GW, Spiess HW, Vill V, editors. *Physical Properties of Liquid Crystals*. Wiley-VCH; 1999
- [44] Guillon D. In: Prigogine I, Rice SA, Vij JK, editors. *Advances in Chemical Physics*; 2007. pp. 1-49
- [45] Niori T, Sekine T, Watanabe J, Takezoe H. Distinct ferroelectric smectic liquid crystals consisting of banana shaped achiral molecules. *Journal of Materials Chemistry*. 1996;6(7):1231-1233. DOI: 10.1039/JM9960601231
- [46] Görtz V, Goodby JW. Enantioselective segregation in achiral nematic liquid crystals. *Chemical Communications*. 2005;(26):3262-3264. DOI: 10.1039/B503846D
- [47] Hegmann T, Peidis F, Diele S, Tschierske C. Combination of molecular rods and half-discs: Transition from lamellar to columnar order in multichain mononuclear ortho-palladated metallomesogens. *Liquid Crystals*. 2000;27(10):1261-1265. DOI: 10.1080/026782900423296
- [48] Mahlstedt S, Janietz D, Schmidt C, Stracke A, Wendorff JH. Novel donor-acceptor triple mesogens incorporating disc-like and rod-like molecular subunits. *Liquid Crystals*. 1999;26(9):1359-1369. DOI: 10.1080/026782999204039
- [49] Hegmann T, Kain J, Diele S, Schubert B, Bogel H, Tschierske C. Molecular design at the calamitic/discotic cross-over point. Mononuclear ortho-metallated mesogens based on the combination of rod-like phenylpyrimidines and -pyridines with bent or half-disc-shaped diketonates. *Journal of Materials Chemistry*. 2003;13:991-1003. DOI: 10.1039/B210250A
- [50] Chen D, Nakata M, Shao RF, Tuchband MR, Shuai M, Baumeister U,

et al. Twist-bend heliconical chiral nematic liquid crystal phase of an achiral rigid bent-core mesogen. *Physical Review E*. 2014;**89**(2). DOI: 10.1103/PhysRevE.89.022506

[51] Tschierske C. Development of structural complexity by liquid-crystal self-assembly. *Angewandte Chemie, International Edition*. 2013;**52**(34):8828-8878. DOI: 10.1002/anie.201300872

[52] Tschierske C, Photinos DJ. Biaxial nematic phases. *Journal of Materials Chemistry*. 2010;**20**(21):4263-4294. DOI: 10.1039/b924810b

[53] Popov P, Mann EK, Jakli A. Thermotropic liquid crystal films for biosensors and beyond. *Journal of Materials Chemistry C*. 2017;**5**(26): 5061-5078. DOI: 10.1039/c7tb00809k

[54] Alaasar M, Prehm M, Poppe S, Tschierske C. Development of polar order by liquid-crystal self-assembly of weakly bent molecules. *Chemistry—A European Journal*. 2017;**23**(23): 5541-5556. DOI: 10.1002/chem.201606035

[55] Tschierske C. Development of structural complexity by liquid-crystal self-assembly. *Angewandte Chemie, International Edition*. 2013;**52**(34):8828-8878. DOI: 10.1002/anie.201300872

[56] Clark NA, Lagerwall ST. Surface-stabilized ferroelectric liquid crystal electrooptics: New multistate structures and devices. *Ferroelectrics*. 1984;**59**:25-67. DOI: 10.1080/00150198408240737

[57] Sutkowski M, Piecek W, Grudniewski T, Parka J, Nowinowski-Kruszelnicki E. Light driven optical switching of the surface stabilized antiferroelectric liquid crystals. *Optics and Lasers in Engineering*. 2011;**49**(11):1330-1334. DOI: 10.1016/j.optlaseng.2011.05.019

Section 2

**Self-Assembling Soft
Functional Materials:
Structure and Phase
Behavior**

Bent-Core Liquid Crystals: Structures and Mesomorphic Properties

Dan Scutaru, Irina Carlescu, Elena-Raluca Bulai (Cioanca), Catalina Ionica Ciobanu, Gabriela Lisa and Nicolae Hurduc

Abstract

Bent-core (BC) molecules became an attractive liquid crystal class due to their potential use in smart displays and photonic devices. In contrast to calamitic mesogens, bent-shaped mesogens are self-organized superstructures with remarkable properties, given the presence of polar order in mesophases, although the molecules themselves are not chiral. A particular interest represents the biaxial nematic liquid crystal materials that are used in display technology and allow a faster switching response, compared to calamitic liquid crystals, with considerably reduced costs. This chapter briefly reviews the bent-core liquid crystals with three different core units in the structure: (1) 2,5-disubstituted oxadiazole, (2) 1,3-disubstituted benzene, and (3) 2,7-disubstituted naphthalene. To the central bent units (BUs) containing reactive functional groups of phenolic or aminic type, various mesogenic groups are symmetrically or asymmetrically connected, via esterification or condensation reactions. The obtained compounds showed biaxial nematic and/or smectic mesophases with high transition temperatures in the case of oxadiazole derivatives or cholesteric and banana-type mesophases with lower transition temperatures in the case of benzene and naphthalene derivatives.

Keywords: liquid crystals, bent-core molecules, resorcinol, naphthalene, oxadiazole, azomesogens, biaxial, nematic, smectic, cholesteric

1. Introduction

Liquid crystal displays (LCDs) are omnipresent in modern world, representing probably the most prevalent, developed, and profitable technology of thermotropic liquid crystals [1, 2]. This application is based on their sensitivity to external electric and magnetic fields, when molecules align fast and at low voltages. This property was the basis for their use in other interesting applications, especially as sensors. Because of their fluid nature at a certain temperature, liquid crystals (LCs) are very easy to process in thin films, along with maintaining optical properties characteristic to crystalline materials, as the ability to rotate the polarized light plane (birefringence).

The discovery of portable devices and the introduction of easily used tactile displays resulted in a new change of direction in LCD technologies. Present researches focus on synthesis, characterization, and analysis of new mesogenic structures with high dielectric anisotropy ($\Delta\epsilon$) (for inducing the decrease of voltage), low

rotational viscosity (γ_1) (allowing fast switching), birefringence (Δn) suitable to accurate display design, good solubility, and a broad nematic phase domain [2].

The increasing interest for bent-core (BC) liquid crystals in the past two decades is due to their ability to provide potential devices with fast switching response [3–7]. Therefore, the main purpose was to analyze the relation between biaxial molecular structures and electro-optical properties in this type of compound. From a technical point of view, the main objective is to look for the improvement of response time in order to reduce the motion effect in the case of large TVs and in displaying information in the case of tactile devices, respectively. The development of reliable functional materials that allow reduced chemical production cost was also considered [8].

Because of the bent shape that strongly deviates from linear symmetry axis, bent-core biaxial molecules are capable of special steric interactions, caused by the tendency to reduce the rotational disordering around the long axis. The bent-core molecules are preferentially packed into bent directions and parallelly aligned to each layer. Because of this imposed framing, each layer presents a spontaneous polarization (P_s), which is parallel or antiparallel to the molecular bent direction, while the molecules present the properties of switching without chirality, particularly useful for display screens. The existing bending angle between the arms permits the formation of unique self-organized systems with mesophases having no counterpart in conventional calamitic liquid crystals [4–7].

The special properties of biaxial molecules stimulated the researches in the field, so that a large number of banana-type compounds with various fragment structural combinations have been synthesized [9–17].

In banana-type compounds, eight different complex mesophase morphologies have been identified until now (B_1, B_2, \dots, B_8), the distinction between phases being made on the basis of optical textures and characteristic differences in X-ray diffraction diagrams [18–22]. Literature data showed that the appearance of B-type mesophases depends mainly on an adequate combination between central unit and lateral rigid units. The general structure of BC molecules includes two symmetrical/asymmetrical mesogenic units of rod-like type connected to central units by linking groups (Figure 1). Usually, the angle between the arms depends mainly on the type of the connecting groups (around 120° and 140°) [23, 24].

Although remarkable progresses have been realized in thermal analysis, a precise correlation between BC chemical structures and their physical properties is still not possible, as for calamitic liquid crystal molecules. In many cases, molecules that present banana-type mesophases have a bent shape, but this does not always assure the mesophase appearance. Data show that for the appearance of B mesophases, two factors are necessary: (1) adequate distribution of charges along the arms [25] and (2) adequate bending angle [24].

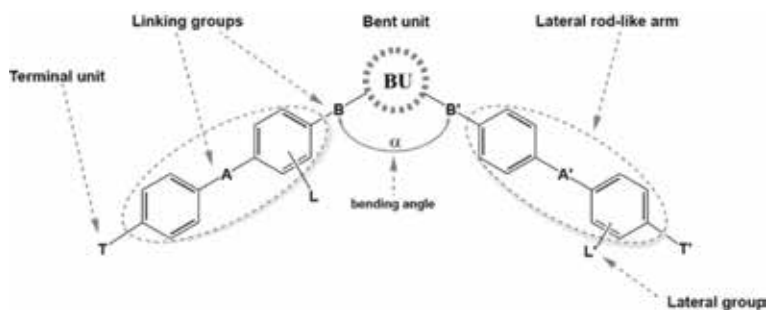


Figure 1.
General structure of banana-type liquid crystals.

The properties of biaxial liquid crystals can be influenced by the substituents of central nucleus, lateral arms, and terminal units. The central aromatic core generally consists of naphthalene, benzene, and heterocyclic units. A considerable influence may have the linking groups used for connecting the chemical structures. The most used connecting groups are of ester, azomethine, azo, stilbene, thiocarbonyl, or acryloyloxy type [26, 27]. The withdrawing or donating electronic groups may strongly affect the electronic density, the molecular flexibility, and the partial polarity of the molecule [25, 28]. The most interesting banana-type mesogenic compounds which presented switchable mesophase have been the ones containing azomethine groups. However, this linking group is thermally unstable in the presence of acidity and metallic surfaces, and some Schiff bases decomposing around 150°C, while others are stable up to 200°C.

Bent-core molecules containing azo linkages present remarkable properties because of the association of the photosensitive nature of azobenzene derivatives with ferroelectric liquid crystalline properties of BC compounds [13, 16, 29]. Although the first bent-core azo liquid crystalline compound was prepared by Vorländer in 1929, the pioneering work has been done by Prasad et al. who synthesized compounds containing aromatic rings and azo groups and presenting smectic phases [30]. Because of *trans-cis* photochemical isomerization of the azobenzene moiety, configurational modifications appear with significant changes on physical properties targeting dipole moment, refractive index, or viscosity [13].

The lateral substitution has a strong impact on liquid crystalline state or mesophase stability, respectively [31, 32]. The packing of molecules may be affected by size, polarity, and substitution position. The liquid crystalline properties may completely disappear after the introduction of bulky lateral substituents. Sometimes, interesting modifications have been observed in the switching behavior after the introduction of small polar substituents [9, 31, 33–35].

Hence, the study of biaxial LC based on bent-core units represents a very actual subject not only from a theoretical point of view but also for designing materials with special properties [36, 37]. The existence of a stable biaxial nematic mesophase can lead to a whole class of devices based on liquid crystals able to considerably improve the switching properties or behave as optical compensation films [38].

This chapter proposes to describe the relationship between the structure and supramolecular ordering properties of symmetrical and asymmetrical bent-core liquid crystals synthesized by our research group. In order to keep this chapter within a certain length, the detailed study on synthesis and complete characterization of compounds is not included here and may be found in the original papers [39–53]. In the following sections, the transition temperature (°C) and the type of mesophase for each compound are given below its chemical structure, while transitions in square brackets refer to monotropic phase. The phase behavior will be discussed in the text, where B stands for banana phase, Cr for crystal, LC for liquid crystal, Iso for isotropic phase, N for nematic phase, Sm for smectic phase, Ch for cholesteric phase, and d for decomposition process.

2. Relationship between structure and liquid crystalline properties

The mesomorphic behavior of bent-core compounds synthesized in our group was described through a systematic study that reviewed the nature of central bent core; the position, size, and the role of lateral substitution in the central unit; the symmetry or non-symmetry of rigid calamitic wings; the length, polarity, and micro-segregation of the terminal flexible chains; and the presence of the cholesteric moiety. The influence of the structure of calamitic wings was also considered,

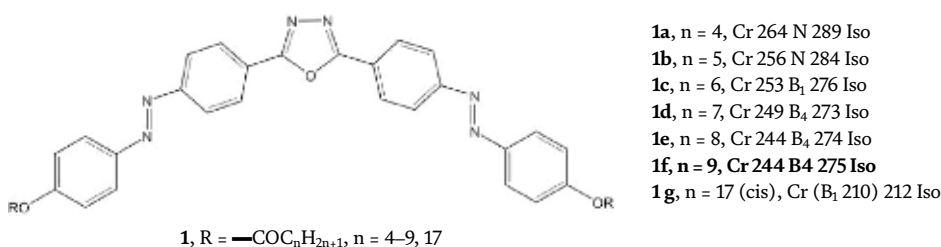
regarding the number of aromatic rings and the nature of linking groups that contribute through polarity, orientation, and flexibility.

According to their core, banana-shaped compounds were divided into three categories: (1) 2,5-disubstituted oxadiazole; (2) 1,3-disubstituted benzene; and (3) 2,7-disubstituted naphthalene.

2.1 Bent-core compounds based on oxadiazole core

Among heterocyclic liquid crystals, the central unit in 2,5-disubstituted-[1,3,4] oxadiazoles assures the optimum geometry for bent-shaped molecules. Generally, the bending angle determined by the presence of 2,5-disubstituted oxadiazole central unit is between 134 and 140°, larger than the typical value of 120° in 1,3-disubstituted benzene unit. Moreover, the presence of three polarizable heteroatoms causes a high dipole moment that affects phase transition temperatures and mesophase types. Therefore, the presence of bent-shape and dipolar nature of the oxadiazole core together makes these compounds very attractive for applications.

When the central unit is symmetrically substituted with two azobenzene units with alkanoyloxy flexible chain ends (compound **1**), the mesomorphic properties vary with the number of carbon atoms.



Thus, for compounds of type **1** containing a smaller number of carbon atoms (n = 4, 5), the mesophase is of nematic type with characteristic Schlieren texture. The change occurs for n = 6, when the compound shows the lowest liquid crystalline domain on heating, but dendritic-like texture on cooling, characteristic of B₁ phase [39]. Further increase of carbon atoms results in progressive growth of the mesomorphic intervals, with B₄ chirally separated domains, evidenced on cooling by dark and bright domains after rotation of one of the polarizers clockwise or anticlockwise from the crossed (90°) position (**Figure 2**). On the other hand, the

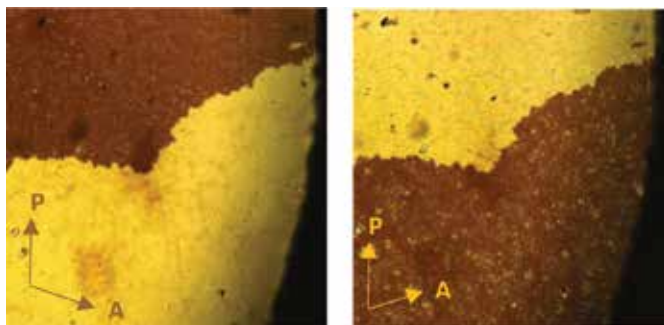
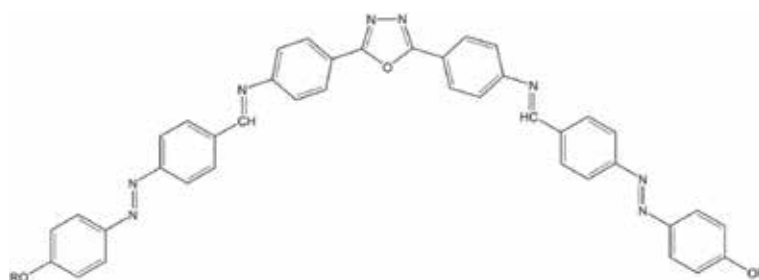


Figure 2. Textures of B₄ chiral domains' phase of compound **1f** at T = 175°C between slightly de-crossed polarizers from 90° by about +/-5°.

introduction of elaidic or oleic units ($n = 17$, *cis*, *trans*) on the terminal chain destabilizes (**1 g**, monotropic) or suppress the mesophase.

Compounds of type **2**, containing one more benzene ring in each side arm and azomethine linking groups, exhibited a rich polymorphism, induced by repulsion effects between the hydrogen atom of the azomethine group and the aromatic system. The compounds presented smectic phase and/or characteristic nematic droplets or Schlieren textures on broad domains (between 89 and 169°C), which go up to high transition temperatures (higher than 330°C), with decomposition before isotropization [40]. Thermal degradation studies revealed that the compounds with even methylene groups show a lower stability compared to those with odd ones [41].



2, R = $-\text{COC}_n\text{H}_{2n+1}$, $n = 4-9$, 1/

3, R = $-\text{C}_n\text{H}_{2n+1}$, $n = 6-10, 18$

2a, $n = 4$, Cr₁ 228 Cr₂ 244 Sm 264 N 333 Iso (d)

2b, $n = 5$, Cr₁ 214 Cr₂ 232 N 342 Iso (d)

2c, $n = 6$, Cr₁ 80 Cr₂ 134 N 253 Iso (d)

2d, $n = 7$, Cr₁ **64** Cr₂ **174** Sm **219** N **343** Iso (d)

2e, $n = 8$, Cr₁ 193 Cr₂ 204 Sm 249 N 321 Iso (d)

2f, $n = 9$, Cr₁ 192 Cr₂ 204 Sm 234 N 332 Iso (d)

2g, $n = 17$, Cr₁ 96 Cr₂ 194 N 335 Iso (d)

3a, $n = 6$, Cr₁ 113 Cr₂ 254 N 326 Iso

3b, $n = 7$, Cr 239 N 327 Iso

3c, $n = 8$, Cr 229 N 330 Iso

3d, $n = 9$, Cr 219 N 322 Iso

3e, $n = 10$, Cr **184** N **321** Iso

3f, $n = 18$, Cr 172 N 280 Iso

Replacing the acyloxy terminal chain with an alkoxy one in compounds of type **3** results in decreasing the isotropization temperatures alongside with mesomorphic domains. For this class, the compound with 10 carbon atoms in the aliphatic chain showed the highest stability of mesophase. All compounds presented similar polymorphism to that of **2**, analogous with nematic droplet phases or Schlieren textures, characteristic of bent-core compounds (**Figure 3**).

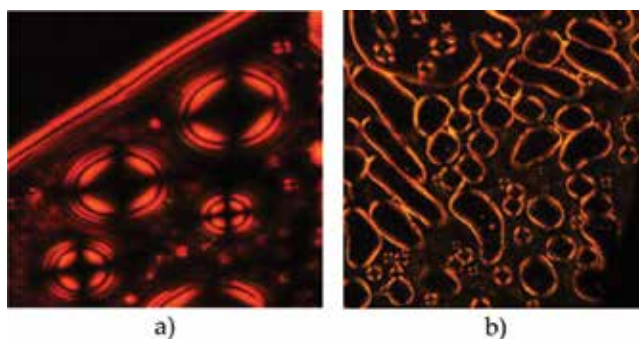
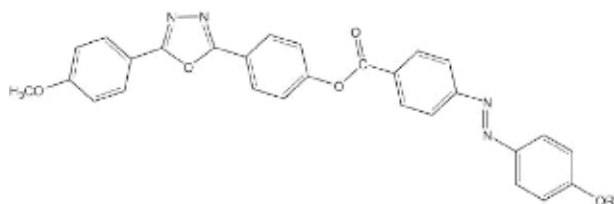


Figure 3.
Optical micrographs of mesophases: (a) **3a**, 285°C, heating; (b) **3e**, 205°C, cooling.

The asymmetric hockey-stick derivatives of type **4** showed the widest meso-phase domains (between 123 and 198°C), compared to compounds **1–3** [42]. The mesophase behavior was explained by the strong dipolar interactions between molecules, determined by the asymmetric substitution of the oxadiazole core with a shorter side arm, where the molecules bend is not emphasized as for classical bent-core compounds.



4a, n = 6, Cr 148 N 346 Iso
4b, n = 7, Cr 138 N 293 Iso
4c, n = 8, Cr 145 N 324 Iso
4d, n = 9, Cr₁ 105 Cr₂ 142 N 275 Iso
4e, n = 10, Cr 141 N 313 Iso
4f, n = 18, Cr₁ 95 Cr₂ 137 Sm 260 Iso

4, R = —C_nH_{2n+1}, n = 6–10, 18

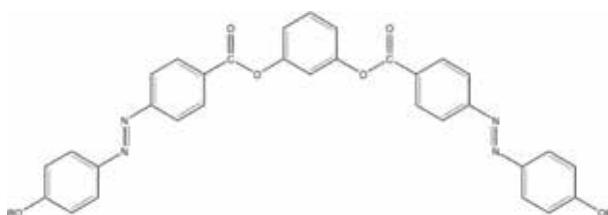
As for previous compounds, the stability of mesophases follows the odd-even effect, because of changing the ability to order into mesophase. Thus, the increase of aliphatic chain to 18 carbon atoms induces changes in supramolecular ordering, which leads to the narrowest mesophase range. All the compounds showed mesophases ordered into nematic phases of ribbon type or with characteristic Schlieren textures. The last compound of the series (n = 18) presented smectic textures.

2.2 Bent-core compounds based on benzene core

1,3-Disubstituted benzene derivatives represent the first class of synthesized bent-core liquid crystals, with the largest number of reported compounds [22]. Our studies are based on two types of benzene core: resorcinol and 1,3-diaminobenzene.

2.2.1 Resorcinol central unit

The symmetric disubstitution of resorcinol with dimeric azomesogens or imino-azo mesogens with terminal flexible chains results in mesomorphic compounds evidencing Sm or B phases with relatively stable mesophase domains. In the case of compound **5a**, SmB dendritic textures were identified from isotropic melt that changed into a B₁ mosaic one at lower temperature [43].



5, R = —C_nH_{2n+1}, n = 6–10

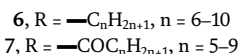
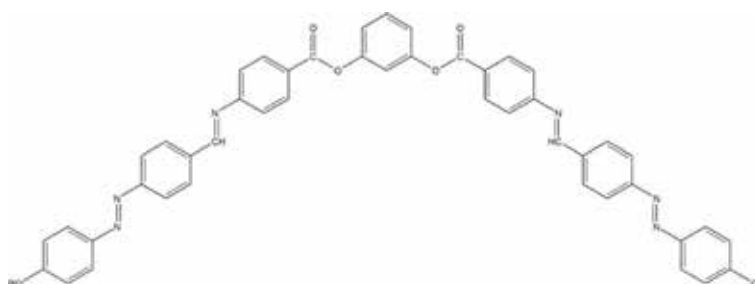
5a, n = 6: Cr₁ 116 Cr₂ (SmB 163) 168 Iso
5b, n = 7: Cr₁ 111 Cr₂ 142 SmB 163 Iso
5c, n = 8: Cr₁ 94 Cr₂ 143 SmB 159 Iso

5d, n = 9: Cr₁ 100 Cr₂ 147 Iso
5e, n = 10: Cr₁ 100 Cr₂ 148 Iso

Increasing the alkyl chain to 7 (compound **5b**) and 8 (compound **5c**) carbon atoms stabilized the mesophase but only on a relatively narrow interval of

temperature. Further increase in the length of the chain completely destabilized the liquid crystalline behavior due to the disorder induced by the flexible unit in relation to the rigid one, so compounds **5d** and **5e** are non mesomorphic [43].

Compounds **6a–e** show predominantly smectic phases with characteristic fan-shaped textures [44]. Oily streak texture was identified in the case of compound **6e** on first heating, that poorly developed into fan-like textures with striations across individual fans from the isotropic melt (**Figure 4a, b**). The mesophase domains are better stabilized for the first (**6a**) and the last compounds (**6e**) of this series. The insertion of polar acyloxy linkage between terminal chain and aromatic ring increases the physical interactions between molecules, with consequences on the isotropization temperatures together with increases of the mesophase domains at around 30°C (compound **7a**) [44].



6a, n = 6: Cr₁ 159 Cr₂ 181 Cr₃ 215 Sm 294 Iso

6b, n = 7: Cr₁ 151 Cr₂ 181 Cr₃ 213 Sm 276 Iso

6c, n = 8: Cr₁ 136 Cr₂ 202 B₁ 267 Iso

6d, n = 9: Cr 195 B₃ 260 Iso

6e, n = 10: Cr₁ 152 Cr₂ 177 B₃ 259 Iso

7a, n = 5: Cr₁ 169 Cr₂ 202 Sm 315 Iso

7b, n = 6: Cr₁ 164 Cr₂ 209 Sm 304 Iso

7c, n = 7: Cr₁ 146 Cr₂ 207 Sm 285 Iso

7d, n = 8: Cr₁ 148 Cr₂ 202 Sm 288 Iso

7e, n = 9: Cr₁ 148 Cr₂ 195 B₂ 287 Iso

As for previous compounds of type **6**, predominately smectic phases were identified on heating and nematic and smectic phases on cooling, respectively. However, banana B₇ phase has been identified in the case of compound **7b** on cooling from the isotropic melt, with characteristic spiral and circular domains and equidistant line pattern (**Figure 5a**). Thin filament texture in a spiral fashion network, which preceded smectic phase, was visible on heating for compounds **7d** and **7e** (**Figure 5b**).

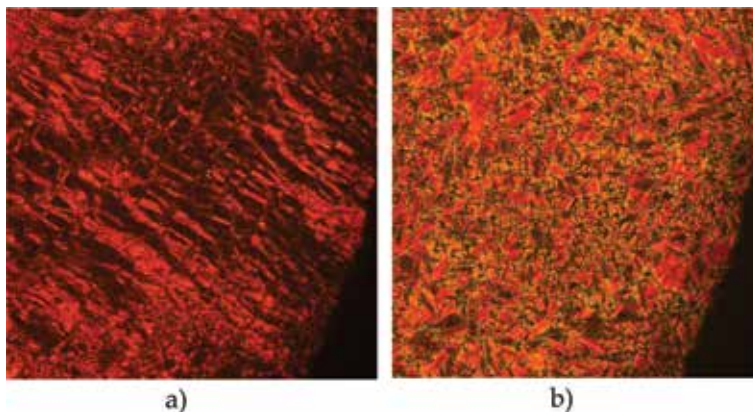


Figure 4.
Optical micrographs of mesophases of compound **6e**, (a) 195°C, heating; (b) 170°C, cooling.

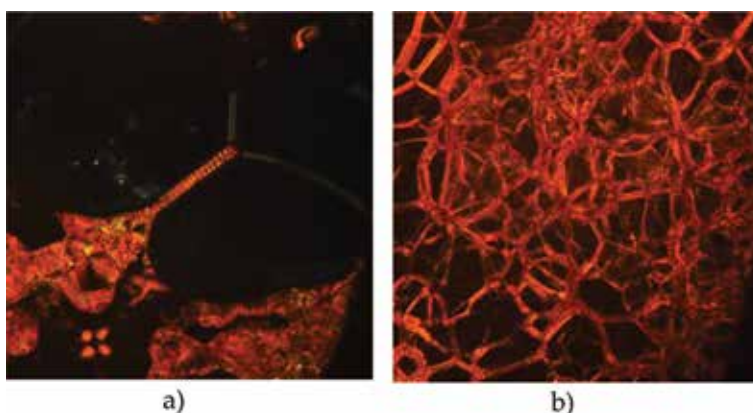
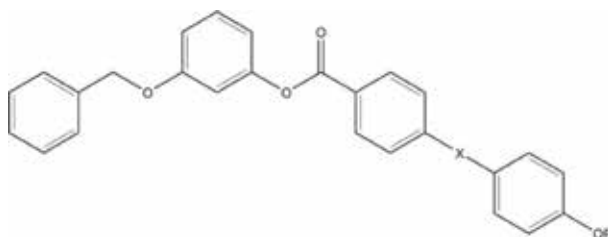


Figure 5.
Optical micrographs of mesophases: (a) **7b**, 280°C, cooling and (b) **7e**, 280°C, heating.

The asymmetric disubstitution of resorcinol resulted in bent-core compounds containing only one typical mesogenic arm, formed by two aromatic rings connected via ester or azo linking groups and containing alkyloxy terminal flexible chains, while the other arm contained only a benzyl unit [45]. In this case, the liquid crystalline behavior depends on the type of the linkage between the aromatic rings in the long arm. Hence, the presence of azo linkage allows the formation only of monotropic phases (compounds **8a–e**).



8, X = —N=N—, R = —C_nH_{2n+1}, n = 6–10

9, X = —OCO—, R = —C_nH_{2n+1}, n = 6–10

8a, n = 6: Cr (B₁ 95) 113 Iso

8b, n = 7: Cr (B₁ 65) 121 Iso

8c, n = 8: Cr (B₁ 95) 117 Iso

8d, n = 9: Cr (B₁ 86) 100 Iso

8e, n = 10: Cr (N 87) 97 Iso

9a, n = 6: Cr **46 B₁ 105 Iso**

9b, n = 7: Cr (B₁ 65) 106 Iso

9c, n = 8: Cr 75 B₁ 94 Iso

9d, n = 9: Cr (B₁ 45) 90 Iso

9e, n = 10: Cr 71 B_x 90 Iso

The mesophase appearance was identified mainly as mosaic textures of the banana B₁ phase that precedes the focal conic domains from isotropic melt on cooling (**Figure 6a**) for compounds **8a–8d**, while the increase of the terminal chain to 10 carbon atoms favors the formation of the nematic phase.

In contrast to compounds **8a–8e**, the presence of the carbonyloxy linkage in compounds **9a–9e** stabilizes the mesophase mostly into enantiotropic behavior, with typical cylindrical focal conic domains that succeed the nematic phase on cooling. In the case of compound **9d**, the coexistence of a fingerprint-like texture and a focal pseudo-isotropic region (black) was observed on cooling (**Figure 6b**). It was noted that the liquid crystalline behavior and transition temperatures follow the odd-even effect in accordance with the number of carbon atoms in the terminal alkyl chain, the most stable mesophases being evidenced by compounds with an even number of carbon atoms.

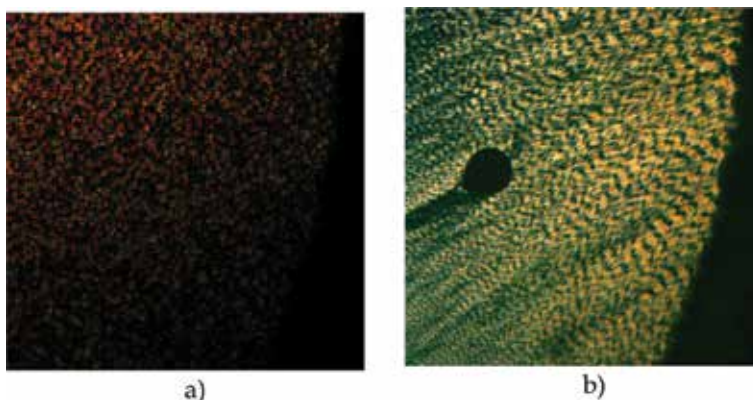
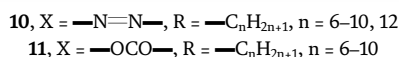
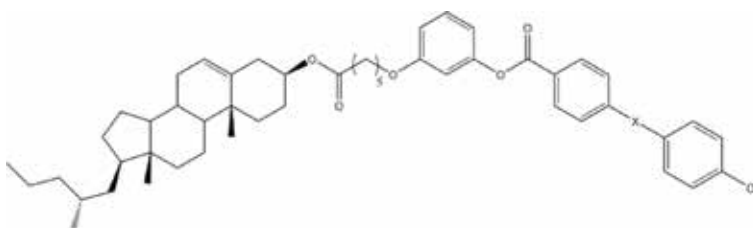


Figure 6.
 Optical micrographs of mesophases: (a) **8b**, 65°C; cooling and (b) **9d**, 43°C, cooling.

When benzyl unit in compounds **8** and **9** is replaced by a cholesteryl moiety linked by a pentamethylene flexible spacer to resorcinol (compounds **10** and **11**), the liquid crystalline behavior changed significantly [46].



10a, n = 6: Cr 59 Sm 146 Iso
10b, n = 7: Cr 83 Sm 142 Iso
10c, n = 8: Cr 77 Sm 133 Iso
10d, n = 9: Cr 78 Sm 133 Iso
10e, n = 10: Cr 80 Sm 122 Iso
10f, n = 12: Cr 82 Sm 97 Iso

11a, n = 6: Cr₁ 33 Cr₂ 52 Cr₃ 91 Sm
109 Sm 115 Iso
11b, n = 7: Cr₁ 50 Cr₂ 70 Cr₃ 87 Sm 102
 Sm 109 Iso
11c, n = 8: Cr₁ 78 Cr₂ 91 Sm 102 Sm
 110 Iso
11d, n = 9: Cr₁ 20 Cr₂ 41 Cr₃ 90 Sm 99
 Sm 107 Iso
11e, n = 10: Cr₁ 21 Cr₂ 45 Cr₃ 80 Sm 85
 Sm 100 Iso

In the case of compounds **10a–10f**, containing azo linkage between the aromatic cycles, only smectic-type textures were observed, the most stable interval of the mesophase being observed for compound **10a**, with the shorter flexible terminal chain (n = 6). Because of strong polar interactions, all compounds presented high viscosity and crystallized very slowly below room temperature. Compared with compounds **10a–10e**, compounds **11a–11e** presented a rich polymorphism on heating with crystalline-crystalline or liquid crystalline-liquid crystalline transitions, on a narrow range of mesophases. However, neither characteristic cholesteric textures were observed as was the case for compounds with azo linkage in the structure; only smectic phases have been observed (**Figure 7a,b**). As for previous compounds **10a–10e**, on cooling, compounds **11a–11e** presented mesophases much below room temperature.

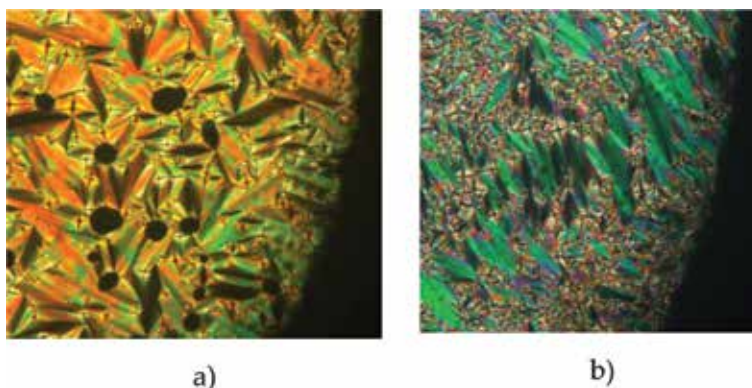
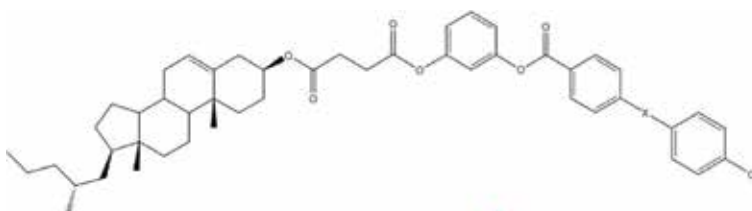


Figure 7.
Optical micrographs of mesophases: (a) **10d**, 115°C, heating and (b) **11c**, 71°C, cooling.

Compounds **12** and **13** were obtained when the flexible spacer between resorcinol and cholesteryl unit in compounds **10** and **11** was changed to a succinate one [47].



12, X = —N=N—, R = —C_nH_{2n+1}, n = 6–10, 12

13, X = —OCO—, R = —C_nH_{2n+1}, n = 6–10

12a, n = 6: Cr 105 Sm 155 Iso

12b, n = 7: Cr₁ 65 Cr₂ 95 Sm 104 Sm 147 Iso

12c, n = 8: Cr₁ 16 Cr₂ 102 Sm 109 Sm 134 Iso

12d, n = 9: Cr₁ 80 Cr₂ 113 Sm 134 Iso

12e, n = 10: Cr₁ 87 Cr₂ 118 Sm 128 Sm 139 Iso

12f, n = 12: Cr 106 Sm 111 Sm 131 Iso

13a, n = 6: Cr (Sm 71) 157 Iso

13b, n = 7: Cr (Sm 91) 139 Iso

13c, n = 8: Cr (Chol 86) 91 Iso

13d, n = 9: Cr (Chol 76) 93 Iso

13e, n = 10: Cr (Chol 99) 101 Iso

Compounds of type **12** presented wider mesophase domains on heating and cooling (compared with compounds of type **10**), suggesting better interactions when the flexible chain inside one arm is shorter.

While compounds **12a–e** showed enantiotropic behavior with smectic-type textures, when switching the azo unit with an ester the mesophases are destabilized, with compounds **13a–e** presenting only monotropic behavior. Whereas the first two compounds, **13a** and **13b**, showed smectic phases, the next homologous compound presented cholesteric phases.

2.2.2. 1,3-Diaminobenzene central core

Symmetric derivatives **14a–14d** presented focal-conic and fan-shaped textures, which are characteristic of the banana B₆ phase (**Figure 8**) (compound **14e** (n = 10) is non mesomorphic) [48]. The mesophase stability ranges decrease with the number of the carbon atoms in the alkyl chain, and the variation of transition temperature follows the odd/even effect, derivatives with an even number of carbon atoms present a larger domain of mesophase.

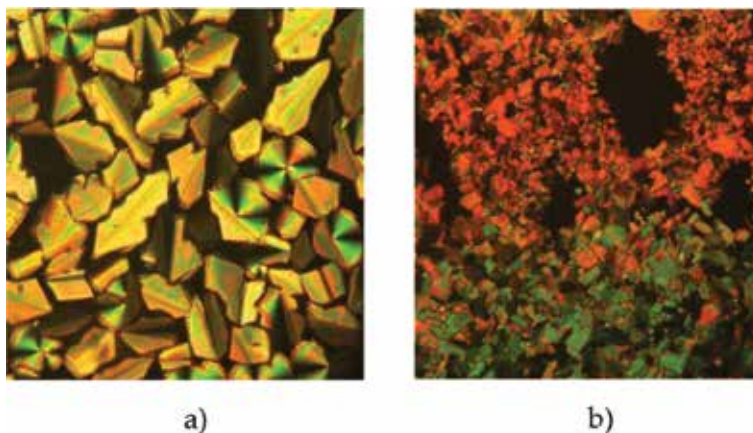
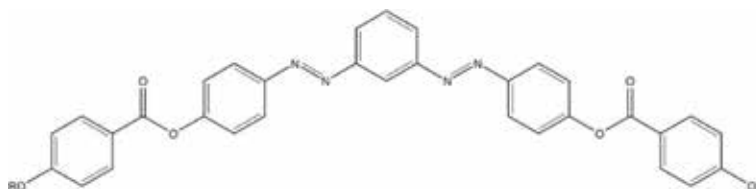


Figure 8.
 Optical micrographs of mesophases: (a) **14c**, 151°C cooling and (b) **18c**, 151°C cooling.



14, R = $-\text{C}_n\text{H}_{2n+1}$, n = 6–10

14a, n = 6: Cr 141 B₆ 171 Iso

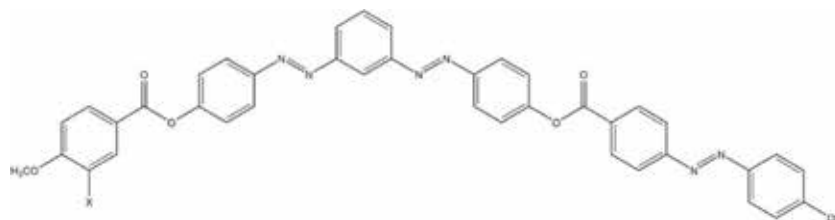
14b, n = 7: Cr 148 B₆ 158 Iso

14c, n = 8: Cr 135 B₆ 155 Iso

14d, n = 9: Cr 140 B₆ 148 Iso

14e, n = 10: Cr 141 Iso

The liquid crystalline properties of asymmetric bent-core derivatives **15** and **16** depend on the nature of the X substituent [49]. Thus, for X = -H, compounds **15a–15e** showed an enantiotropic behavior with fan-shaped texture characteristic of the banana B₆ phase while replacement of hydrogen atom with $-\text{Br}$ decreased the mesophase stability, so compounds **16a–16d** presented only monotropic behavior with narrow intervals of mesophases.



15, X = $-\text{H}$, R = $-\text{C}_n\text{H}_{2n+1}$, n = 6–10

16, X = $-\text{Br}$, R = $-\text{C}_n\text{H}_{2n+1}$, n = 6–10

15a, n = 6: Cr₁ 113 Cr₂ 156 B₆ 183 Iso

15b, n = 7: Cr₁ 125 Cr₂ 146 B₆ 205 Iso

15c, n = 8: Cr₁ 131 Cr₂ 158 B₆ 181 Iso

15d, n = 9: Cr₁ 133 B₆ 159 Iso

15e, n = 10: Cr₁ 128 B₆ 142 Iso

16a, n = 6: Cr (166) B₆ 175 Iso

16b, n = 7: Cr (179) B₆ 172 Iso

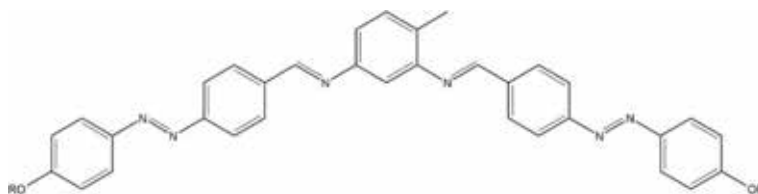
16c, n = 8: Cr (166) B₆ 176 Iso

16d, n = 9: Cr (159) B₆ 166 Iso

16e, n = 10: Cr 168 Iso

Compounds of type **17** and **18** were obtained by condensing 4-methylbenzene-1,3-diamine with 4'-alkyloxy-4-formylazobenzene and 4'-acyloxy-4-formylazobenzene, respectively [50].

Compounds with alkyloxy terminal flexible chain (compounds **17a–17f**) evidenced nematic phases on heating and smectic textures on cooling. Introduction of an acyl group as terminal chain (compounds **18a–18f**) has as result the slight increase of the transition temperatures but a decrease of meso-phase stability, such that only compounds **18c–18f** showed mesomorphic behavior.



17, R = $-\text{C}_n\text{H}_{2n+1}$, n = 6–10, **18**
18, R = $-\text{COC}_n\text{H}_{2n+1}$, n = 5–9, **17**

17a, n = 6: Cr 154 N 172 Iso

17b, n = 7: Cr 158 N 164 Iso

17c, n = 8: Cr₁ 72 Cr₂ 155 N 160 Iso

17d, n = 9: Cr₁ 112 Cr₂ 145 N 164 Iso

17e, n = 10: Cr 155 N 165 Iso

17f, n = 18: Cr 120 N 137 Iso

18a, n = 5: Cr₁ 146 Cr₂ 177 Iso

18b, n = 6: Cr₁ 128 Cr₂ 172 Iso

18c, n = 7: Cr₁ 135 Cr₂ 158 Sm 166 Iso

18d, n = 8: Cr₁ 123 Cr₂ 151 Sm 159 Iso

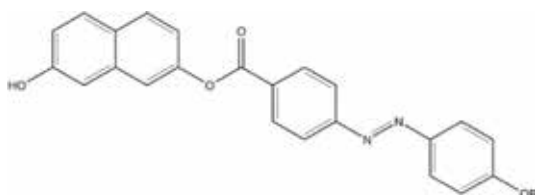
18e, n = 9: Cr₁ 122 Cr₂ 147 Sm 156 Iso

18f, n = 17: Cr 128 Sm 150 Iso

However, the optical microscope observations revealed focal-conic or fan-like textures for compounds **18c–18f** on cooling, characteristic of the banana B₂ phase, with striations across individual fans which on further cooling transform into mosaic textures (**Figure 8**).

2.3. Bent-core compounds based on 2,7-dihydroxynaphthalene core

The presence of a naphthalene unit in banana-shaped compounds is characterized by increased temperature transitions, compared to previous compounds with a benzene central core. Hence, the nematic mesophase domains of compounds **19a–19e** are situated between 175 and 214°C. The nematic phases were identified by characteristic Schlieren textures and nematic droplets or ribbon-like textures [51].



19, R = $-\text{C}_n\text{H}_{2n+1}$, n = 6–10

19a, n = 6: Cr 190 N 214 Iso

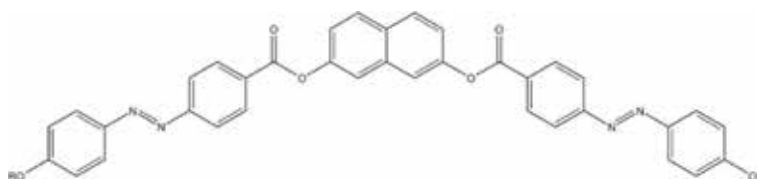
19b, n = 6: Cr 178 N 190 Iso

19c, n = 6: Cr 183 N 198 Iso

19d, n = 6: Cr 177 N 197 Iso

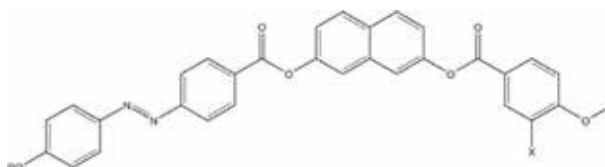
19e, n = 6: Cr 175 N 196 Iso

The symmetric disubstitution of compounds of type **19** gave compounds of type **20**, which are non mesomorphic [51].



20, R = $-\text{C}_n\text{H}_{2n+1}$, n = 6–10

The asymmetric disubstituted compounds **21** and **22** that differ only by X substituent showed similar monotropic behavior, mainly with nematic textures [52].



21, X = -H, R = $-\text{C}_n\text{H}_{2n+1}$, n = 6–10

22, X = -Br, R = $-\text{C}_n\text{H}_{2n+1}$, n = 6–10

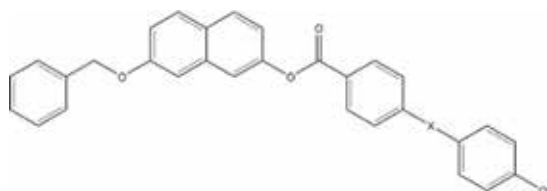
21a, n = 6: Cr (N 137) 140 Iso
 21b, n = 7: Cr (N 130) 133 Iso
 21c, n = 8: Cr (N 135) 140 Iso
 21d, n = 9: Cr (N 146) 150 Iso
 21e, n = 10: Cr (N 142) 146 Iso

22a, n = 6: Cr (N 99) 149 Iso
 22b, n = 7: Cr (N 108) 159 Iso
 22c, n = 8: Cr (N 109) 147 Iso
 22d, n = 9: Cr (B₆ 106) 129 Iso
 22e, n = 10: Cr 130 N 146 Iso

If compared with previous naphthalene derivatives, transition temperatures were relatively low, something higher in brominated derivatives **22a–22e**. While the mesophase ranges on cooling for compounds **21a–21e** are larger, the mesophase domains of derivatives **22a–22e** are much narrower, proving the destabilizing effect of the bulky bromine atom.

Anyway, compound **22e** showed enantiotropic behavior, meaning that a length of 10 carbon atoms on the alkyl terminal chain compensated the negative effect of bromine and stabilized the liquid crystalline character. Only the last two compounds of this series showed fan-shaped textures of banana B₆ growing from the isotropic melt on cooling.

The introduction of benzyl unit to compounds **19a–19e** led to compounds **23a–23e**, where only the last three compounds of the series showed enantiotropic behavior [53]. It was noted that though the melting and isotropization transition temperatures were lower, considering the hydrogen bonding interaction in compounds **19a–19e**, but at the same time, the mesophase domains were larger, up to 35°C in compound **23e**.



23, X = $-\text{N}=\text{N}-$, R = $-\text{C}_n\text{H}_{2n+1}$, n = 6–10

24, X = $-\text{OCO}-$, R = $-\text{C}_n\text{H}_{2n+1}$, n = 6–10

23a, n = 6: Cr (B₁ 126) 155 Iso
 23b, n = 7: Cr (N 118) 143 Iso
 23c, n = 8: Cr₁ 107 Cr₂ 120 N 150 Iso
 23d, n = 9: Cr 110 N 137 Iso
 23e, n = 10: Cr 113 N 148 Iso

24a, n = 6: Cr 122 B₁ 144 Iso
 24b, n = 7: Cr₁ 109 Cr₂ 116 B₁ 129 Iso
 24c, n = 8: Cr 127 B₁ 148 Iso
 24d, n = 9: Cr (B₁ 108) 146 Iso
 24e, n = 10: Cr (B₁ 108) 136 Iso

Comparing this series with compounds **8a–8e**, where the central core derived from resorcinol, the favorable effect of naphthalene as central core was observed, since compounds **8a–8e** showed only a monotropic behavior.

Changing the azo linkage in compounds **23a–23e** with ester results in compounds **24a–24e**, where only the first three homologous compounds, with shorter alkyl chains, presented enantiotropic behavior [53]. The presence of ester linkage increases the transition temperatures but decreases the mesophase range, if one considers compound **24c** (21°C), compared with **23c** (30°C).

3. Conclusions

We have presented here, in brief, a part of the work carried out by our group over a period of 16 years, from the standpoint of relationship between the structure and mesomorphic properties on some banana-shaped compounds. Our purpose was to investigate a variety of new compounds in order to design bent-shaped liquid crystals with large mesophase intervals at low transition temperatures, which might expand the field of electro-optical applications. It was found that the mesomorphic behavior depends upon the type of the bent unit, the number of aromatic units in the calamitic substituents, the nature of the linkages, the lateral substitution, and the length as well as the type of the terminal flexible chains. Hence, biaxial nematic, smectic, and cholesteric banana phases as well as less conventional mesophases were identified. The use of resorcinol as central bent unit had proved to be very useful in inducing various mesophases, with some transitions being evidenced even at low temperatures. Derivatives with the smallest length of terminal chains (especially $n = 6$) presented the widest mesophase interval. In terms of symmetrical derivatives, while the presence only of two aromatic cycles on each arm was not enough to stabilize or to induce the mesophase, the introduction of a third aromatic cycle has substantially improved the liquid crystalline properties. In asymmetrical derivatives, the presence of ester and azo linkages between aromatic rings influenced better the mesophase behavior or stability, compared with the situation when only ester linkages were present, except for derivatives with benzyl unit on the shorter arm. Moreover, the introduction of a cholesteryl hexanoate moiety on the second asymmetric arm led to mesophase transitions much below room temperature. In 1,3-diaminobenzene derivatives, the presence of bromine atom as lateral substituent on a calamitic arm destabilized or suppressed the mesophase. However, compared with resorcinol symmetrical derivatives with two aromatic cycles on each arm, just switching the places of ester and azo linkages between cycles had a better influence on liquid crystalline properties. Of the oxadiazole compounds, the hockey-stick derivatives showed the widest nematic ranges, particularly for the homologous compound with smallest number of carbon atoms in the terminal chain ($n = 6$). In symmetrical derivatives, the presence of three aromatic cycles on each arm and of acyloxy linkage on terminal chain induced better interactions and favorable packing, especially for compounds with higher number of carbon atoms in terminal flexible chain ($n = 9–11$), but increased too much the isotropization temperatures up to the beginning of the degradation processes. The presence of 2,7-disubstituted naphthalene as central core in bent-core compounds mainly destabilized the mesophases, compared with 1,3-disubstituted benzene derivatives.

Overall, considering the high impact of liquid crystal displays in everyday life and the multiple possibilities that bent-core compounds offer to vary the properties of materials, it is expected that the present study will contribute to future research directions, hopefully not only in fundamental or theoretical research but also in practical applications.

Conflict of interest

No potential conflict of interest was reported by the authors.

Author details

Dan Scutaru¹, Irina Carlescu^{1*}, Elena-Raluca Bulai (Cioanca)^{1,2},
Catalina Ionica Ciobanu^{1,3}, Gabriela Lisa¹ and Nicolae Hurduc¹


1 “Cristofor Simionescu” Faculty of Chemical Engineering and Environmental Protection, “Gheorghe Asachi” Technical University of Iasi, Iasi, Romania

2 “Stefan cel Mare” University of Suceava, Suceava, Romania

3 Research Department, Faculty of Chemistry, “Al. I. Cuza” University, Iasi, Romania

*Address all correspondence to: icarlescu@ch.tuiasi.ro

IntechOpen

© 2018 The Author(s). Licensee IntechOpen. This chapter is distributed under the terms of the Creative Commons Attribution License (<http://creativecommons.org/licenses/by/3.0>), which permits unrestricted use, distribution, and reproduction in any medium, provided the original work is properly cited. 

References

- [1] Bremer M, Kirsch P, Klasen-Memmer M, Tarumi K. The TV in your pocket: Development of liquid-crystal materials for the new millennium. *Angewandte Chemie (International Ed. in English)*. 2013;**52**(34):8880-8896. DOI: 10.1002/anie.201300903
- [2] Kato T, Uchida J, Ichikawa T, Sakamoto T. Functional liquid crystals towards the next generation of materials. *Angewandte Chemie (International Ed. in English)*. 2018;**57**(16):4355-4371. DOI: 10.1002/anie.201711163
- [3] Acharya BR, Primak A, Kumar S. Biaxial nematic phase in bent-core thermotropic mesogen. *Physical Review Letters*. 2004;**92**(14):145506. DOI: 10.1103/PhysRevLett.92.145506
- [4] Jakli A. Liquid crystals of the twenty-first century—nematic phase of bent-core molecules. *Liquid Crystals*. 2013;**1**(1):65-82. DOI: 10.1080/21680396.2013.803701
- [5] Gleeson HF, Kaur S, Gortz V, Belaissaoui A, Cowling S, Goodby JW. The nematic phases of bent-core liquid crystals. *ChemPhysChem*. 2014;**15**(7):1251-1260. DOI: 10.1002/cphc.201400014
- [6] Buka A, Eber N, Fodor-Csorba K, Jakli A, Salamon P. Physical properties of a bent-core nematic liquid crystal and its mixtures with calamitic molecules. *Phase Transitions*. 2015;**85**(10):872-887. DOI: 10.1080/01411594.2012.689834
- [7] Khan RK, Turlapati S, Rao NVS, Ghosh S. Elastic and dielectric properties of ferroelectric nanoparticles/bent-core nematic liquid crystal blend. *European Physical Journal E: Soft Matter and Biological Physics*. 2017;**40**(9):75. DOI: 10.1140/epje/i2017-11564-x
- [8] Barche J, Janietz S, Ahles M, Schmechel R, von Seggern H. Cross-linked liquid-crystalline materials—A possible strategy to ordered organic semiconductors. *Chemistry of Materials*. 2004;**16**(22):4286-4291. DOI: 10.1021/cm049352l
- [9] Pelzl G, Diele S, Weissflog W. Banana-shaped compounds—A new field of liquid crystals. *Advanced Materials*. 1999;**11**(9):707-724. DOI: 10.1002/(SICI)1521-4095(199906)11:9<707::AID-ADMA707>3.3.CO;2-4
- [10] Marx VM, Girgis H, Heiney PA, Hegmann T. Bent-core liquid crystal (LC) decorated gold nanoclusters: Synthesis, self-assembly, and effects in mixtures with bent-core LC hosts. *Journal of Materials Chemistry*. 2008;**18**(25):2983-2994. DOI: 10.1039/b802554a
- [11] Etxebarria J, Ros MB. Bent-core liquid crystals in the route to functional materials. *Journal of Materials Chemistry*. 2008;**18**(25):2919-2926. DOI: 10.1039/b803507e
- [12] Alaasar M, Prehm M, Poppe S, Tschierske C. Development of polar order by liquid-crystal self-assembly of weakly bent molecules. *Chemistry – A European Journal*. 2017;**23**(23):5541-5556. DOI: 10.1002/chem.201606035
- [13] Alaasar M. Azobenzene-containing bent-core liquid crystals: An overview. *Liquid Crystals*. 2016;**43**(13-15):2208-2243. DOI: 10.1080/02678292.2016.1175676
- [14] Alaasar M, Prehm M, Tschierske C. Mirror symmetry breaking in fluorinated bent-core mesogens. *RSC Advances*. 2016;**6**(86):82890-82899. DOI: 10.1039/c6ra18482k
- [15] Kohout M, Alaasar M, Poryvai A, Novotna V, Poppe S, Tschierske C,

- et al. Photosensitive bent-core liquid crystals based on methyl substituted 3-hydroxybenzoic acid. *RSC Advances*. 2017;7(57):35805-35813. DOI: 10.1039/c7ra05632j
- [16] Srinivasa HT. New symmetric azobenzene molecules of varied central cores: Synthesis and characterisation for liquid crystalline properties. *Liquid Crystals*. 2017;44(9):1384-1393. DOI: 10.1080/02678292.2017.1280620
- [17] Khan RK, Turlapati S, Begum N, Mohiuddin G, Rao NVS, Ghosh S. Impact of terminal polar substitution on elastic, electro-optic and dielectric properties of four-ring bent-core nematic liquid crystals. *RSC Advances*. 2018;8(21):11509-11516. DOI: 10.1039/c8ra00575c
- [18] Niori T, Sekine T, Watanabe J, Furukawa T, Takezoe H. Distinct ferroelectric smectic liquid crystals consisting of banana shaped achiral molecules. *Journal of Materials Chemistry*. 1996;6(7):1231-1233. DOI: 10.1039/jm9960601231
- [19] Tschierske C, Dantlgraber G. From antiferroelectricity to ferroelectricity in smectic mesophases formed by bent-core molecules. *Pramana*. 2003;61(2):455-481. DOI: 10.1007/BF02708325
- [20] Acharya BR, Primak A, Dingemans TJ, Samulski ET, Kumar S. The elusive thermotropic biaxial nematic phase in rigid bent-core molecules. *Pramana*. 2003;61(2):231-237. DOI: 10.1007/BF02708305
- [21] Acharya BR, Primak A, Kumar S. Biaxial nematic phase in bent-core thermotropic mesogens. *Physical Review Letters*. 2004;92(14):145506. DOI: 10.1103/PhysRevLett.92.145506
- [22] Kumar S, Gowda AN. The chemistry of bent-core molecules forming nematic liquid crystals. *Liquid Crystals*. 2015;3(2):99-145. DOI: 10.1080/21680396.2015.1061958
- [23] Shen D, Diele S, Pelzl G, Wirth I, Tschierske C. Designing banana-shaped liquid crystals without Schiff's base units: m-terphenyls, 2,6-diphenylpyridines and V-shaped tolane derivatives. *Journal of Materials Chemistry*. 1999;9(3):661-672. DOI: 10.1039/a808275h
- [24] Kang S, Saito Y, Watanabe N, Tokita M, Takanishi Y, Takezoe H, et al. Low-birefringent, chiral banana phase below calamitic nematic and/or smectic C phases in oxadiazole derivatives. *The Journal of Physical Chemistry. B*. 2006;110(11):5205-5214. DOI: 10.1021/jp057307a
- [25] Bedel JP, Rouillon JC, Marcerou JP, Laguerre M, Nguyen HT, Achard MF. Influence of fluoro substituents on the mesophase behaviour of banana-shaped molecules. *Journal of Materials Chemistry*. 2002;12(8):2214-2220. DOI: 10.1039/b201467j
- [26] Nguyen HT, Rouillon JC, Marcerou JP, Bedel JP, Barois P, Sarmiento S. Mesomorphic and electro-optical properties of new achiral banana-shaped molecule. *Molecular Crystals and Liquid Crystals*. 1999;328:177-184. DOI: 10.1080/10587259908026057
- [27] Sadashiva BK, Reddy AR, Pratibha R, Madhusudana NV. Biaxial smectic A liquid crystal in a pure compound. *Chemical Communications*. 2001;20:2140-2141. DOI: 10.1039/b106084h
- [28] Bedel JP, Rouillon JC, Marcerou JP, Laguerre M, Nguyen HT, Achard MF. New switchable smectic phases in banana-shaped compounds. *Liquid Crystals*. 2001;28(9):1285-1292. DOI: 10.1080/02678290110039949
- [29] Alaasar M, Prehm M, Tschierske C. New azobenzene containing

bent-core liquid crystals based on disubstituted resorcinol. *Liquid Crystals*. 2014;**41**(1):126-136. DOI: 10.1080/02678292.2013.840393

[30] Prasad V, Rao DSS, Prasad SK. A novel class of banana-shaped azo compounds exhibiting antiferroelectric switching behaviour. *Liquid Crystals*. 2001;**28**(4):643-646. DOI: 10.1080/02678290010020887

[31] Dunemann U, Schroder MW, Reddy RA, Pelzl G, Diele S, Weissflog W. The influence of lateral substituents on the mesophase behaviour of banana-shaped mesogens. Part II. *Journal of Materials Chemistry*. 2005;**15**(37):4051-4061. DOI: 10.1039/b507458d

[32] Weissflog W, Baumeister U. Laterally aryl-substituted bent-core mesogens. *Liquid Crystals*. 2013;**40**(7):959-967. DOI: 10.1080/02678292.2013.786797

[33] Jakli A, Lischka C, Weissflog W, Pezl G, Rauch S, Heppke G. Structural transitions of smectic phases formed by achiral bent-core molecules. *Ferroelectrics*. 2000;**243**(1-4):239-+. DOI: 10.1080/00150190008008025

[34] Ros MB, Serrano JL, de la Fuente MR, Folcia CL. Banana-shaped liquid crystals: A new field to explore. *Journal of Materials Chemistry*. 2005;**15**(48):5093-5098. DOI: 10.1039/b504384k

[35] Findeisen-Tandel S, Weissflog W, Baumeister U, Pelzl G, Murthy HNS, Yelamaggad CV. Laterally substituted symmetric and nonsymmetric salicylideneimine-based bent-core mesogens. *Beilstein Journal of Organic Chemistry*. 2012;**8**:129-154. DOI: 10.3762/bjoc.8.15

[36] Fleischmann EK, Zentel R. Liquid-crystalline ordering as a concept in materials science: From semiconductors to stimuli-responsive devices.

Angewandte Chemie, International Edition. 2013;**52**(34):8810-8827. DOI: 10.1002/anie.201300371

[37] Tschierske C. Development of structural complexity by liquid-crystal self-assembly. *Angewandte Chemie, International Edition*. 2013;**52**(34):8828-8878. DOI: 10.1002/anie.201300872

[38] Prasad V, Kang SW, Suresh KA, Joshi L, Wang QB, Kumar S. Thermotropic uniaxial and biaxial nematic and smectic phases in bent-core mesogens. *Journal of the American Chemical Society*. 2005;**127**(49):17224-17227. DOI: 10.1021/ja052769n

[39] Bulai ER, Carlescu I, Scutaru D. Synthesis and characterisation of liquid crystalline compounds based on symmetric 1, 3, 4 oxadiazole core. *Revista de Chimie*. 2015;**66**(4):439-443

[40] Cioanca ER, Carlescu I, Wilson D, Scutaru D. Liquid crystalline schiff bases containing a 2, 5-(p-aminophenyl)-[1, 3, 4]oxadiazole bent core. *Revista de Chimie*. 2010;**61**(12):1158-1163

[41] Lisa G, Cioanca ER, Tudorachi N, Carlescu I, Scutaru D. Thermal degradation of some [1, 3, 4]oxadiazole derivatives with liquid crystalline properties. *Thermochemica Acta*. 2011;**524**(1-2):179-185. DOI: 10.1016/j.tca.2011.07.01

[42] Cioanca ER, Epure EL, Carlescu I, Lisa G, Wilson D, Hurduc N, et al. Hockey stick liquid crystals based on a 2, 5-asymmetric disubstituted [1, 3, 4] oxadiazole core. *Molecular Crystals and Liquid Crystals*. 2011;**537**:51-63. DOI: 10.1080/15421406.2011.556444

[43] Ciobanu CI, Drochioiu G, Carlescu I, Lisa G, Antoci V, Vasilache V, et al. Thermal behaviour of some bent-core resorcinol derivatives with azo-type spacers and variable flexible

- chain. *Letters in Organic Chemistry*. 2016;**13**(2):156-161. DOI: 10.2174/1570178612666150916010459
- [44] Ciobanu CI, Carlescu I, Lisa G, Scutaru D. Symmetric bent-core liquid crystals of some schiff bases containing azo linkage. *Croatica Chemica Acta*. 2014;**87**(1):7-16. DOI: 10.5562/cca2150
- [45] Simion A, Carlescu I, Lisa G, Scutaru D. Unsymmetrical bent-core liquid crystals based on resorcinol core. *Revista de Chimie*. 2016;**67**(3):446-450
- [46] Huzum CC, Carlescu I, Lisa G, Scutaru D. New cholesteryl containing bent core liquid crystals. *Journal of the Serbian Chemical Society*. 2013;**78**(5):669-680. DOI: 10.2298/JSC120810114H
- [47] Huzum CC, Carlescu I, Lisa G, Scutaru D. Nonsymmetric liquid crystalline cholesteric dimers derived from resorcinol. *Revista de Chimie*. 2013;**64**(1):60-67
- [48] Iuganu D, Carlescu I, Lisa G, Scutaru D. Symetric bent-core liquid crystals based on 1, 3-bis-(4'-hydroxyphenylazo) benzene core. *Revista de Chimie*. 2012;**63**(5):501-506
- [49] Iuganu D, Carlescu I, Lisa G, Scutaru D. Asymmetric bent-core liquid crystals based on 1, 3-bis-(4'-hydroxyphenylazo)benzene central core. *Studia Universitatis Babes-Bolyai Chemia*. 2011;**56**(4):63-74
- [50] Ciobanu C, Carlescu I, Lisa G, Scutaru D. Synthesis and mesomorphic properties of some bent-core schiff bases containing azo linkage. *Revista de Chimie*. 2013;**64**(3):249-253
- [51] Simion G, Carlescu I, Lisa G, Scutaru D. Synthesis and characterization of some liquid crystalline compounds based on a 2, 7-dihydroxynaphtalene core. *Revista de Chimie*. 2012;**63**(4):407-411
- [52] Simion G, Carlescu I, Lisa G, Scutaru D. Asymetric bent-core liquid crystals based on 2, 7-dihydroxynaphtalene core with an azo and esteric connecting groups. *Studia Universitatis Babes-Bolyai Chemia*. 2011;**56**(4):75-88
- [53] Simion A, Huzum CC, Carlescu I, Lisa G, Balan M, Scutaru D. Unsymmetrical banana-shaped liquid crystalline compounds derived from 2, 7-dihydroxynaphtalene. *Journal of the Serbian Chemical Society*. 2015;**80**(5):673-683. DOI: 10.2298/JSC140725126S

Binary Mixture Composed of Nematic Liquid Crystal and Carbon Nanotubes: A Theoretical Description

Vlad Popa-Nita and Robert Repnik

Abstract

Based on the phenomenological model first presented by van der Schoot et al., which predicts the alignment of carbon nanotube (CNT) dispersions in thermotropic nematic liquid crystals, we present the extensive results concerning the phase diagram and the orientational properties of the mixture in this chapter.

Keywords: liquid crystal, carbon nanotube, phase transition

1. Introduction

A method to obtain aligned CNTs (necessary for applications) is to disperse them into liquid crystals (LCs) [with their self-organization (long-range orientational order) and fluidity] [1–9]. The thermotropic [10–13] and the lyotropic LCs [14–17] have been used to align CNTs parallel as well as perpendicular to average direction of alignment of long axes of LC molecules called the director. As a consequence, the orientational order parameter of CNTs could have the values between 0.6 and 0.9. The study of mixture composed by LCs and CNTs is also important due to the influence of CNTs on the physical properties of LCs (increased dielectric anisotropy, decreased threshold voltage, much accelerated electrooptical response) [18–25].

The main hypothesis used in the theoretical study of the collective behavior of CNTs dispersed in the isotropic solvents [26–28] as well as in LCs [29–36] is that they can be considered as rigid rod polymers [37].

Using the density functional theory, the isotropic-liquid crystal phase transition has been analyzed considering the van der Waals attractive interactions [26]. Onsager theory of rigid rods [38] was used to study the phase behavior of CNTs dispersed into organic and aqueous solutions [27]. Also, the Onsager model including length polydispersity and solvent-mediated interaction was considered to study the dispersions of CNTs in superacids [28]. These theoretical studies lead to the conclusion that to obtain orientational order of CNTs at room temperature it is necessary that the van der Waals interactions must be screened out, i.e., the CNTs must be dispersed in a good solvent. In the case of a non-good solvent, no liquid crystalline phases of CNTs form at room temperature because only dilute solutions are thermodynamically stable.

Matsuyama [29, 30] used a mean field theory to analyze the phase behavior of a mixture composed of low-molecular-weight liquid crystal and a rigid rod-like polymer such as CNTs. The free energy is constructed on the basis of Onsager model for excluded volume interactions, the Maier-Saupe model for orientational-dependent attractive interactions, and the Flory-Huggins theory for binary mixtures.

In the previous papers [31, 32, 34–36], we have presented a phenomenological theory to describe the alignment of CNT dispersions in thermotropic nematic LCs. We combined the Landau-de Gennes [39, 40] free energy for thermotropic ordering of the LC solvent and the Doi free energy [41–43] for the lyotropic orientational order of CNTs. Because the CNT is much thinner than the elastic penetration length, the alignment of CNTs in the nematic solvent is caused by the coupling of the LC director field to the anisotropic interfacial tension of the CNTs. This is true only for very dilute solutions without large aggregates [33]. Density functional calculations [44] show that CNT alignment mechanism in LC is associated with a strong interaction due to surface anchoring with a binding energy of -2eV for $\pi - \pi$ electron stacking between LC molecules and CNT.

In the present chapter, we extend this model to generalize the anisotropic interaction form between a CNT and the liquid crystal molecules including the possibility of perpendicular alignment.

The remainder of this chapter is organized as follows. In Section 2, we describe the model. In Section 3, we illustrate the results and finally give the main conclusions in Section 4.

2. Model

The free energy density of the binary mixture composed of CNTs and thermotropic nematic LC contains three terms:

$$f = f_{CNT} + f_{LC} + f_{CNT/LC} \quad (1)$$

where f_{CNT} represents the Doi free energy density of CNTs, f_{LC} represents the Landau-de Gennes free energy density of the nematic liquid crystal order, and $f_{CNT/LC}$ takes into account the interaction of these two components.

2.1 Free energy of carbon nanotubes

At the mesoscopic level of description, the free energy of CNTs can be written in the following form [31]:

$$f_{CNT} = k_B T \left[\frac{1}{v_{LC}} (1 - \phi) \ln (1 - \phi) + \frac{1}{v_{CNT}} \phi \ln \phi \right] + k_B T \frac{L\phi^2}{6v_{CNT}} \left[\left(\frac{3}{L\phi} - 1 \right) S_{CNT}^2 - \frac{2}{3} S_{CNT}^3 + S_{CNT}^4 \right] \quad (2)$$

where the first two terms represent the entropy of isotropic mixing of CNTs and LC components [45] and the third one is obtained from the Onsager theory [38] using the Smoluchowski Equation [41, 42]. In this form, the van der Waals attractions between CNTs are neglected. The long-ranged intermolecular attractions between CNTs were considered in [36]. $v_{LC} \approx \pi l d^2 / 4$ represents the volume of one LC molecule with length $l \approx 3 \text{ nm}$ and diameter $d \approx 0.5 \text{ nm}$, and $v_{CNT} \approx \pi L_0 D^2 / 4$ is the volume of one CNT with length $L_0 \approx 400 \text{ nm}$ and diameter $D \approx 2 \text{ nm}$. The values cited

above are those used in this paper. In Eq. (2), k_B is the Boltzmann constant, T is the absolute temperature, ϕ represents the volume fraction of CNTs, $1 - \phi$ defines the volume fraction of the LC, and $L = L_0/D$ is the aspect ratio of a CNT.

Eq. (2) defines a first-order isotropic-nematic phase transition of CNTs with the equilibrium values of the order parameters $S_{CNT,iso} = 0$ and $S_{CNT,nem} = 0.3365$ and of the volume fractions, respectively, $\phi_{iso} = 0.01349$ and $\phi_{nem} = 0.01351$. These equilibrium values of the parameters are obtained minimizing the free energy (2) with respect to S_{CNT} and equating the chemical potentials of CNTs ($\mu_{CNT} = v_{CNT} [f_{CNT} + (1 - \phi)\partial f_{CNT}/\partial\phi]$) and of LC ($\mu_{LC} = v_{LC}(f_{CNT} - \phi\partial f_{CNT}/\partial\phi)$) in the two phases. The model predicts a relative variation of the volume fraction of CNTs (the Flory “chimney”) at the transition of 0.19%, while the prediction of Onsager and Flory [38, 46] for monodisperse lyotropic LC is about 1%, and the experimental results obtained by the polarized light microscopy for an aqueous dispersion of multiwall carbon nanotube indicate a biphasic region that range between 1 and 4% [47, 48]. The discrepancy is due to polydispersity, as well as the possibility of segregation which the model does not consider.

2.2 Free energy of thermotropic liquid crystal

To characterize the isotropic-nematic phase transition of thermotropic LC, we use the Landau-de Gennes [39] free energy:

$$f_{LC} = (1 - \phi) \left[\frac{3}{2} a (T - T^*) S_{LC}^2 - \frac{3}{4} B S_{LC}^3 + \frac{9}{4} C S_{LC}^4 \right] \quad (3)$$

where T^* is the undercooling limit temperature of stability of the isotropic phase and the constant coefficients a , B , and C depend on the material. Later, in our numerical calculations presented in Section 3, we consider the following values: $T^* = 307.55$ K, $a \approx 3.5 \cdot 10^4$ J · m⁻³ · K⁻¹, $B \approx 7.1 \cdot 10^5$ J · m⁻³, and $C \approx 4.3 \cdot 10^5$ J · m⁻³ [40, 49–51], values specific for pentylcyanobiphenyl (5CB). For this nematogen, the first-order isotropic-nematic phase transition takes place at temperature $T = T_{NI} = T^* + B^2/24aC = 308.95$ K with $S_{LC,iso} = 0$ and $S_{LC,nem} = B/6C = 0.2752$.

2.3 The coupling free energy

The condition of weak anchoring limit of the interaction between the two components is $D \ll \xi$, where the diameter of a CNT is $D \approx 2$ nm and $\xi = K/W \approx 10^{-5}$ m is the elastic penetration length ($K \approx 10^{-11}$ N is a typical elastic constant, and $W \approx 10^{-6}$ N/m is a typical anchoring energy).

The coupling free energy has been explained in [31], and it has the following form:

$$f_{CNT/LC} = -\gamma\phi S_{LC} S_{CNT} \left(1 - \frac{1}{2} S_{CNT} \right) \quad (4)$$

where $\gamma \equiv \frac{4}{3} W/D$ defines the coupling parameter. Thus, for the same anchoring energy, the coupling parameter in the case of thin rods is larger than that of the thick one. From the experimental results, we find that the value of the coupling parameter can be between $10^{-3} - 10^3$ N · m⁻². In the limit of large coupling $\gamma \rightarrow \infty$, the orientational order of CNTs is perfect $S_{CNT} \rightarrow 1$.

We note that positive values of γ characterize a parallel alignment of LC molecules to CNTs. In this chapter we extend our analysis considering also negative

values of γ which characterize a perpendicular alignment. Depending on the orientational order parameters S_{CNT} and S_{LC} , two nematic phases could be defined: (i) the N_1 phase with $S_{CNT} > 0$ and $S_{LC} > 0$ (parallel alignment of CNT and LC molecules) and (ii) the N_2 phase with $S_{CNT} < 0$ and $S_{LC} > 0$ (perpendicular alignment of CNT and LC molecules). These two phases are experimentally obtained depending on the surface treatment of the CNTs.

2.4 The total free energy density of the binary mixture

Finally, the total free energy density of the binary mixture (1) is the sum of the free energy densities of CNTs (2), thermotropic LC (3), and interaction between nematic CNTs and nematic LC (4):

$$\begin{aligned}
 f = & k_B T \left[\frac{1}{v_{LC}} (1 - \phi) \ln(1 - \phi) + \frac{1}{v_{CNT}} \phi \ln \phi \right] \\
 & + k_B T \frac{L\phi^2}{6v_{CNT}} \left[\left(\frac{3}{L\phi} - 1 \right) S_{CNT}^2 - \frac{2}{3} S_{CNT}^3 + S_{CNT}^4 \right] \\
 & + (1 - \phi) \left[\frac{3}{2} a(T - T^*) S_{LC}^2 - \frac{3}{4} B S_{LC}^3 + \frac{9}{4} C S_{LC}^4 \right] \\
 & - \gamma \phi S_{LC} S_{CNT} \left(1 - \frac{1}{2} S_{CNT} \right)
 \end{aligned} \tag{5}$$

3. Results

We present the main results concerning the phase behavior of the CNT-LC binary mixture as a function of temperature, volume fraction ϕ of CNTs, and coupling strength γ .

3.1 Positive γ : critical point of CNT phase transition

The positive value of the interaction parameter γ defines the nematic N_1 phase with $S_{CNT} > 0$ and $S_{LC} > 0$ (the rod and the LC molecules are parallel to each other). The isotropic phase of CNTs is transformed into a nematic phase with a small degree of order which is called paranematic phase (by analogy with the magnetism). The phase transition nematic-paranematic of the CNTs is first order for small values of the interaction parameter (so-called subcritical regime of CNTs). For large values of γ , the phase transition of CNTs becomes continuous. The critical point is given by the equations $\partial f / \partial S_{CNT} = \partial^2 f / \partial S_{CNT}^2 = \partial^3 f / \partial S_{CNT}^3 = 0$, giving $S_{CNT,c} = 1/6$ and the effective volume fraction $(L\phi)_c = 2.592$, while the critical value of the interaction parameter is given by the equation:

$$\gamma_c = \frac{k_B T}{125 v_{CNT} S_{LC,c}}. \tag{6}$$

The dependence of γ_c as a function of temperature is shown in **Figure 1**.

In the nematic phase of the liquid crystal, the critical interaction parameter is relatively small (because $S_{LC,c}$ has relatively large values between 0.28 and 0.8), while in the isotropic phase of the liquid crystal, the value of the order parameter is very small ($\simeq 10^{-4}$), and the values of γ_c are relatively large. As a consequence there is a jump of γ_c at T_{NI} .

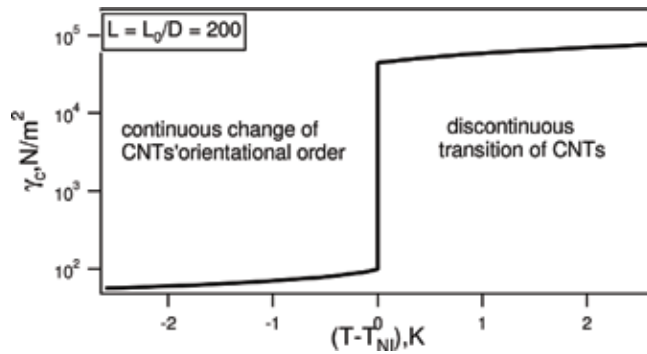


Figure 1.
 The critical value of the coupling parameter γ_c as a function of temperature.

The dependence of γ_c on the lengths of CNTs for a fixed value of the temperature is shown in **Figure 2** (we mention that for the value of the temperature shown ($T - T_{NI} = -1.4K$) the LC is in the nematic phase). The critical value of the coupling parameter decreases when the length of CNTs increase, meaning that the continuous paranematic-nematic transition of CNTs is favored.

In **Figure 3** the volume fractions of CNTs at the transition as a function of the coupling parameter for a fixed value of the temperature are shown. For negative values of γ (region I in the figure, perpendicular alignment), the volume fraction

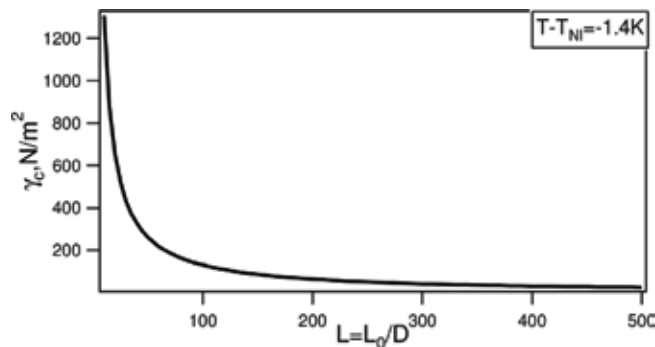


Figure 2.
 The critical value of the coupling parameter γ_c as a function of the lengths of CNTs for a fixed temperature in the nematic region of the liquid crystal.

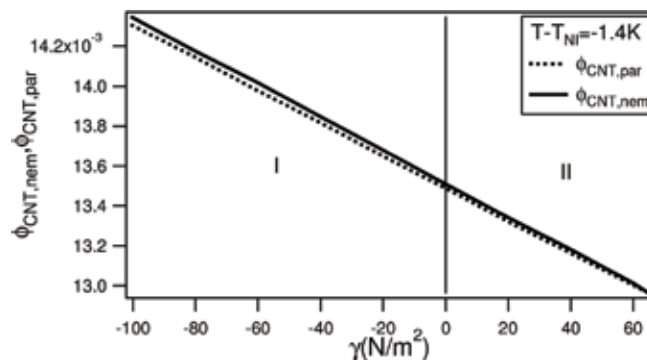


Figure 3.
 The volume fractions of CNTs at the transition as a function of coupling parameter for a fixed value of temperature in the nematic region of LC.

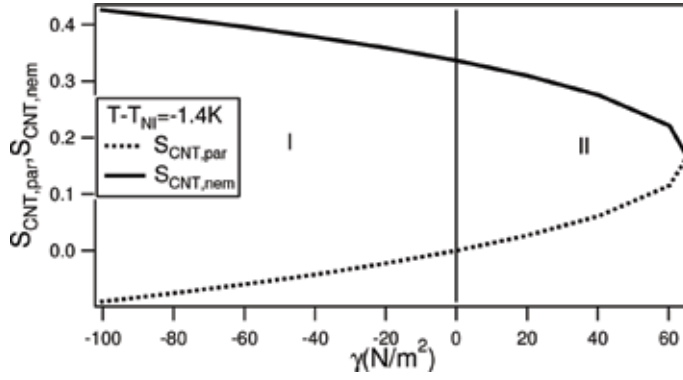


Figure 4.

The order parameter of the two phases of CNTs at the transition as a function of the coupling parameter for a fixed value of the temperature in the nematic region of LC.

gap of CNTs remains practically constant, while for positive values (region II in the figure, parallel alignment), the volume fraction gap decreases with increasing γ until it cancels for critical value γ_c .

The CNT order parameters at the transition as a function of the coupling parameter for a fixed value of the temperature are plotted in **Figure 4**. For negative values of the coupling parameter (the region I in the figure), the first-order phase transition of CNTs takes place between a paranematic phase with a negative order parameter (perpendicular alignment) and a nematic phase with a positive order parameter (parallel alignment). For positive values of γ (region II in the figure), the transition takes place between a paranematic phase and a nematic phase, both with positive order parameters (parallel alignment). If the coupling increases the degrees of alignment of the two phases become smaller until the critical value of the coupling parameter when they are identical.

3.2 Phase diagram

The equilibrium phase diagram can be obtained by minimizing the free energy with respect to S_{CNT} and S_{LC} :

$$\frac{\partial f}{\partial S_{CNT}} = \frac{\partial f}{\partial S_{LC}} = 0 \quad (7)$$

and equating the chemical potentials of CNTs and LC in the two phases. The chemical potentials are given by

$$\begin{aligned} \mu_{CNT} &= v_{CNT} \left[f + (1 - \phi) \frac{\partial f}{\partial \phi} \right] \\ \mu_{LC} &= v_{LC} \left(f - \phi \frac{\partial f}{\partial \phi} \right) \end{aligned} \quad (8)$$

where the free energy density is given by Eq. (5).

3.2.1 Positive coupling constant

A positive coupling parameter corresponds to a paranematic ($S_{CNT,par}$ very small and positive) and nematic ($S_{CNT,nem}$ large and positive) phase transition of CNTs. The corresponding $T(\phi)$ phase diagram is shown in **Figure 5**, where the

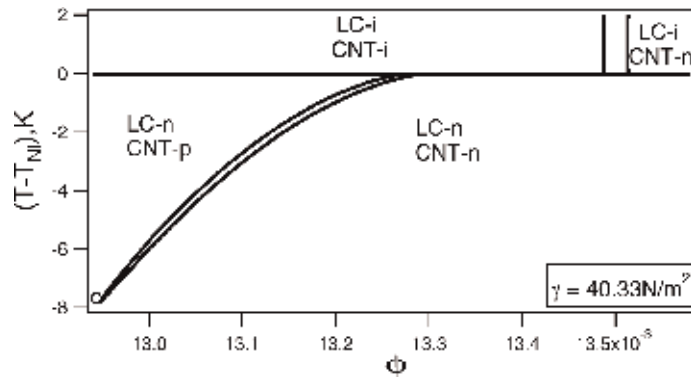


Figure 5. The $T(\phi)$ phase diagram for a constant positive coupling parameter. The horizontal line shows the isotropic-nematic phase transition of LC.

smaller case letters i, p, and n stand for isotropic, paranematic (parallel alignment), and nematic phases, respectively.

For $T < T_{NI}$, LC is in the nematic phase, and the paranematic-nematic phase transition of CNTs is first order. With decreasing temperature, the bi-phase region (the Flory “chimney” [45]) becomes smaller and cancels at the critical point (for the value $\gamma = 40.33 \text{ N/m}^2$, the critical temperature is given by $T_c - T_{NI} = -7.84 \text{ K}$). On the contrary, for $T > T_{NI}$, LC is in the isotropic phase. The isotropic-nematic phase transition of CNTs is first order with a constant Flory “chimney” that does not depend on temperature (because $S_{LC} = 0, f_{LC} = f_{CNT/LC} = 0$, and the problem is equivalent with the dispersion of CNTs in an isotropic solvent). The triple points are the intersection points between the CNT phase transition equilibrium curves and LC phase transition equilibrium curve (the horizontal lines).

To see in more detail the orientational order of the two components, in **Figure 6**, we have plotted the order parameter profiles S_{LC} and S_{CNT} along the binodal lines as a function of temperature.

The transition between the isotropic and nematic phases of LC is first order (see **Figure 6a**), and the values of the LC order parameter depend only on temperature and are not influenced by CNT phase transition (because of $v_{CNT} \gg v_{LC}$, the concentration of LC component is much larger than for CNTs). But each particle contributes with $k_B T$ to the free energy, so that the free energy of LC is significantly larger than that of CNTs. The order parameters of CNTs as functions of temperature are shown in **Figure 6b**. Lowering the temperature, the jump of the order parameters cancels at the critical temperature. In the isotropic phase of LC ($T > T_{NI}$), the jump of the CNT order parameter remains constant independent on temperature (see the discussion of the results plotted in **Figure 5**).

3.2.2 Negative coupling constant

The negative coupling parameter corresponds to a paranematic ($S_{CNT,par}$ very small and negative) and nematic ($S_{CNT,nem}$ large and positive) phase transition of CNTs. The corresponding $T(\phi)$ phase diagram is shown in **Figure 7**, where the smaller case letters i, p, and n stand for isotropic, paranematic (perpendicular alignment), and nematic phases, respectively.

For $T < T_{NI}$, LC is in the nematic phase, and the paranematic (perpendicular)-nematic (parallel) phase transition of CNTs is first order. Contrary to the positive coupling parameter, here with decreasing temperature, the bi-phase region (the Flory “chimney” [45]) becomes larger. For $T > T_{NI}$, the characteristic of the phase

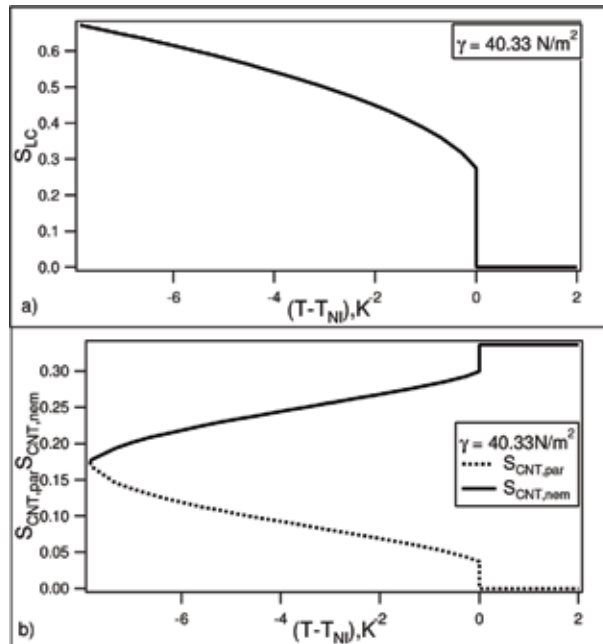


Figure 6. The order parameters along the binodal lines for a constant positive coupling parameter. (a) The LC order parameter and (b) the CNT order parameters.

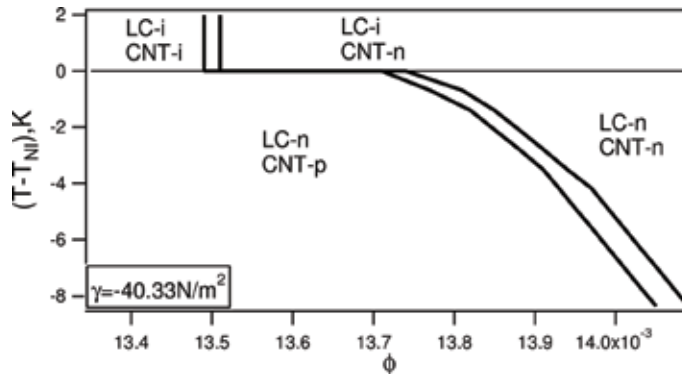


Figure 7. The $T(\phi)$ phase diagram for a constant negative coupling parameter. The horizontal line shows the isotropic-nematic phase transition of LC.

diagram remains the same; because LC is in the isotropic phase, the isotropic-nematic phase transition of CNTs is first order with a constant Flory “chimney” that does not depend on temperature.

The order parameter profiles S_{LC} and S_{CNT} along the binodal lines as a function of temperature are plotted in **Figure 8**.

Again the transition between the isotropic and nematic phases of LC is first order (see **Figure 8a**), and the values of the LC order parameter depend only on temperature. The behavior of CNT orientational order with temperature is shown in **Figure 8b**. In the nematic phase of LC ($T < T_{NI}$), the CNT jump of the order parameters at transition slowly decreases with increasing temperature, while in the isotropic phase of LC ($T > T_{NI}$), the jump of the CNT order parameter remains constant independent on temperature.

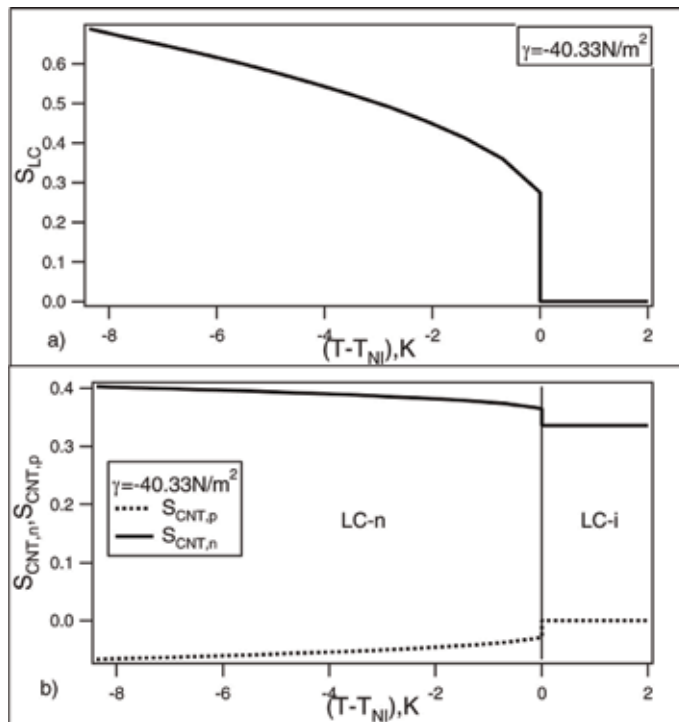


Figure 8. The order parameters along the binodal lines for a constant negative coupling parameter. (a) The LC order parameter and (b) the CNT order parameters.

4. Conclusions

In the present chapter, we have extended the previous mesoscopic phenomenological model [31, 32, 34–36] (used to describe the phase behavior of a binary mixture composed of CNTs and thermotropic nematic LC) to include the possibility of a perpendicular alignment of CNTs to LC molecules. The model contains the CNT free energy density (2), the Landau-de Gennes free energy (3) for thermotropic LC order, and an interaction term between the nematic CNTs and nematic LC (4). This interaction term generates the possibility of existence of two nematic phases of CNTs: (i) the mean direction of orientation of CNTs is parallel with the direction of the director of LC molecules, when $S_{CNT} > 0$ and $S_{LC} > 0$, and (ii) the two direction of orientation are perpendicular with each other, $S_{CNT} < 0$ and $S_{LC} > 0$. It is to be mentioned that the order parameter of CNTs can be negative (perpendicular alignment) only for a paranematic phase for which the degree of orientational order is very low. The model predicts in this case a first-order paranematic (perpendicular alignment)-nematic (parallel alignment) phase transition of CNTs. When the coupling constant is positive, the first-order paranematic (parallel alignment)-nematic (parallel alignment) phase transition of CNTs cancels at a critical point, when the transition becomes continuous.

The phase behavior and orientational properties of the mixture are discussed considering different values of temperature T , volume fraction of CNTs ϕ , and coupling strength γ .

The theoretical model we have presented describes quite well (comparing with experimental results) the phase properties of the CNTs into thermotropic

nematic LC. The model could be improved by considering the polydispersity of the CNT component and by considering, in more detail, the form of the interaction energy between the two components.

Author details


Vlad Popa-Nita^{1*} and Robert Repnik²

1 Faculty of Physics, University of Bucharest, Bucharest, Romania

2 Faculty of Natural Sciences and Mathematics, University of Maribor, Maribor, Slovenia

*Address all correspondence to: v.popanita@gmail.com

IntechOpen

© 2018 The Author(s). Licensee IntechOpen. This chapter is distributed under the terms of the Creative Commons Attribution License (<http://creativecommons.org/licenses/by/3.0>), which permits unrestricted use, distribution, and reproduction in any medium, provided the original work is properly cited. 

References

- [1] Lynch MD, Patrick DL. Organizing carbon nanotubes with liquid crystals. *Nano Letters*. 2002;**2**:1197
- [2] Dierking I, Scalia G, Morales P, LeClere D, Adv D. Aligning and reoriented carbon nanotubes with nematic liquid crystals. *Maternité*. 2004;**16**:865-869
- [3] Dierking I, San SE. Magnetically steered liquid crystal-nanotube switch. *Applied Physics Letters*. 2005;**87**:233507
- [4] Zakri C. Carbon nanotubes and liquid crystalline phases. *Liquid Crystal Today*. 2007;**16**:1
- [5] Lagerwall JPF, Scalia G. Carbon nanotubes in liquid crystals. *Journal of Materials Chemistry*. 2008;**18**:2890
- [6] Rahman M, Lee W. Scientific duo of carbon nanotubes and nematic liquid crystals. *Journal of Physics D: Applied Physics*. 2009;**42**:063001
- [7] Scalia G. Alignment of carbon nanotubes in thermotropic and lyotropic liquid crystals. *ChemPhysChem*. 2010;**11**:333
- [8] Lagerwall JPF, Scalia G. A new era for liquid crystal research: Application of liquid crystals in soft matter nano-, bio-, and microtechnology. *Current Applied Physics*. 2012;**12**:1387
- [9] Dierking I, Scalia G, Morales P. Liquid crystal- carbon nanotubes dispersions. *Journal of Applied Physiology*. 2005;**97**:044309
- [10] Schymura S, Kuhnast M, Lutz V, Jagiella S, Dettiaff-Weglikowska U, Roth S, et al. Towards efficient dispersion of carbon nanotubes in thermotropic liquid crystals. *Advanced Functional Materials*. 2010;**20**:3350
- [11] Ji Y, Huang YY, Terentjev EM. Dissolving and alignment carbon nanotubes in thermotropic liquid crystals. *Langmuir*. 2011;**27**:13254
- [12] Lebovka NI, Lisetski LN, Goncharuk AI, Minenko SS, Ponevchinsky VV, Soskin MS. Phase transitions in smectogenic liquid crystal BBBA doped by multiwall carbon nanotubes. *Phase Transitions*. 2013;**86**:463
- [13] Kumar S. Nanoparticles in the supramolecular order of discotic liquid crystals. *Liquid Crystals*. 2014;**41**:353
- [14] Weiss V, Thiruvengadathan R, Regev O. Preparation and characterization of a carbon nanotube-lyotropic liquid crystal composite. *Langmuir*. 2006;**22**:854-856
- [15] Lagerwall J, Scalia G, Haluska M, Dettlaff-Weglikowska U, Roth S, Giesselmann F. Nanotubes alignment using lyotropic liquid crystal. *Advanced Materials*. 2007;**19**:359
- [16] Schymura S, Enz E, Roth S, Scalia G, Lagerwall JPF. Macroscopic-scale carbon nanotube alignment via self-assembly in lyotropic liquid crystals. *Synthetic Metals*. 2009;**159**:2177
- [17] Ould-Moussa N, Blanc C, Zamora-Ledezma C, Lavrentovich OD, Smalyukh II, Islam MF, et al. Dispersion and orientation of single-walled carbon nanotubes in a chromonic liquid crystal. *Liquid Crystals*. 2013;**40**:1628
- [18] Duran H, Gazdecki B, Yamashita A, Kyu T. Effect of carbon nanotubes on phase transition of nematic liquid crystals. *Liquid Crystals*. 2005;**32**:815
- [19] Chen HY, Lee W, Clark NA. Faster electro-optical response characteristic of a carbon-nanotube-nematic suspension.

- Applied Physics Letters. 2007;**90**:033510
- [20] Basu R, Iannacchione GS. Carbon nanotube dispersed liquid crystal: A nano electromechanical system. Applied Physics Letters. 2009;**95**:173113
- [21] Basu R, Iannacchione GS. Orientational coupling enhancement in a carbon nanotube dispersed liquid crystal. Physical Review E. 2010;**81**:051705
- [22] Sigdel KP, Iannacchione GS. Effect of carbon nanotubes on the isotropic to nematic and the nematic to smectic-A phase transitions in liquid crystal and carbon nanotubes composites. European Physical Journal E: Soft Matter and Biological Physics. 2011;**34**:34
- [23] Schymura S, Scalia G. On the effect of carbon nanotubes on properties of liquid crystals. Philosophical Transactions of the Royal Society A. 2013;**371**:20120261
- [24] Lee KJ, Park HG, Jeong HC, Kim DH, Seo DS, Lee JW, et al. Enhanced electro-optical behavior of a liquid crystal system via multi-walled carbon nanotube doping. Liquid Crystals. 2014;**41**:25
- [25] Basu R, Iannacchione GS. Dielectric hysteresis, relaxation dynamics, and nonvolatile memory effect in carbon nanotube dispersed liquid crystal. Journal of Applied Physics. 2009;**106**:124312
- [26] Somoza AM, Sagui C, Roland C. Liquid crystal phases of capped carbon nanotubes. Physical Review B. 2001;**63**:081403-1
- [27] Sabba Y, Thomas EL. High-concentration dispersion of single-wall carbon nanotube. Macromolecules. 2004;**37**:4815
- [28] Green MJ, Parra-Vasquez ANG, Behabtu N, Pasquali M. Modelling the phase behavior of polydispersed rigid rods with attractive interaction with application to single-walled carbon nanotubes in superacids. The Journal of Chemical Physics. 2009;**131**:084901
- [29] Matsuyama A, Kato T. Phase separation in mixture of a liquid crystal and a nanocolloidal particle. Physics Review. 1999;**E59**:763
- [30] Matsuyama A. Theory of binary mixture of a rodlike polymer and a liquid crystal. The Journal of Chemical Physics. 2010;**132**:214902
- [31] van der Schoot P, Popa-Nita V, Kralj S. Alignment of carbon nanotubes in nematic liquid crystals. The Journal of Physical Chemistry. B. 2008;**112**:4512
- [32] Popa-Nita V, Kralj S. Liquid crystal-carbon nanotubes mixtures. The Journal of Chemical Physics. 2010;**132**:024902
- [33] Lisetski LN, Lebovka NI, Naydenov SV, Soskin MS. Dispersions of multi-walled carbon nanotubes in liquid crystals: A physical picture of aggregation. Journal of Molecular Liquids. 2011;**164**:143
- [34] Popa-Nita V, Barna V, Repnick R, Kralj S. In: Suzuki S, editor. Syntheses and Applications of Carbon Nanotubes and Their Composites. Rijeka, Croatia: InTech; 2013. Chap. 7
- [35] Popa-Nita V. Mixtures composed of liquid crystals and carbon nanotubes. The Journal of Chemical Physics. 2014;**140**:164905
- [36] Popa-Nita V. The phase behavior of rigid rods in an anisotropic mean field with application to carbon nanotubes in nematic liquid crystals. The Journal of Chemical Physics. 2015;**143**:094901

- [37] Green MJ, Behabtu N, Pasquali M, Adams WW. Nanotubes as polymers. *Polymer*. 2009;**50**:4979
- [38] Onsager L. The effect of shape on the interaction of colloidal particles. *Annals of the New York Academy of Sciences*. 1949;**51**:727
- [39] de Gennes PG, Prost J. *The Physics of Liquid Crystals*. Oxford: Oxford University Press; 1993
- [40] Oswald P, Pieranski P. Nematic and cholesteric liquid crystals; concepts and physical properties illustrated by experiments. In: *Liquid Crystals Book Series*. Boca Raton: Taylor and Francis Group/CRC Press; 2005
- [41] Doi M. Molecular dynamics and rheological properties of concentrated solutions of rodlike polymer in isotropic and liquid crystalline phases. *Journal of Polymer Science Part B: Polymer Physics*. 1981;**19**:229
- [42] Doi M, Edwards SF. *Theory of Polymer Dynamics*. Oxford: Clarendon; 1989
- [43] Kuzuu N, Doi M. Constitutive equations for nematic liquid crystals under weak velocity gradient derived from a molecular kinetic equation. *Journal of the Physical Society of Japan*. 1983;**52**:3486
- [44] Park KA, Lee SM, Lee SH, Lee YH. Anchoring a liquid crystal molecule on a single-walled carbon nanotube. *Journal of Physical Chemistry C*. 2007;**111**:1620
- [45] Flory PJ. *Principles of Polymer Chemistry*. Ithaca: Cornell University Press; 1953
- [46] Flory PJ. Statistical thermodynamics of semi-flexible chain molecules. *Proceedings of the Royal Society of London A*. 1956;**243**:73
- [47] Song W, Kinloch IA, Windle AH. Nematic liquid crystallinity of multiwall carbon nanotubes. *Science*. 2003;**302**:1363
- [48] Song W, Windle AH. Isotropic-nematic phase transition of dispersion of multiwall carbon nanotubes. *Macromolecules*. 2005;**38**:6181
- [49] Faetti S, Palleschi V. Measurements of the interfacial tension between nematic and isotropic phase of some cyanobiphenyls. *The Journal of Chemical Physics*. 1984;**81**:6254
- [50] Faetti S, Palleschi V. Nematic-isotropic interface of some members of the homologous series of 4-cyano-4'-(n-alkyl)biphenyl liquid crystals. *Physical Review A*. 1984;**30**:3241
- [51] Faetti S, Palleschi V. Molecular orientation and anchoring energy at the nematic-isotropic. *Journal de Physique Lettres (France)*. 1984;**45**:L313

Section 3

Electro-Optic
Switching Behavior and
Photorefractive Effect
in Ferroelectric Liquid
Crystals

In-Plane Retardation Switching Behavior at Certain Types of Smectic Liquid Crystals

Akihiro Mochizuki

Abstract

Smectic liquid crystals' layer structures and their influence on electro-optic characteristic properties are studied. Some background research works have revealed that a certain type of tilted smectic liquid crystal to the smectic layer normal showed some distorted out-of-plane retardation change. With intentional distortion of out-of-plane retardation change even provides almost in-plane only retardation change. In a certain type of smectic liquid crystal and its specific alignment condition, such a certain type of smectic liquid crystal panel shows in-plane only retardation switching. A more comprehensive study is still required, and such type of smectic liquid crystal panel provides unique electro-optic properties that have not been reported.

Keywords: smectic liquid crystal, smectic layer, tilted smectic, in-plane retardation, out-of-plane retardation, chevron layer, bookshelf layer

1. Introduction

Some smectic liquid crystals are known to show very different electro-optic effect compared to those of most of nematic liquid crystals. Although among nematic liquid crystals, some show unique electro-optic effect, most of nematic liquid crystals use their anisotropy of dielectric constant originated from dipole-momentum as their driving torque coupled with externally applied electric field. Under the restriction of orientational order on nematic liquid crystals, the dipole-momentum driving torque is fairly predictable. On the other hand, smectic liquid crystal molecules have some more restriction in their molecular switching than those of nematic liquid crystals due to their higher order molecule-molecule interactions than those for nematic liquid crystals. Such restriction may not be simply interpreted by higher viscosity as a bulk effect, but would be considered more intrinsic molecule-molecule interaction. Since the meaning of restriction does not mean slower optical response, but rather faster optical response than much less viscous nematic liquid crystal cases in a certain case of smectic liquid crystal electro-optic device. One of the purposes of this series of investigations is to understand how such restriction influences on retardation switching behavior such as in-plane and/or out-of-plane switching under the premise of in use for electro-optic devices such as display devices, phase modulation devices, beam steering devices and so on. In general, weaker molecule-molecule interaction gives more straightforward driving torque as the result of driving torque coupling from externally applied stimulation such as electric field application. Since

externally applied electric field is literally a field effect regardless the applied field is on liquid crystal layer, alignment layer, and more complex portion of interface area between those two different dielectric layers. Some detailed investigation of dielectric relaxation effect and its influence both on electro-optic response profile and surface accumulated charge influence on electro-optic performance are widely investigated [1–12]. Thanks to orientational order nature of most of nematic liquid crystal molecules, their electro-optic response profile is mostly described and predictable without significant consideration of those different dielectric layers relaxation and surface charges influence except for some unique cases. One of the unique cases includes even existence of second harmonic generation with nematic liquid crystal molecules such as 5CB [13]. In spite of some unique cases, most of nematic liquid crystal cases, their electro-optic behavior is still somewhat predictable, and more importantly, such unique cases in nematic liquid crystal cases may be beneficial to consider more complicated smectic liquid crystal cases' electro-optic behavior.

It would be one of the interested topics to investigate smectic liquid crystal molecular switching behavior governed by the smectic layer structure, specifically the layer restriction influence on in-plane and out-of-plane retardation change. With expected smectic liquid crystals' two-dimensional order, it is reasonably expected showing some different retardation switching behavior familiar with most of nematic liquid crystal cases. One of the examples is surface stabilized Ferroelectric Liquid Crystal (SSFLC) case using artificially unwounded helical structure of chiral smectic liquid crystals such as SmC* phase liquid crystals [14]. Unlike most of nematic liquid crystal devices in use which use the concept of strong anchoring, SSFLC device prefers much weaker surface anchoring as long as it has well enough uniform molecular initial alignment at the surface of the substrate. This requirement comes from SSFLC panel's driving torque origin. Unlike dielectric momentum based driving torque for most of nematic liquid crystal devices, SSFLC devices use spontaneous polarization as their driving torque origin. Spontaneous polarization gives applied voltage polarity sensitive torque. Therefore, if its surface anchoring is strong anchoring, which means no molecular orientation change regardless applied voltage, such a strong anchored SSFLC device shows asymmetric electro-optic effect due to surface electrical polarization effect formed by asymmetric surface anchoring in terms of surface area's smectic liquid crystal molecular packing mainly governed by non-uniform smectic layer stacking such as Chevron 1 uniform structure described in later on this chapter. Therefore, an ideal surface anchoring for SSFLC panels is one-time surface anchoring just to have initial alignment, and once uniform alignment is obtained, surface should not have any restriction to molecular switching as "zero-anchoring force". However, even it is an ideal situation, such surface anchoring may not be easy to realize as an actual device, so that it would be necessary to find out any alternative way to provide substantial "zero-anchoring" after obtained initial alignment with smectic liquid crystal devices. One of such approaches is so-called slippery SSFLC device, [15], or weak surface anchoring effect on nematic liquid crystals [16]. A slippery surface is effective to avoid some significant conflict between the strong anchored surface area's liquid crystal molecules and bulk area's much less influenced surface anchoring effect liquid crystal molecules under application of externally applied electric field. Thanks to almost freely moving surface area's liquid crystal molecules, surface area's and bulk area's could eliminate any catastrophic conflict under applied electric field, resulting in more natural and stable molecular switching. However, such slippery surface is not easy to provide large area in uniform manner; moreover, such weak surface anchoring

may have some long-term reliability concern. Since one of the reasons in current nematic liquid crystal devices' strong anchoring choice was long term reliability and stability reason. However, using spontaneous polarization as a smectic liquid crystal driving torque, choice of surface anchoring whether strong or weak is still a big question. Some approaches to get rid of this dilemma have been investigated. Surface clinic effect [17–31] is one of those investigations. Use of DeVries type of smectic liquid crystals is also one of the potential approaches [32, 33]. Unlike SSFLC cases, surface clinic effect is like induced polarization base. Anti-ferroelectric liquid crystals are also other approaches [34–38]. Both surface clinic and anti-ferroelectric liquid crystal cases have the common ground in their initial surface anchoring. Both do not have spontaneous polarization at the initial alignment stage, but show induced spontaneous polarization. The expression of induced spontaneous polarization is contradiction. However, this expression gives intrinsic effect of those cases. Absence of externally applied electric field, both cases do not show any spontaneous polarization. Once externally applied electric field unpins a certain balance, each liquid crystal's potential polarization synchronizes, resulting in bulk level of spontaneous polarization. Both cases are certainly providing some great hint to get rid of the dilemma discussed above. This series of research works are to seek out any practical means to get rid of the dilemma between strong and weak surface anchoring in a smectic liquid crystal device. For the sake of this purpose, first, current known ferroelectric liquid crystal device's molecular alignment effect on its electro-optic effect was investigated. Then, any possible way to avoid using spontaneous polarization as a driving torque was investigated. As the investigation means, it turned out that knowing in-plane and out-of-plane retardation switching behavior as the result of molecular switching is very effective to learn a certain type of smectic liquid crystal molecular stacking. In addition to above investigation, it is also discussed that how in-plane only retardation switching is beneficial for some phase modulation devices.

A clarification of actual definitive relationship between smectic layer structure and electro-optic switching behavior requires comprehensive research works. Even such a comprehensive research work is a large amount of work, some approaches penetrating specific point would be beneficial as one of the large amount of works. This series of research works have focused on tilted smectic liquid crystals as their influence on electro-optic performance, specifically on in-plane and out-of-plane retardation switching behavior.

2. Ideal SSFLC molecular stacking geometry

Before some unique molecular switching behaviors are discussed, first, an ideal SSFLC molecular switching would be confirmed in terms of initial molecular stacking models and their switching behavior. As shown in **Figure 1**, with an ideal bookshelf layer structure, each liquid crystal molecule rotates its spontaneous polarization uniformly and simultaneously from the top to the bottom substrates. At an ideal smectic layer structure, all of smectic liquid crystal molecules move simultaneously known as Goldstone mode [39], and maximize the power of spontaneous polarization. This movement is also reciprocal in terms of spontaneous polarization switching. Since the spontaneous polarization switching is completely reciprocal, there is no smectic layer structure change during the switching. Therefore, the bookshelf smectic layer structure is supposed to provide the most stable electro-optical switching.

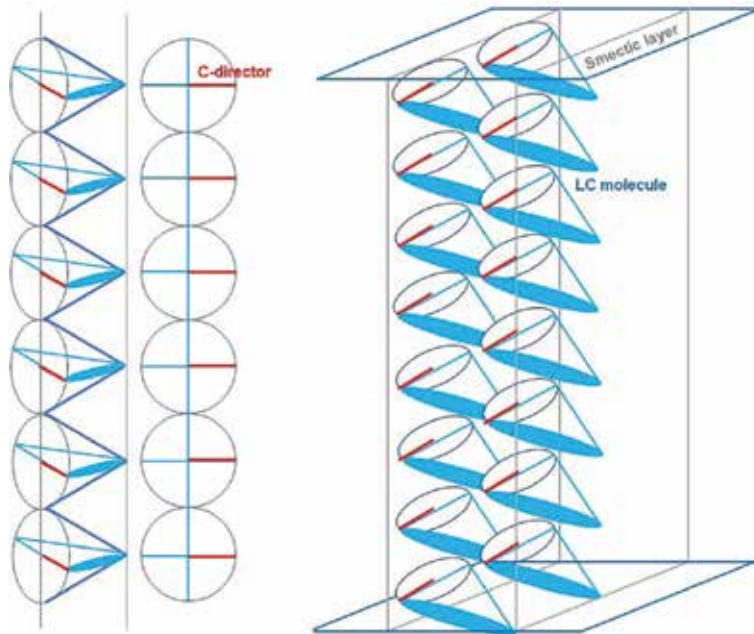


Figure 1. An ideal smectic layer structure known as “bookshelf” layer. At an ideal bookshelf layer structure, all of smectic liquid crystal molecules move simultaneously known as goldstone mode, resulting in maximizing power of the spontaneous polarization.

3. Typical SSFLC molecular stacking geometries

Most of typical smectic layer structures with tilted smectic liquid crystals are, however, not a bookshelf structure, but a chevron layer structure. Actual chevron layer structure has many variations in its detail structure; however, there are two typical chevron layer structures widely known as Chevron C1 uniform and Chevron C2 uniform as shown in **Figures 2** and **3**, respectively. In a Chevron C1 uniform layer structure, c-directors at the upper half of the chevron layer structure and c-directors at the bottom half of the chevron structure have opposite direction, resulting in reduction of the power of bulk spontaneous polarization as shown in **Figure 2**. This situation is, however, just the initial molecular alignment structure, and such uneven c-director structure creates some complicated electro-optic switching behavior. In a Chevron C1 structure, at the kink area where the two opposite chevron leaning angles meet together, two different directions of c-directors have conflict to rotate their direction under the externally applied electric field. Actual dynamics of the kink area’s conflict is not easy to clarify, specifically when time resolved local kink area’s chevron layer structure change requires nano-scale layer analysis. Some local smectic layer structure analysis has been published using soft X-ray (Synchrotron Radiation) beam [40, 41]. Even using soft X-ray beam, it is still not easy to clarify sub-milliseconds dynamic response of local layer structure. Therefore, until new time resolved local smectic layer structure analysis methodology is developed, most of practical means to estimate influence of c-director packing on electro-optic switching behavior would be an optical measurement at visible wavelength including in-plane and out-of-plane retardation measurement.

At a Chevron C2 uniform geometry shown in **Figure 3**, the kink area’s c-directors have almost the same direction, but not really the same direction unlike those of a bookshelf layer structure. Even such kink area’s c-director conflict is not easy to

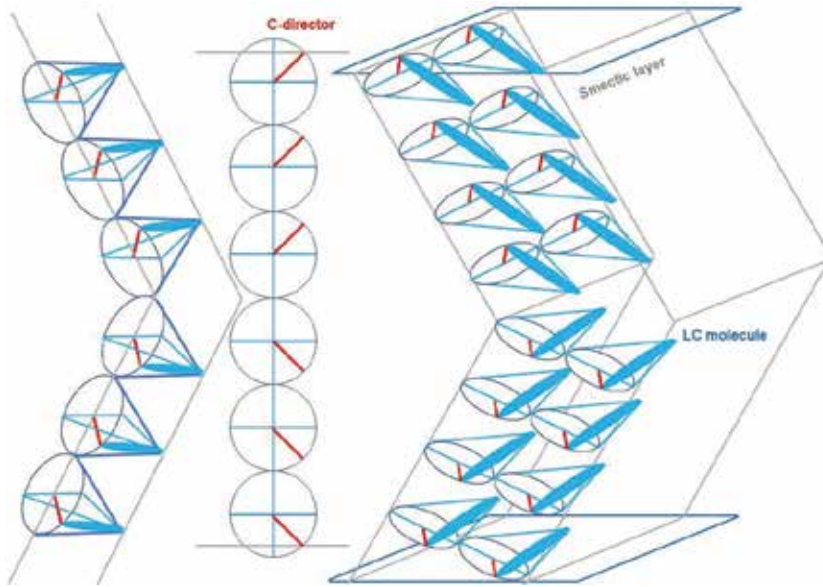


Figure 2. *c*-Director packing geometry of a Chevron C1 uniform layer structure. Due to opposite *c*-director directions from the top substrate and from the bottom substrate, at the center area known as “kink” area, two opposite directions of *c*-directors have conflict of their packing. Such *c*-director packing conflict is also problematic when externally applied electric field induces *c*-director packing change.

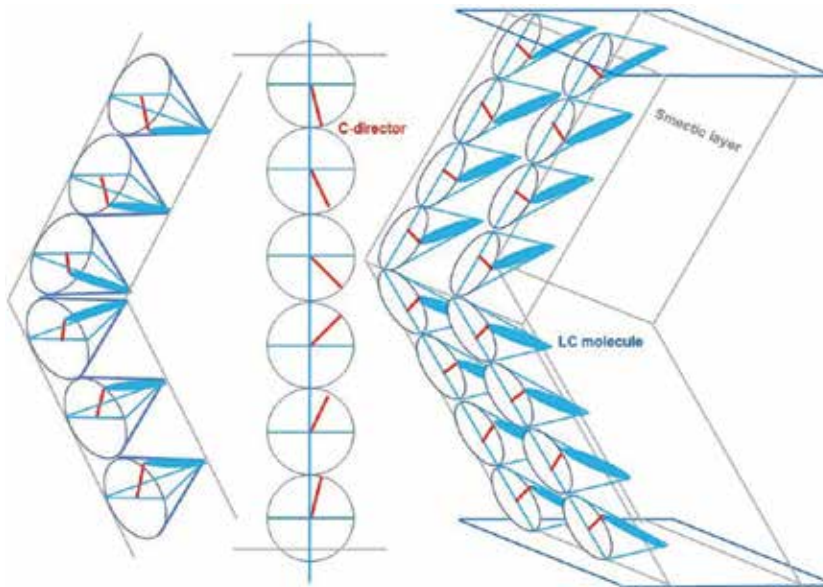


Figure 3. *c*-Director packing geometry of a Chevron C2 uniform layer structure. Unlike C1 uniform configuration, at the kink area, *c*-director's directions both from the upper and the bottom substrates have nearly same direction. This is effective to minimize conflict in *c*-director packing while molecular switching is in process by an externally applied electric field.

minimize, C2 structure's kink area's conflict is less competitive than at C1 structure. A kink area's *c*-director conflict is sometimes making even irreversible smectic layer structure change. There are many published reports on smectic layer instabilities, most of them are about rotation of smectic layer itself which is a large scale of layer

structure change [42–46]. This investigation's interest is, however, some local areas' layer structure distortion, and its consecutive electro-optic response behavior. As discussed above, such local area's smectic layer structure change is not easy to retrieve directly. One of the practical means to estimate if there is an irreversible or non-reciprocal local smectic layer structure change would be electro-optic response change, specifically a ratio between in-plane/out-of-plane retardation change as discussed later in this chapter. As a realistic choice of smectic layer structure, most of practical approaches using ferroelectric liquid crystals are using Chevron C2 uniform configuration. Thanks to overall same direction of c-directors both from the upper and the lower substrates directions, at the kink area, a minimum conflict in c-director packing geometry is reasonably expected. This minimum c-directors conflict at the kink area would be able to avoid irreversible or non-reciprocal smectic layer structure change as illustrated in **Figure 4**.

Depending on the kink area's influence, mainly size wise as how many numbers of liquid crystal molecules are restricted by the kink effect at the center portion of the panel, reciprocal and non-reciprocal layer structure change provides some significantly different optical effect. In an actual SSFLC device case, not only smectic layer structure, but also depolarization effect should be in consideration, though [47]. The depolarization effect is the result of dielectric relaxation or rearrangement by polarization switching. In addition to a typical dielectric relaxation of dielectric materials, switch of spontaneous polarization creates a large amount of charge transfer, and the transferred charges remain in the panel at least for a while due to the nature of spontaneous polarization (with absence of externally applied electric field, spontaneous polarization still keeps internal electric field in the SSFLC panel), resulting in formation of depolarization effect. Such depolarization works as weakening of externally applied electric field, when next time an externally electric field is applied. This weakening effect of the applied electric field requires very complicated driving voltage control. It is about transient charge transfer including liquid crystal's

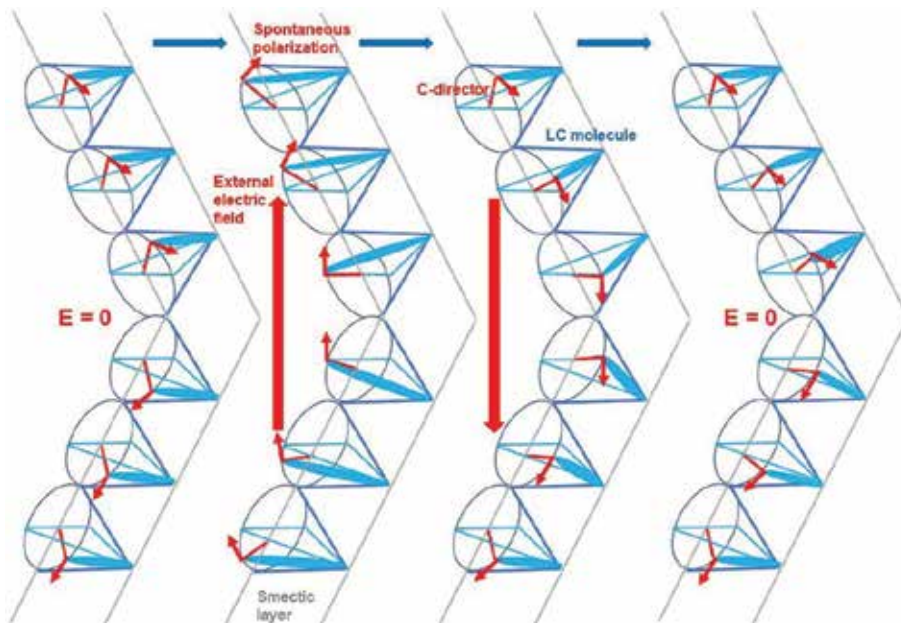


Figure 4. A non-reciprocal smectic layer switching of Chevron C1 uniform structure. Due to significant conflict in c-director packing at the kink area, repeating driving sometimes provides irreversible c-director packing after removing driving voltage. This results in instable electro-optic switching.

own charge mobility, liquid crystal-surface alignment layer interface potential barrier, and electrode-alignment layer potential barrier, and so on. These charge transfer matters are common with nematic liquid crystal devices; however, more complicated situation at SSFLCDs is their polarity sensitive behavior. Dielectric anisotropy based driving torque does not tell the difference of polarity, resulting in much more room for the surface charge influence. On the other hand, spontaneous polarization based driving torque tells the difference in polarity, resulting in bias voltage effect, if internal polarization has asymmetric structure in terms of polarity.

4. Polarization shielded smectic liquid crystals

As previous works clarified [42, 47], depolarization effect is one of the most influential factors to destabilize spontaneous polarization switching, which disturbs SSFLC cells memory effect accompanied with the cell's internal depolarization structure. At a typical SSFLC cell, due to existence of permanent spontaneous polarization, regardless absence of externally applied electric field, the SSFLC cell forms internal polarization structure. Once externally electric field is applied, most of liquid crystal molecules change their orientation making total spontaneous polarization direction along with the applied electric field. In this process, due to spontaneous polarization switching, the cell internal dielectric materials which are the ferroelectric liquid crystal layer and its alignment layer try to neutralize polarization. This process is known as depolarization process. Such depolarization process is, however, ends up weakening total spontaneous polarization structure in the cell. This is the major reason why the memory effect of an SSFLC cell is destabilized [42, 47].

Through the investigation of SSFLC molecular switching in terms of both the smectic layer and surface accumulated charges influence, the authors group proposed and showed some new approach minimizing influence of surface accumulated charges as well as layer structure influence on molecular orientation change. The concept of this new approach was to minimize spontaneous polarization keeping the basic response of an SSFLC cell. According to this concept, such a modified SSFLC driving mode is called as polarization shielded smectic (PSS) liquid crystal mode [48–50]. Although it was not clear of the reason, in the course of the PSS-LCD investigations, it turned out that some of PSS-LC cells showed a quasi-bookshelf layer structure. One of the reasonable assumptions of the bookshelf layer structure of the PSS-LC cell was very small spontaneous polarization, and its consecutive small depolarization effect. Major component of the PSS-LC chemical formula is shown in **Figure 5**. They have Naphthalene-ring core structure connected by carbonyl polar portion as the common structure [51–53].

Using the same smectic liquid crystal mixture shown in **Figure 5**, polymer assisted ferroelectric liquid crystal response phenomenon was investigated how the bookshelf layer structured small spontaneous polarization liquid crystal molecules show any specific electro-optic response, specifically its retardation switching behavior using polymer assisted ferroelectric liquid crystal configuration [54–56]. The detail of this empirical result is published [57]. **Figure 6** shows the result.

In **Figure 6**, Δ is in-plane retardation angle, and Ψ is out-of-plane retardation angle. The significant difference in retardation angle change behavior between Δ and Ψ with doped oligomer amount strongly suggests some enhancement and suppression effects in polarization switching behavior. With relatively small doping ratio such as 5 mol%, in-plane retardation (Δ) shows significant increase. On the other hand, out-of-plane retardation shows opposite tendency. These two retardation switching behavior suggests possible suppression of out-of-plane retardation change keeping in-plane retardation change large enough.

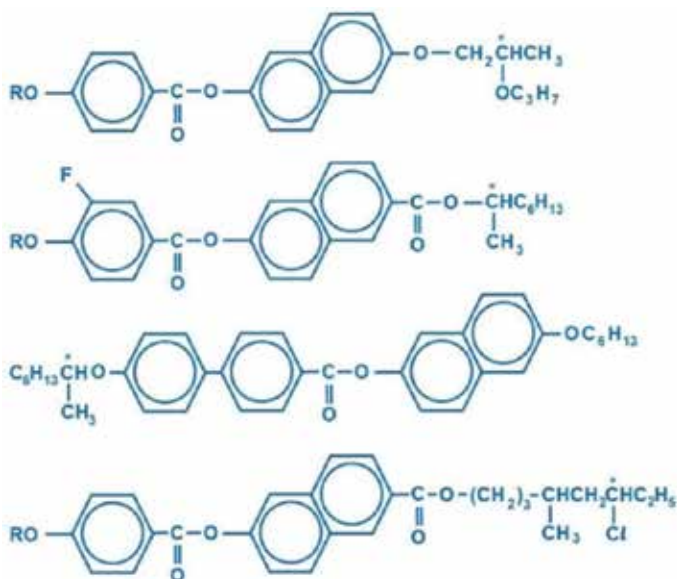


Figure 5. Major component of naphthalene-ring base chiral smectic liquid crystal molecules for the bookshelf SSFL panel preparation.

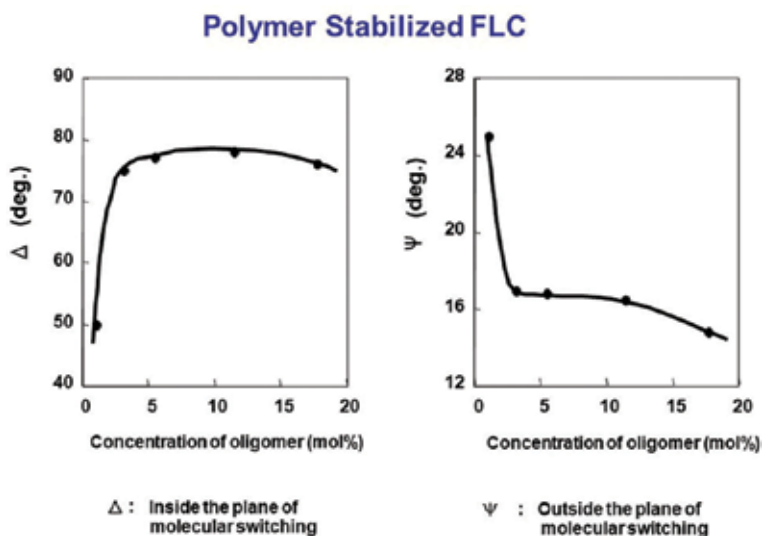


Figure 6. In-plane (Δ) and out-of-plane (Ψ) retardation change depending on doping rate of photoreactive oligomer with the bookshelf layer structure ferroelectric liquid crystal panels.

5. Possibility of active suppression of out-of-plane retardation change

Above experimentally clarified possible suppression of out-of-plane retardation switching in chiral smectic C phase liquid crystal panel may naturally lead possible completely in-plane only retardation switching without showing any out-of-plane retardation switching. If it happens, molecular switching behavior does not follow half circle cone edge anymore like a typical SSFLCD's case, and liquid crystal molecules swing in the same plane where the liquid crystal molecules' initial alignment plane. For this specific purpose to investigate possible in-plane only molecular

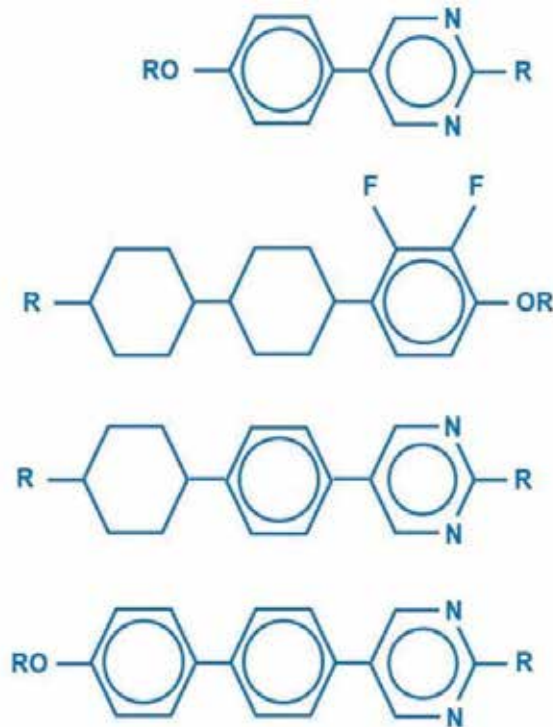


Figure 7.
Major liquid crystal component for smectic C phase mixture.

swing movement behavior, new smectic C phase liquid crystal mixture was formulated. **Figure 7** shows main component of the smectic C phase (non-chiral) liquid crystal mixture. This mixture does not contain any chiral materials, resulting in non-Chiral mixture showing smectic C phase at room temperature as a bulk liquid crystal. With this mixture, if the mixture shows artificial smectic A like alignment, which means no molecular tilt to the smectic layer normal, was investigated using RN-1199 mechanical buffed alignment layer and 2.4–2.6 μm gap panels. The texture at the extinction angle with the crossed Nicole set polarized microscope photo is shown in **Figure 8**. This photo was taken with 2.4 μm gap panel. The prepared liquid crystal mixture showed smectic C phase at over 32°C, and it kept smectic C phase at most 47°C. Over the smectic C phase in temperature, the mixture showed smectic A phase. The **Figure 8** texture photo was taken at 35°C elevated temperature from the room temperature. At 35°C, the obtained uniform liquid crystal molecular alignment gives over 4000:1 static contrast ratio using coherent 514 nm diode laser optical system with crossed Nicole configuration that would be good enough for most of application (refer **Figure 15**). Since the series of investigation is under the premise of applying electro-optic devices such as display devices and phase modulation devices, not only large area's uniform molecular alignment, but also very tiny area's pixel to pixel uniformity with its unit size of few tens of microns square are required with static contrast ratio of over 3000:1 for a consideration of application.

As shown in the texture in **Figure 8**, this liquid crystal panel shows smectic A like texture at smectic C phase temperature as a bulk liquid crystal. It also showed electro-optic response above 32°C, however, below 32°C, and over 47°C temperature, the liquid crystal panel did not show any electro-optic response. The extinction angle of the liquid crystal panel at 35°C was slightly shifted from mechanical buffed angle. However, such slight angle shift from mechanical buffing direction is not unique

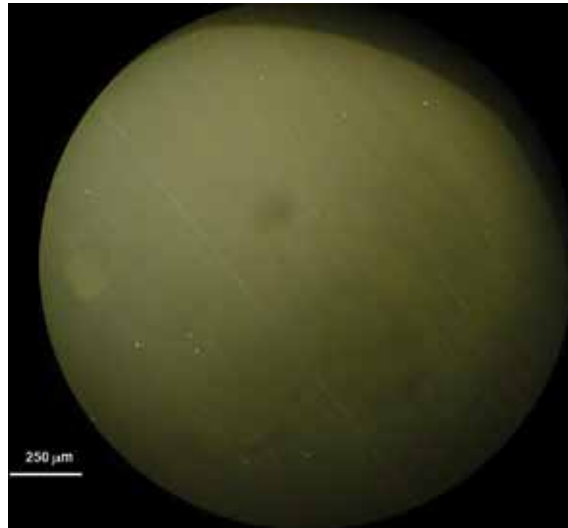


Figure 8. A texture of artificial smectic A liquid crystal panel using smectic C phase mixture as a bulk state. This panel uses RN-1199 mechanical buffed alignment layer with panel gap of 2.4 μm .

with this particular case, and sometimes an alignment layer gives relatively large retardation as the alignment layer itself shows an angle shift between liquid crystal panel's extinction angle and mechanical buffing direction. The shifting angle around 3–4° was not the same with that at smectic A phase of the panel. At the smectic A phase temperature, the panel shows ~1 to 2° shift at the extinction angle. The shifting angle direction was same both at the smectic A and artificial smectic A phase. This mixture has nematic phase above smectic A phase, however, its temperature range was very narrow such as less than 2°, and it was not easy to confirm its extinction angle with accurate enough measurement. Using these panels with elevated temperature at 35°C, if the smectic A like aligned panel shows in-plane only retardation switching was measured. For in-plane only retardation change confirmation, two different electro-optical measurements were compared. As illustrated in **Figure 9**, crossed Nicole linear polarizers measurement and crossed Nicole with quarter wave plates measurement were investigated. The crossed Nicole measurement does not distinguish in-plane and out-of-plane retardation change. Regardless in-plane only or mix between in-plane and out-of-plane retardation change, the crossed Nicole set up shows some electro-optical light throughput changes. On the other hand, the crossed Nicole with quarter wave plate measurement whose incident light to a liquid crystal panel is circularly polarized light shows some light throughput change only with out-of-plane retardation change.

Figures 10–12 compared crossed Nicole and crossed Nicole with $\frac{1}{4}$ lambda plates measurements of the smectic A like initial alignment panel by changing applied electric field strength. **Figure 10(a)** was from crossed Nicole result, and **Figure 10(b)** was with $\frac{1}{4}$ lambda plates result. The applied voltage both for crossed Nicole and with $\frac{1}{4}$ lambda plates set-up were the same: 2 ms duration bi-polar pulse voltage having 2 V height both for positive and negative directions. Light intensity scale at crossed Nicole and with $\frac{1}{4}$ lambda plates is different. Using circularly polarized light, if the liquid crystal panel's retardation change does include out-of-plane retardation change, basically, the light throughput from the liquid crystal panel is through without any light intensity modulation. In these experimental works, the designed panel gap was 2.4 μm at 35°C. Therefore, externally applied electric field strength is 2 V/2.4 μm –0.83 V/ μm . It would be

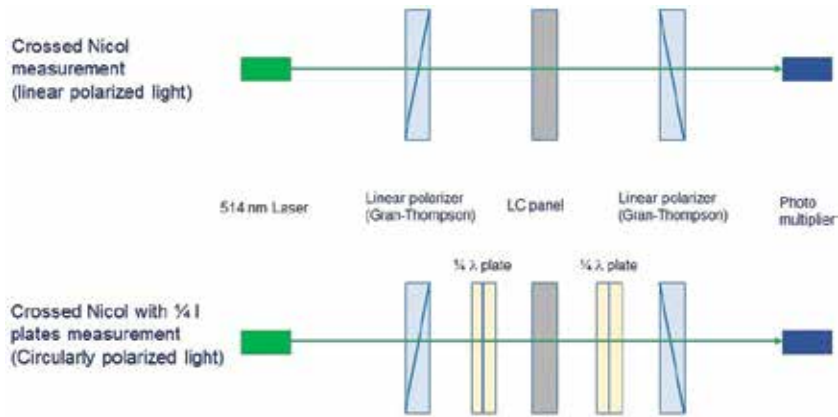


Figure 9. Electro-optic measurement set-ups. One is using crossed Nicole linear polarizers. Linearly polarized incident 514 nm laser beam is modulated by the liquid crystal panel. The crossed Nicole set-up shows some light intensity change either the liquid crystal panel's retardation change including both in-plane and out-of-plane retardation change or only in-plane retardation change. The bottom set-up uses a pair of $\frac{1}{4}$ lambda wave plates, which change the incident light to circularly polarized light instead of linearly polarized light. In this measurement set-up, if the liquid crystal panel has both in-plane and out-of-plane retardation change, or only out-of-plane retardation change, the photo multiplier detects some light intensity change. If the liquid crystal panel has only in-plane retardation change, circularly polarized incident light does not have any amplitude modulation, resulting in no light intensity change.

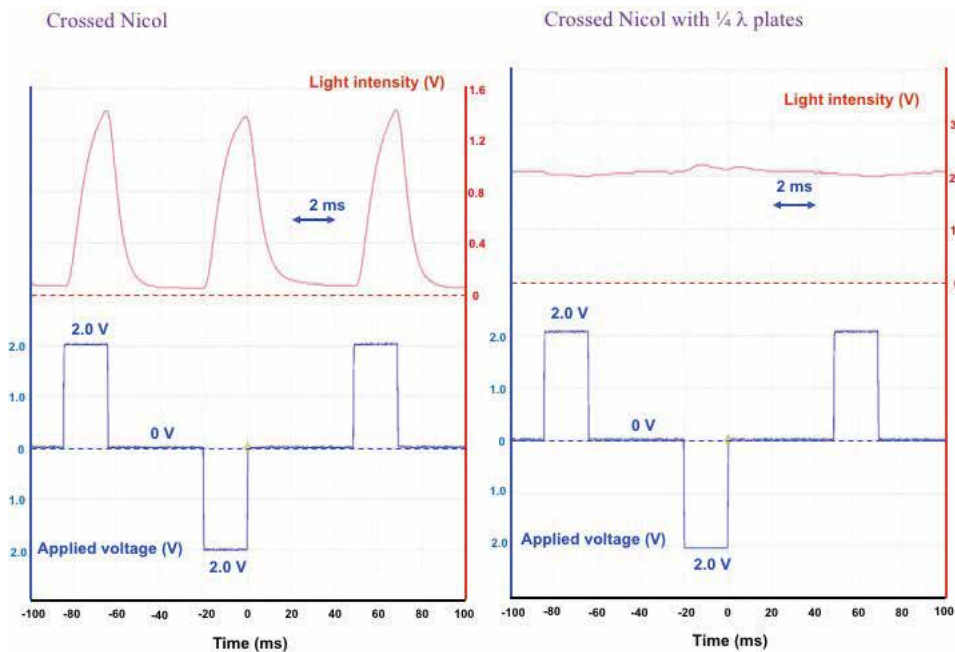


Figure 10. (a) Light intensity profile with crossed. Nicole optical set-up with 2 V pulse. (b) Light intensity profile with crossed. Nicole and $\frac{1}{4}$ lambda plates set-up with 2 V pulse.

reasonable to discuss molecular response behavior with applied electric field strength, rather than voltage. On the other hand, at this particular molecular stacking configuration case, it is still not clear if externally applied electric field represents effective applied electric field. Because the expected driving torque on

this particular case is still not clear, but clear that it is not from dielectric anisotropy coupling, not from spontaneous polarization. Most likely, it would be quadrupole momentum base [57, 58], and if it is really from quadrupole momentum

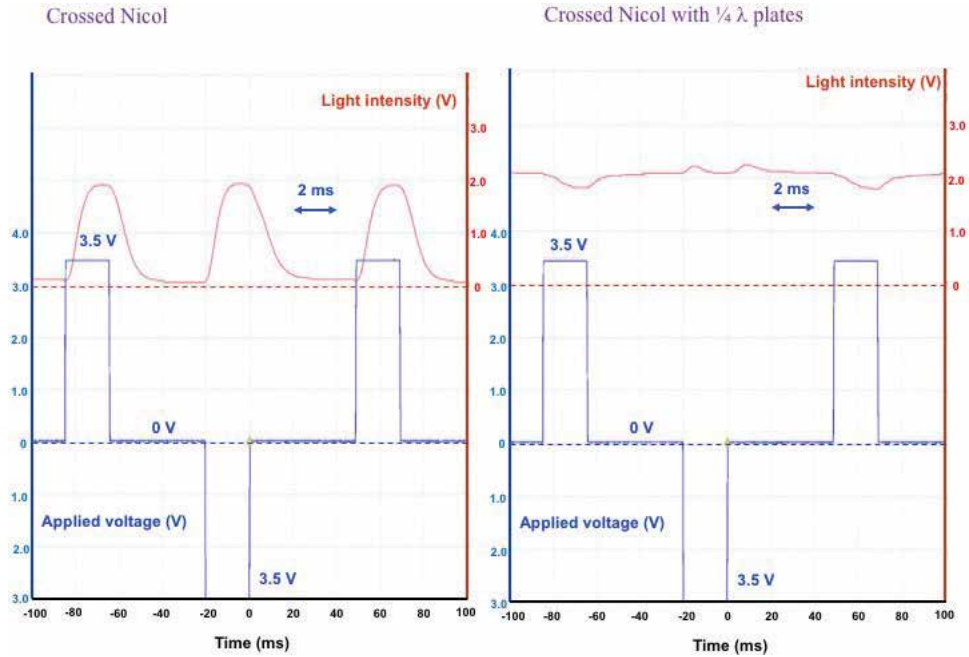


Figure 11. (a) Light intensity profile with crossed. Nicole optical set-up with 3.5 V pulse. (b) Light intensity profile with crossed. Nicole and $\frac{1}{4}$ lambda plates set-up with 3.5 V pulse.

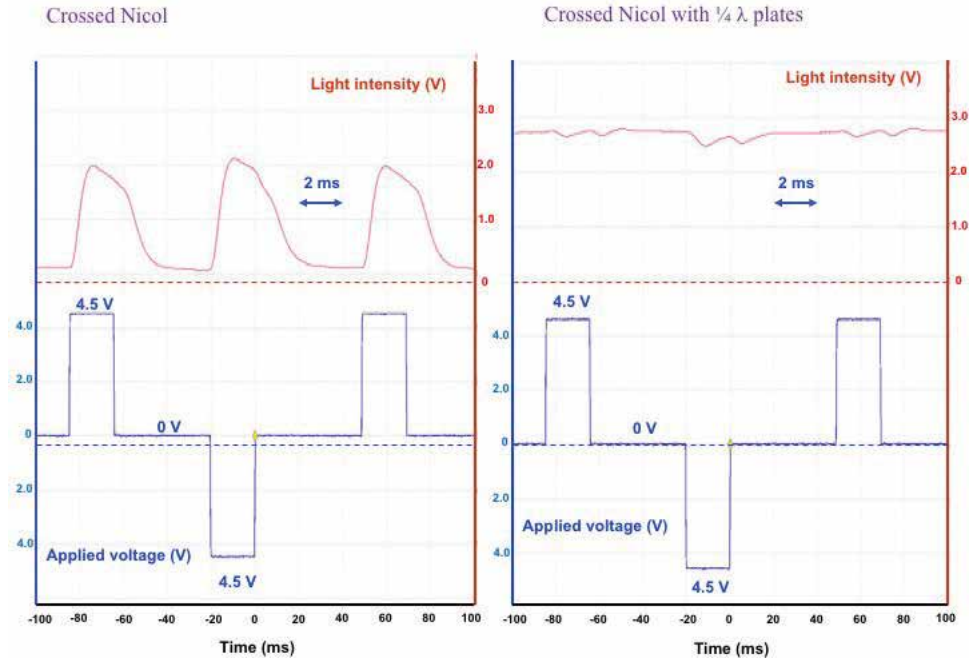


Figure 12. (a) Light intensity profile with crossed. Nicole optical set-up with 4.5 V pulse. (b) Light intensity profile with crossed. Nicole and $\frac{1}{4}$ lambda plates set-up with 4.5 V pulse.

base, we may need to figure out what external excitation is the most appropriate to discuss the influence, however, it might be too early to conclude from current obtained empirical results, yet.

Figure 10(a) and **(b)** comparison clearly suggests the smectic A like initial alignment smectic liquid crystal panel has almost in-plane only retardation change. Following **Figures 11** and **12** show some influence of further increase in applied voltage on the in-plane/out-of-plane retardation change.

With increase in applied voltage, **Figure 11(b)** shows no-complete flat light intensity profile, but shows some change at each applied pulse voltage edge. This change strongly indicates some involvement of out-of-plane retardation change. Further higher applied voltage shows some interesting amplitude modulation profile as shown in **Figure 12(a)** and **(b)**. **Figure 12(a)** and **(b)** show the light intensity profiles both at crossed Nicole and with $\frac{1}{4}$ lambda plates set-up results with 4.5 V pulse voltage, respectively. Unlike lower applied voltage cases, 4.5 V voltage gave at least two-step wise light intensity profile at **Figure 12(a)**: crossed Nicole set-up case. The measured liquid crystal panel has 2.4 μm gap between two counter transparent electrodes gap. Therefore, applied electric field strength at 4.5 V would be ca. 1.88×10^6 V/m. From typical liquid crystal device point of view, this level of electric field is somehow typical strength. Therefore, it is reasonably assumed that there was no particular electric field discharge influence on these measurements. A comparison between **Figures 11(a)** and **12(a)** also suggests possible over 45° molecular optical axis rotation under the premise of almost in-plane only retardation change. **Figure 11(a)** clearly shows saturated light intensity during 2 ms pulse voltage application. On the other hand, **Figure 12(a)** shows decrease in light intensity after the light intensity reached at the peak light after the pulse voltage was applied, also shows slower light intensity decay after the pulse voltage is removed. The light intensity decrease during the pulse voltage application suggests over 45° liquid crystal molecular axis rotation under the premise of almost only in-plane retardation change.

Since the measurement set-up used cross Nicole, if birefringence optical medium changes its optical axis over 45° , light intensity should be decreased.

Slower light intensity decrease right after the applied pulse voltage is removed also supports possible over 45° molecular optical axis rotation. It is reasonably assumed that during pulse voltage application, molecular optical axis rotates over 45° , and right after the pulse voltage is removed, the liquid crystal molecular axis continuously comes back to the original position which gives the light extinction. If this view is correct, apparent two-step wise light intensity change is not really two-step, but monotonical decrease in light intensity along with liquid crystal optical axis rotation from over 45° to heading to 0° . For further detail investigation whether really the smectic liquid crystal optical axis rotates over 45° , slightly different formulated smectic liquid crystal mixtures were prepared showing more uniform initial molecular alignment. Using the newly formulated smectic liquid crystal mixtures, if really the optical axis rotates over 45° was investigated. **Figure 13** is the result of this investigation.

Figure 13 strongly indicates over 45° optical axis rotation under the premise of almost in-plane only retardation change. In **Figure 13**, at 4 V pulse voltage application, the reached light intensity is close to the light intensity given by the parallel Nicole configuration. This suggests that the optical axis at 4 V pulse voltage application gave almost 45° rotation from the initial extinction angle (0°). At 8 V pulse voltage, during 1 ms pulse voltage application duration, the light intensity shows decrease right after it reached the maximum. Also right after the pulse voltage is removed, the light intensity showed sharp increase, then decrease continuously. This light intensity change profile is reasonably interpreted as over 45° rotation.

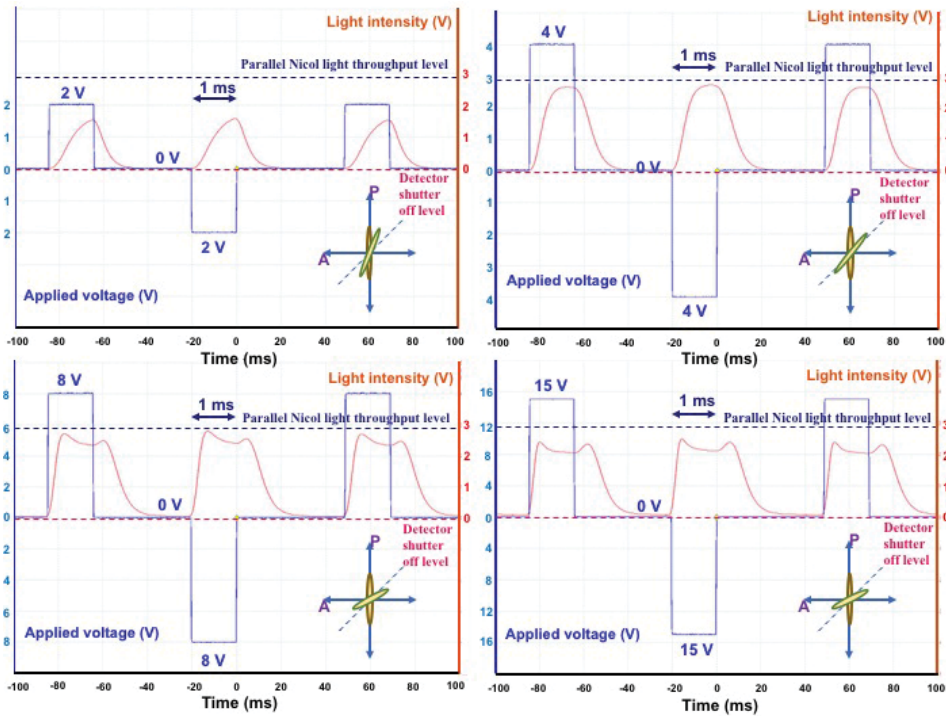


Figure 13. Light intensity profiles depending on applied electric field strength using the crossed Nicol optical set-up with 1 ms pulse voltage. Up to 4 V pulse voltage, light intensity gives almost maximum intensity. 8 V pulse voltage gives “bump” in light intensity during pulse voltage application, which strongly indicates over 45° optical axis rotation. Further increase in pulse voltage such as 15 V even gave lower reachable light intensity during pulse voltage application. This also indicates over 45° rotation under the premise of almost in-plane only retardation change.

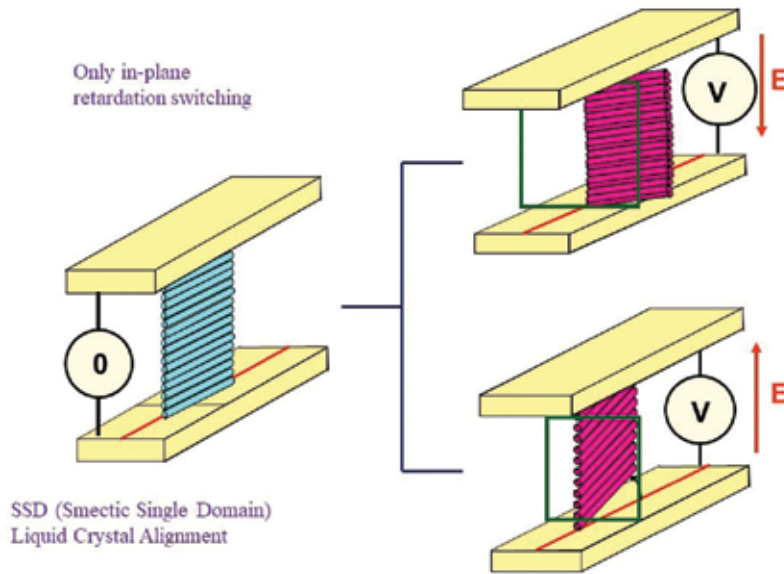


Figure 14. An overall concept of smectic single domain (SSD) liquid crystal molecular switching behavior. At the initial molecular alignment configuration, all of smectic liquid crystal molecules align uniformly forming like “liquid crystal wall”. When downward voltage is applied to the liquid crystal panel, the “liquid crystal wall” rotates clockwise direction. When upward voltage is applied, the “liquid crystal wall” rotates counter-clockwise direction.

With further increase in applied voltage such as 15 V, the apparent reachable light intensity is even decreased. This is possibly due to photo detector's sampling time issue. It is still required more detail investigation to conclude in-plane only retardation switching with this particular smectic liquid crystal cases, as a general understanding with above investigations, an overall liquid crystal molecular behavior is illustrated in **Figure 14**.

Although some detail is still missing, as an overall concept for the smectic single domain (SSD) liquid crystal molecular switching behavior may be reasonable. However, there is one big question here. The question is "Is it possible to rotate over 45 degrees" in a smectic layer structure? As of today, this question has no rational answer yet. As discussed above, to give a rational answer to the question, it would be required intense local smectic layer structure analysis, specifically some dynamic layer structure change. Therefore, at this moment, only some speculation is given here. All of the speculation should be subjected to be verified with reasonable enough both empirical and theoretical evidences, though.

6. Necessity of further investigations

As discussed above, whether over 45° optical axis rotation is really happening or not is based on all assumption based on some indirect empirical results. Although they are all assumptions, there are some suggestive empirical results. **Figure 15** shows light leakage amount depending on applied pulse voltage strength at **Figure 9** type of crossed Nicole optical set-up measurement. As shown in **Figure 10**, when applied pulse voltage is relatively low such as 2 V for 2.4 μm gap, during zero voltage application time duration, the SSD-LC panel shows very low light leakage, which means most of liquid crystal molecular optical axis stays at the initial extinction position. However, when applied pulse voltage increased over ca. 4.5 V, suddenly the light leakage level increased. This indicates that voltage application

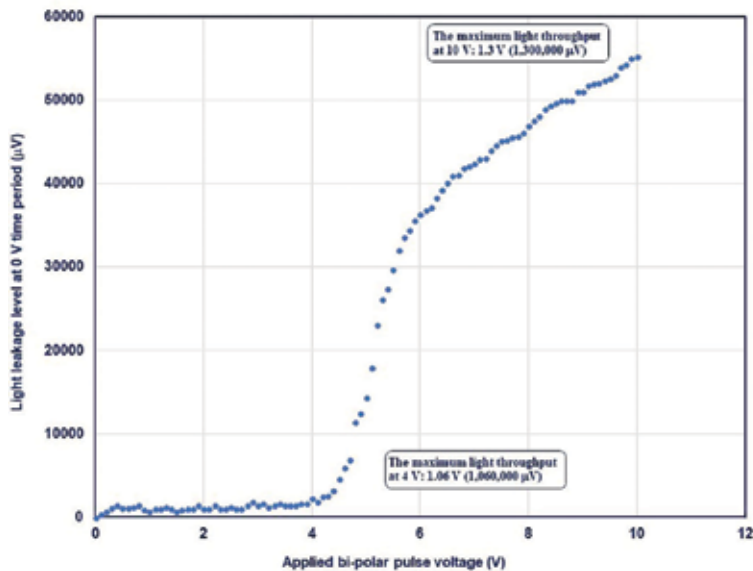


Figure 15. Light leakage level during zero-voltage application depending on pulse voltage strength of the SSD-LC panel. Up to ca. 4.5 V, light leakage level is very low, and over 4.5 V, light leakage shows significant increase by voltage increase. This pulse voltage dependence of light leakage level strongly suggests some influence on the initial liquid crystal optical axis position change.

to the SSD-LC panel induced some smectic layer structural change, resulting in no more initial extinction position at zero voltage duration. It looks like dependent on SSD-LC mixtures; some mixtures did not show reversible measurement result. This means that once over ca. 6 V pulse voltage was applied to 2.4 μm gap, the SSD-LC panel never showed the original very low light leakage. Some SSD-LC mixtures, however, showed reversible light leakage phenomenon even after higher voltage was applied. There are some potentially relevant research works to give some reasonable interpretation to above empirical results. One is very local smectic layer structure change by high voltage application. Iida et al. investigated local smectic layer structures of ferroelectric liquid crystal panels using Synchrotron radiation beam [40]. This research works clarified existence of narrow walls in a smectic layer structures. Such narrow walls might be possible interpretation of **Figure 15** result. Even the SSD-LC molecular optical axis stays at extinction position normal to the smectic layer, if for some reason, the smectic layer itself changes its structure, liquid crystal molecular optical axis is no more parallel to the incident linear polarized light, resulting in light leakage at zero voltage application duration. The other relevant possibility is giant-block twist grain boundary reported by Fernsler et al. [59] This possibility might be, however, relatively small, or righter in the SSD-LC case. Since most of SSD-LC panels, the initial alignment textures are quite clean, and there is no particular microscope level of visible size of defects. However, it might be possible having much smaller size of grain boundary structure than visible wavelength size.

A narrow wall and possible local twisted boundary effects might be fairly possible interpretation to understand **Figure 15** results. Moreover, why over 45° of SSD-LC molecular swing in the same orientation plane is possible with significant layer spacing shrink (if it really shrinks, though) is the question. It would be more intense research works not only local, but relatively large scale structures, but also much larger area of continuous theory deal might be necessary [60–63].

7. Concluding remarks

Smectic liquid crystals have been somewhat difficult to obtain clean molecular alignment for display and phase modulation devices purpose level of high static contrast ratio such as over 3000:1, and this difficulty would be one of the major reasons preventing from practical applications. The difficulty in uniform and clean molecular alignment might be mainly due to existence of smectic layer structure. Required well enough balance between healthy construction of smectic layer structure and surface anchoring needs somewhat tricky technique. However, at least in a certain type of smectic liquid crystals case, an initial liquid crystal molecular alignment is already equivalent from those of most of nematic liquid crystals. Still some specific difficulty remains that are not necessary to consider at most of nematic liquid crystal cases. Even if the initial liquid crystal molecular alignment is perfect, the remaining difficulty is if the initially obtained alignment is preserved by driving with externally applied electric field. One of the practical means to get rid of instability of smectic layer and molecular alignment has been clarified to use non-spontaneous, non-anisotropy of dielectric constant base driving torque. At this moment, however, it is not clear yet what is the real driving torque of SSD-LC cells except for some reasonable assumption of quadrupole momentum base. This remaining difficulty still needs further investigation. Regardless required further detail investigation, this series of investigations clarified possible in-plane only retardation switching. Moreover, such an in-plane only retardation switching also indicates over 45° molecular optical axis rotation. In-plane only retardation

switching with over 45° swing angles would provide a liquid crystal device new application field. Under the premise of smectic layer restriction, it would be required to give a reasonable interpretation why over 45° rotation is allowed.


This series of investigation may open both practical application opportunity of some smectic liquid crystal devices, specifically for fast response (~200 μs) in-plane only retardation switching devices, and fundamental research necessity to clarify nature of such smectic layer structures.

Author details

Akihiro Mochizuki
i-CORE Technology, LLC, USA

*Address all correspondence to: akihiros@i-coretechnology.com

IntechOpen

© 2018 The Author(s). Licensee IntechOpen. This chapter is distributed under the terms of the Creative Commons Attribution License (<http://creativecommons.org/licenses/by/3.0>), which permits unrestricted use, distribution, and reproduction in any medium, provided the original work is properly cited. 

References

- [1] Matsuda T, Nasuno T, Saito S. Occurrence condition of bistability in BTN-LCDs and a possibility of displaying gray scales. Digest of Technical Papers, AM-LCD 98, LC p-3. 1998. pp. 129-132
- [2] Kizu Y. Simulation of dynamic motion of inversion wall in TN-LCD cell with three-dimensional flow profile. Digest of Technical Papers, AM-LCD 98, LC p-4. 1998. pp. 133-136
- [3] Ikeno H, Oh-saki A, Nitta M, Ozaki N, Yokoyama Y, Nakaya K, et al. Electrooptic bistability of a ferroelectric liquid crystal device prepared using polyimide Langmuir-Blodgett orientation films. Japanese Journal of Applied Physics. 1989;27:L116-L119
- [4] Yang KH, Chieu TC. Dominant factors influence the bistability of surface-stabilized ferroelectric liquid crystal devices. Japanese Journal of Applied Physics. 1989;28:L1599-L1602
- [5] Ono K, Nakanowatari J. A method for the determination of the internal electric field of ion-doped ferroelectric liquid crystals. Japanese Journal of Applied Physics. 1991;30:L2832-L2838
- [6] Mochizuki A, Yoshihara T, Yoneda Y, Motoyoshi K, Kobayashi S. Elimination of crosstalk in highly multiplexed STN-LCDs by using conductive orientation films. Proceedings of the SID. 1990;31/4:327-332
- [7] Seitz T, Stelzer J, Trebin H-R. Switching of surface-stabilized ferroelectric liquid crystal cells by motion of defects. Journal of Applied Physics. 1996;80(3):1381-1389
- [8] Saishu T, Takatoh K, Lida R, Nagata H, Mori Y. Voltage-holding properties of thresholdless antiferroelectric liquid crystals driven by active matrices. In: SID (Symposium for Information Display) 96 Digest. 1996. pp. 703-706
- [9] Patel JS. Ferroelectric liquid crystal modulator using twisted smectic structure. Applied Physics Letters. 1992;60(3):280-282
- [10] Mochizuki A, Yoshihara T, Motoyoshi K, Kobayashi S. An electrical bilayer model of the transient current in a nematic liquid crystal cell. Japanese Journal of Applied Physics. 1990;29:L322-L325
- [11] Mochizuki A, Motoyoshi K, Kobayashi S. A ferroelectric layer in a cell containing a polar molecular mixture in nematic and isotropic phases. Japanese Journal of Applied Physics. 1990;29(10):L1898-L1900
- [12] Mochizuki A, Makino T, Shiroto H, Kiyota Y, Yoshihara T. Threshold properties of SSFLC in terms of polarization structure. Molecular Crystals and Liquid Crystals. 1997;303:391-401
- [13] Mochizuki A, Sotoyama W, Tatsuura S, Ishitsuka T, Motoyoshi K, Kobayashi S. Second-harmonic generation from an interfacial layer between orientation films and liquid crystal layers of nematic liquid crystal cell. Japanese Journal of Applied Physics. 1991;30(3B):L504-L506
- [14] Clark NA, Lagerwall ST. Submicrosecond bistable electro-optic switching in liquid crystals. Applied Physics Letters. 1980;36:899-901
- [15] Yamamoto J, Yamashita M, Inaba R, Takamoto K, Takanishi Y, Sakatsuji W, et al. Principle and design for the slippery interface. In: 27th ILCC (International Liquid Crystal Conference). Vol. 2-B1-15. 2018

- [16] Bryan-Brown GP, Wood EL, Sage IC. Weak surface anchoring of liquid crystals. *Nature*. 1999;**399**:338-340
- [17] Garoff S, Meyer RB. Electroclinic effect at the A-C phase change in a chiral smectic liquid crystal. *Physical Review Letters*. 1977;**38**:848-851
- [18] Meyer RB, Pelcovits RA. Electroclinic effect and modulated phases in smectic liquid crystals. *Physics Review*. 2002;**65**:061704-1-061704-7
- [19] Selinger JV, Collings PJ, Shashidhar R. Field-dependent tilt and birefringence of electroclinic liquid crystals: Theory and experiment. *Physical Review E*. 2001;**64**:061705-1-061705-5
- [20] Langer SA, Sethna JP. Textures in a chiral smectic liquid-crystal film. *Physical Review A*. 1986;**34**:5035-5046
- [21] Hinshaw GA, Petschek RG, Pelcovits RA. Modulated phases in thin ferroelectric liquid-crystal film. *Physical Review Letters*. 1988;**60**:1864-1867
- [22] Hinshaw GA, Petschek RG. Transitions and modulated phases in chiral tilted smectic liquid crystals. *Physical Review A*. 1989;**39**:5914-5926
- [23] Gorecka E, Glogarova M, Lejoek L, Sverenyak H. Periodic in-layer director modulations responsible for the stripe texture formation in chiral smectic-C phase. *Physical Review Letters*. 1995;**75**:4047-4050
- [24] Matkin LS, Watson SJ, Gleeson HF, Pindak R, Pitney J, Barois P, et al. Resonant x-ray scattering study of the antiferroelectric and ferroelectric phases in liquid crystal devices. *Physics Review*. 2001;**E64**:021705-1-021705-5
- [25] Matkin LS, Gleeson HF, Mach P, Huang CC, Pindak R, Srajer G, et al. Resonant X-ray scattering at the Se edge in liquid crystal free-standing films and devices. *Applied Physics Letters*. 2000;**76**:1863-1865
- [26] Crandall KA, Tripathi S, Rosenblatt C. Surface-mediated electroclinic effect in a chiral nematic liquid crystal. *Physical Review A: Rapid Communications*. 1992;**46**:R715-R718
- [27] Gregory ZL, Lisi AD, Petschek RG, Rosenblatt C. Nematic electroclinic effect. *Physical Review A*. 1990;**41**:1997-2004
- [28] de Vries A, Ekachai A, Spielberg N. Why the molecules are tilted in all smectic A phases, and how the layer thickness can be used to measure orientational disorder. *Molecular Crystals and Liquid Crystals*. 1979;**49**:143-152
- [29] Clark NA, Bellini T, Shao RF, Coleman D, Bardon S, Link DR, et al. Electro-optic characteristics of de vries tilted smectic liquid crystals: Analog behavior in the smectic A* and smectic C* phases. *Applied Physics Letters*. 2002;**80**:4097-4099
- [30] Saunders K. de Vries behavior of the electroclinic effect in the smectic-A* phase near a biaxiality-induced smectic-A*-smectic-C* tricritical point. *Physical Review*. 2009;**E80**:011703-1-011703-16
- [31] Lagerwall JPE, Giesselmann F, Radcliffe MD. Optical and x-ray evidence of the “de Vries” Sm-A*-Sm-C* transition in a non-layer-shrinkage ferroelectric liquid crystal with very weak interlayer tilt correlation. *Physics Review*. 2002;**E66**:031703-1-031703-10
- [32] Manna U, Song JK, Panarin YP, Fukuda A, Vij JK. Electro-optic and dielectric study of the de Vries-type smectic-A* phase exhibiting transitions to smectic-CA* and smectic-C* phases. *Physics Review*. 2008;**E77**:041707-1-041707-11

- [33] Hayashi N, Kocot A, Lineham MJ, Fukuda A, Vij JK, Heppke G, et al. Experimental demonstration, using polarized Raman and infrared spectroscopy, that both conventional and de Vries smectic-A phases may exist in smectic liquid crystals with a first-order-A-C* transition. *Physics Review*. 2006;**E74**:051706-1-051706-11
- [34] Oton JM, Quintana X, Castillo PL, Lara A, Urruchi V, Bennis N. Antiferroelectric liquid crystal displays. *Opto-Electronics Review*. 2004;**12**(3):263-269
- [35] Coleman DA. Polarization-modulated smectic liquid crystal phases. *Science*. 2003;**301**:1204-1205
- [36] O'Callaghan MJ. Switching dynamics and surface forces in thresholdless 'V-shaped' switching ferroelectric liquid crystals. *Physical Review E*. 2003;**67**:011710
- [37] Yoshida T, Tanaka T, Ogura J, Wakai H, Aoki H. A full-color thresholdless antiferroelectric LCD exhibiting wide viewing angle with fast response time. In: *SID'97 International Symposium Digest*. SID (Symposium for Information Display). Vol. 28. 1997. pp. 841-844
- [38] Nishiyama I. Antiferroelectric liquid crystals. *Advanced Materials*. 1994. DOI: 10.1002/adma.19940061215
- [39] Gouda F, Sarp K, Lagerwall ST. Dielectric studies of the soft mode and goldstone mode in ferroelectric liquid crystals. *Ferroelectrics*. 1991;**113**:165-206
- [40] Iida A, Noma T, Miyata H. Characterization of the local layer structure of a narrow wall in a surface stabilized ferroelectric liquid crystal using synchrotron X-ray micro-diffraction. *Japanese Journal of Applied Physics*. 2001;**40**:1345-1351
- [41] Reiker TP, Clark NA, Smith GS, Parmer DS, Sirota EB, Safinya CR. Chevron local layer structure in smectic surface-stabilized ferroelectric smectic-C cells. *Physical Review Letters*. 1987;**59**:2658-2661
- [42] Clark NA, Coleman D, MacLennan JE. Electrostatic and the electro-optic behavior of chiral smectic C: 'Block' polarization screening of applied voltage and 'V-shaped' switching. *Liquid Crystals*. 2000;**27**:985-991
- [43] Srajer G, Pindak R, Patel JS. Electric-field-induced layer reorientation in ferroelectric liquid crystals: An X-ray study. *Physical Review A*. 1990;**43**:5744-5748
- [44] Morse AS, Gleeson HF, Cummings S. Time resolved X-ray diffraction studies of electric field induced layer motion in a chevron geometry smectic A liquid crystal device. *Liquid Crystals*. 1997;**23**:717-722
- [45] Dierking I, Mitov M, Osipov MA. Smectic layer instabilities in liquid crystals. *The Royal Society of Chemistry, Soft matter, Review*. 2015;**10**:1039
- [46] Terada M, Yamada S, Katagiri K, Yoshihara S, Kanbe J. Static and dynamic properties of chevron uniform FLC. *Ferroelectrics*. 1993;**149**:283-294
- [47] Hartmann WJAM. Charge-controlled phenomena in the surface-stabilized ferroelectric liquid crystal structure. *Journal of Applied Physics*. 1989;**66**(3):1132-1136
- [48] Mochizuki A. An introduction to PSS-LCDs: A fast-optical-response smectic LCD. *Journal of the SID*. 2006;**14**(6):1-6
- [49] Mochizuki A. Fundamental performance of PSS-LCDs. In:

Proceedings of 13th IDW (International Display Workshop). 2008. pp. 1547-1550

[50] Mochizuki A. A fast response smectic LCD using induced polarization. *Journal of Information Display*. 2005;**6**(3):6-11

[51] US Patent No. USP. Federal Government of the United States of America. 5,169,556

[52] US Patent No. USP. 5,348,685

[53] Takanishi Y, Ouchi Y, Takezoe H, Fukuda A, Mochizuki A, Nakatsuka M. Spontaneous formation of quasi-bookshelf layer structure in new ferroelectric liquid crystals derived from a naphthalene ring. *Japanese Journal of Applied Physics*. 1990;**29**:L984-L986

[54] Kataoka S, Taniguchi Y, Iimura Y, Kobayashi S, Hasebe H, Takatsu H. Liquid crystalline polymer stabilized FLCs with conventional rubbed films or photo alignment films of poly (vinyl cinnamate). *Molecular Crystals and Liquid Crystals*. 1997;**292**:333-343

[55] Fujisawa T, Nishiyama I, Katsusaka K, Kobayashi S. Field sequential full color LCDs using polymer stabilized V-shaped ferroelectric liquid crystal. *Ferroelectric*. 2008;**363**:78-85

[56] Kikuchi H, Yokota M, Hisakado Y, Yang H, Kajiyama T. Polymer-stabilized liquid crystal blue phases. *Nature Materials*. 2002;**1**:64-68

[57] Mochizuki A. Molecular tilting effect on smectic liquid crystal sub-phase stability from its retardation switching behavior. *Journal of Molecular Liquids* (in print). 2018. DOI: 10.1016-2017.12.117 0167-7322

[58] Mochizuki A. In-plane only retardation switching by certain type of smectic liquid crystal panels. *Proceedings of SPIE*. 2018;**10555**:1055517-1-1055517-9

[59] Fernsler J, Hough L, Shao R, Maclennan JE, Navailles L, Brunet M, et al. Giant-block twist grain boundary smectic phases. *Proceedings of the National Academy of Sciences*. 2005;**102**(40):14191-14196

[60] Carlsson T, Stewart IW, Leslie FM. Theoretical studies of SmC liquid crystals confined in a wedge. *Liquid Crystals*. 1991;**9**:661-678

[61] Leslie FM, Gill SPA. Some topic from continuum theory for SmC liquid crystals. *Ferroelectrics*. 1993;**148**:11-24

[62] Stewart IW, Leslie FM, Nakagawa M. Smectic liquid crystals and the parabolic cyclides. *Quarterly Journal of Mechanics and Applied Mathematics*. 1994;**47**:511-525

[63] McKay G, Leslie FM. A continuum theory for smectic liquid crystals allowing layer dilation and compression. *European Journal of Applied Mathematics*. 1997;**8**:273-280

The Photorefractive Effect in Liquid Crystals

*Takeo Sasaki, Khoa Van Le, Yumiko Naka
and Takafumi Sassa*

Abstract

This chapter summarizes the state of the art of research regarding photorefractive liquid crystals. Photorefractive effect is of interest because it can be used to obtain dynamic holograms, based on interference between dual laser beams within a liquid crystal to generate a refractive index grating. This technique can be employed in numerous diffraction optics applications, such as optical amplifiers, phase-conjugate wave generators, 3D displays, novelty filters, and optical tomography. The photorefractive effect in liquid crystals is especially pronounced, and both ferroelectric and nematic liquid crystals have been researched for this purpose, with the former showing special promise in practical applications. As an example, ferroelectric liquid crystals have been found to readily produce a refractive index grating in conjunction with a significant gain and a formation time of 900 ms.

Keywords: photorefractive effect, hologram, photoconductivity, nonlinear optics, optical amplification

1. Introduction

Photorefractive effect is a nonlinear optical phenomenon by which the refractive index of a medium can be modified. This effect can be used to produce rewritable, dynamic (that is, temporal) holographic images [1, 2]. Associated applications include the production of phase-conjugate beams and the amplification of optical signals. There are numerous potential uses of this effect in optical devices, such as in the fabrication of electrical transistors. As an example, the photorefractive phenomenon can result in the appearance of both electro-optic and photovoltaic properties in optically transparent materials. Numerous such substances have been reported, including organic molecular crystals, inorganic ferroelectric photoconductive crystals, amorphous organic photoconductive materials, photoconductive liquid crystals (LCs), photoconductive amphiphilic compounds, and photoconductive organic polymers [3–5]. Among these, organic compounds tend to have the shortest response times and greatest photorefractivity values, and hence these are of special interest [6]. Both electro-optic and photovoltaic mechanisms contribute to variations in refractive index that are associated with the photorefractive effect (**Figure 1**). The separation of photo-induced charges in a photorefractive substance and associated refractive index variations resulting from the electro-optic effect can produce a refractive index grating. The application of an electric field to such devices can also enhance the efficiency of charge generation. Photoconductive

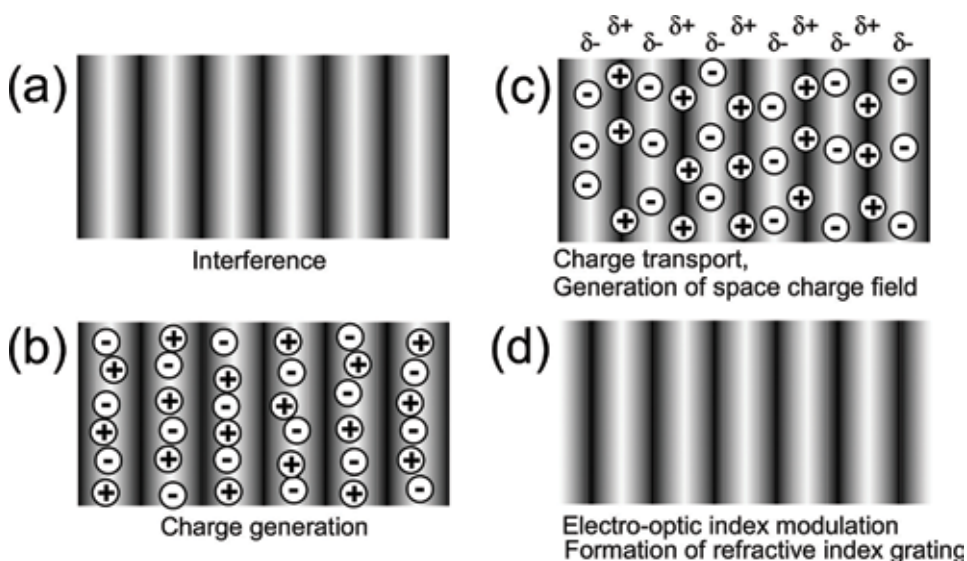


Figure 1.

A diagram summarizing the photorefractive effect mechanism. (a) Dual laser beams undergo interference in a photorefractive compound; (b) charges are produced at the light regions associated with interference fringes; (c) trap sites in the light regions hold electrons, while hole migration occurs via drift or diffusion due to an external electric field, such that an internal electric field is produced between the dark and light regions; and (d) the refractive index in specific areas is modified as a result of the internal electric field.

glassy polymers containing high levels of D- π -A chromophores (comprising π -conjugated systems with both donor and acceptor moieties) tend to exhibit especially high photorefractivity [3–7]. These materials have been suggested for use in 3D displays, real-time edge enhancement, and holographic interferometry [7]. Nevertheless, it remains necessary to reduce the electric field values of 30–50 V/ μm that must be applied to activate photorefractivity, as well as to improve the sluggish response times of these materials (approximately 100 ms). LCs, which are essentially in the liquid state and thus can be driven by the application of lower electric fields, have also been investigated with regard to their photorefractive properties [7]. Nematic LCs were reported to show photorefractivity in 1994 [8], and this effect was especially pronounced when the compounds were subjected to a low electric field (several V/ μm) [9]. Surface-stabilized ferroelectric liquid crystals (SS-FLCs) combined with photoconductive materials have also shown photorefractivity [10, 11]. Ferroelectric liquid crystals (FLCs) have a layered helical structure [12, 13] in conjunction with a chiral smectic C (SmC*) phase. Interestingly, these materials only exhibit ferroelectricity in the form of thin films (several μm in thickness) [12]. When such films are contained between the glass plates, the SmC* phase helix uncoils to generate a surface-stabilized (SS) state that shows spontaneous polarization (Ps) (**Figure 2**). Typically, a film thickness of 2 μm is employed for practical applications, such that the FLC molecules are forced into a two-dimensional SS alignment, the direction of which varies with the Ps direction (**Figure 3**). Applying an alternating electric field to the film results in an ongoing back-and-forth motion of the molecules on a time scale of less than 1 ms. The electric field determines the Ps direction, which in turn affects the properties of the film. An internal electric field can also modify the Ps direction in SS-FLCs, and **Figure 4** presents a diagram showing the photorefractive effect mechanism in an FLC. The interference between laser beams in an FLC mixed with a photoconductive material results in an internal electric field due to charge separation between dark and light regions. This field modifies the Ps direction between the dark and light locations within the

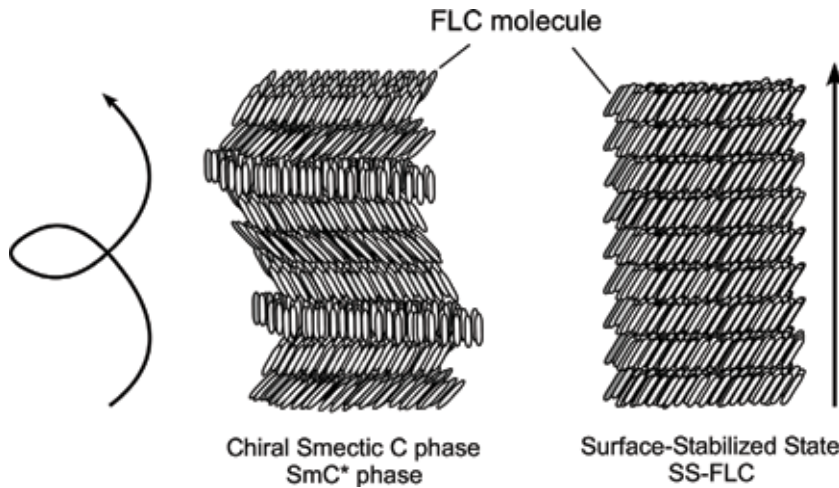


Figure 2.
SmC phase and SS state (SS-FLC) structures.

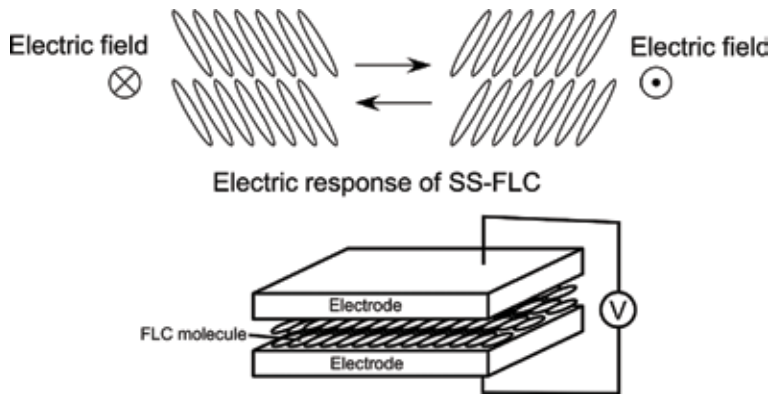


Figure 3.
Electro-optical switching of an FLC in the SS state.

interference fringes, which in turn produces periodic variations in the FLC molecular orientation. Whereas in some organic photorefractive materials there is a bulk polarization response to the internal electric field, in the case of an FLC there is a molecular dipole response. Thus, the exceptionally rapid FLC molecular switching is a consequence of the bulk polarization response.

1.1 Characteristics of the photorefractive effect

The photorefractive effect induces variations in refractive index between the dark and light points in interference fringes. As a result, the refractive index grating phase is moved away from these fringes. In the case that one photogenerated charge is not moved from the light region, the magnitude of this shift is $\pi/2$. If a substance exhibits photochemical activity but not photorefractivity, the phasing of the resulting refractive index grating is equivalent to that of the interference fringes because only a photochemical reaction takes place at the light regions (**Figure 5a**), and this grating diffracts the laser beams. In the case that the interfering beams have the same intensity, symmetric diffraction is obtained and so there is no change in the transmission intensities of the beams. As shown in the figure, beams 1 and 2 are diffracted toward each other. In contrast, if a photorefractive material is employed,

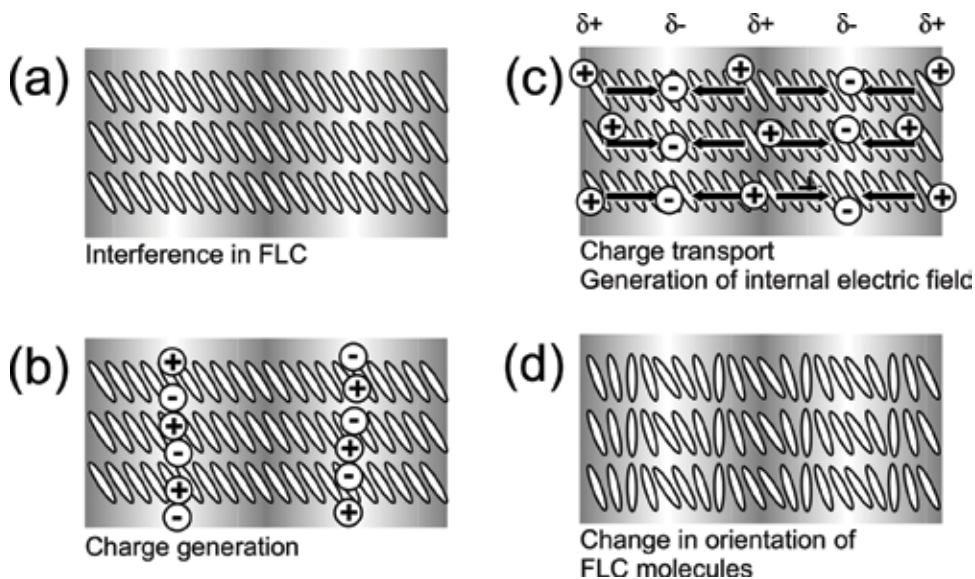


Figure 4. A diagram showing the FLC photorefractivity mechanism. (a) Dual laser beams undergo interference in a mixture of an FLC in the SS state with a photoconductive compound; (b) charge generation takes place within the light regions of the interference fringes; (c) trap sites in the light regions hold electrons, while holes move via drift or diffusion due to an external electric field, producing an internal electric field between the dark and light zones; (d) the spontaneous polarization vector orientation (that is, the mesogen orientation in the FLC) is modified by the internal electric field.

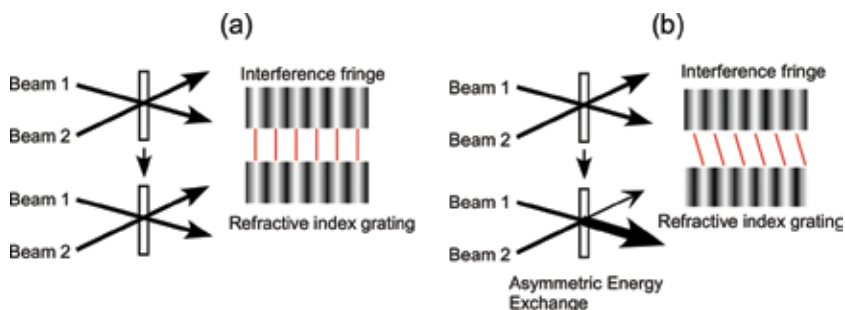


Figure 5. Diagrams of refractive index grating formations. (a) Photochromic and (b) photorefractive gratings.

there is a phase shift of the grating relative to the fringes that modifies both beams. Specifically, both beams undergo energetic coupling such that beams 1 and 2 become less and more intense, respectively (**Figure 5b**). This amplification of one beam by the second beam as a result of dual-beam coupling is referred to as asymmetric energy exchange [3]. The appearance of this phenomenon, which can be applied to numerous optical devices, is characteristic of a photorefractive material.

1.2 Evaluation of photorefractivity

Dual-beam coupling is often used to assess the appearance of photorefractivity. In this technique, two beams are obtained from a p-polarized laser beam, using a beam splitter, and these beams interfere with one another inside a film specimen to which a high-voltage electric field has been applied to enhance charge generation. Variations in the intensity of the transmitted beam are tracked, and photorefractive substances will exhibit asymmetric energy exchange. The gain coefficient is

determined from changes in the beam intensity due to dual-beam coupling, and is used to communicate the magnitude of the photorefractivity. As a prerequisite to calculating this term, it is necessary to ascertain whether Bragg or Raman-Nath diffraction occurs, based on the dimensionless parameter Q , calculated as:

$$Q = 2\pi\lambda L/n\Lambda^2. \quad (1)$$

Specifically, a Q value greater than 1 indicates Bragg diffraction. In such cases, only a single diffraction order is obtained as multiple scattering does not take place. In contrast, a Q value less than 1 is associated with Raman-Nath diffraction involving numerous diffraction orders. Q values in excess of 10 ensure that solely Bragg diffraction occurs. The dual-beam coupling gain coefficient, Γ [cm^{-1}], can be calculated using the equation:

$$\Gamma = \frac{1}{D} \ln \left(\frac{gm}{1+m-g} \right) \quad (2)$$

Here, $D = L/\cos(\theta)$ is the signal beam interaction path (where L is the sample thickness and θ is the angle of beam propagation in the sample), g is the signal beam intensity behind the sample with the pump beam ratioed to that without, and m is the pump/signal intensity ratio in front of the sample [1–3].

2. Photorefractive effect of FLCs

2.1 Two-beam coupling experiments with FLCs

Research regarding the photorefractivity of commercial FLCs combined with photoconductive materials began circa 2000 [10, 11] and was continued by Sasaki et al. and Golemme et al. [7, 14]. This prior experimental work was based on dual-beam coupling trials incorporating a 488-nm Ar^+ laser, employing the photoconductive materials presented in **Figure 6** along with SCE8 (Clariant, SmC^* at 60°C , SmA at 80°C , N^* at 104°C , $\text{Ps} = 4.5 \text{ nC}/\text{cm}^2$), a combination of chiral and LC compounds, such as the FLC. In these trials, a mixture of the FLC with trinitrofluorenone (TNF, 0.1 wt.%) and carbazole diphenylhydrazone (CDH, 2 wt.%) was injected into a 10- μm gap in a glass cell having an alignment layer composed of polyimide and 1 cm^2 indium tin oxide electrodes (**Figure 7**). The typical asymmetric energy exchange obtained upon applying a 0.1 $\text{V}/\mu\text{m}$ DC electric field to an FLC (SCE8)/CDH/TNF specimen is presented in **Figure 8** [15]. In these trials, one beam exhibited enhanced transmittance while the other showed reduced intensity following interference within the FLC, resulting in symmetric variations in the transmitted intensities. These results demonstrate that a refractive index grating was

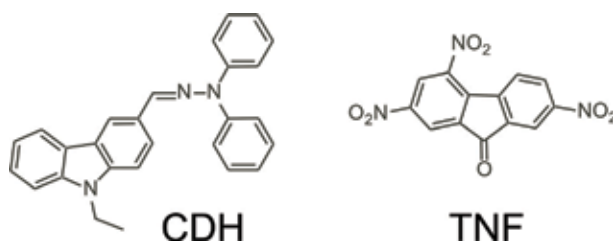


Figure 6. Molecular structures of the photoconductive chemical CDH and the sensitizer (that is, electron trap) TNF.

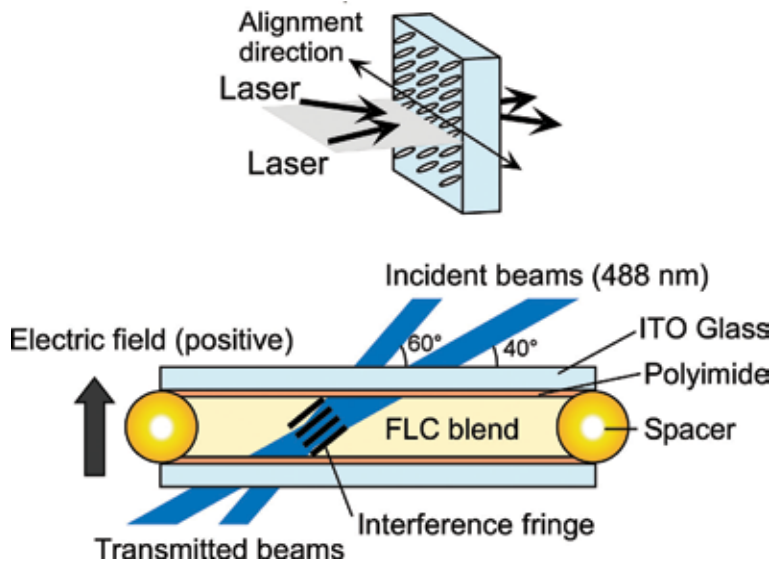


Figure 7.
The structure of an LC cell and the associated laser beam incidence.

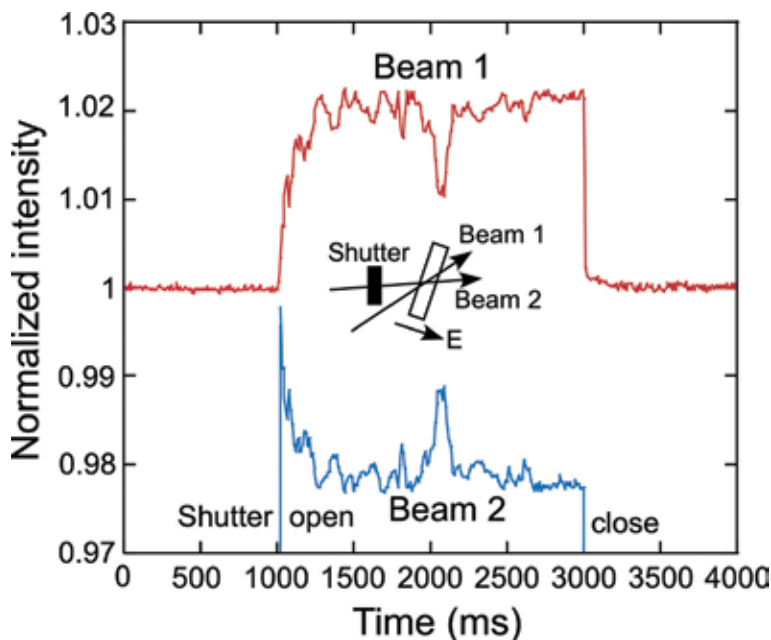


Figure 8.
A typical asymmetric energy exchange obtained within the FLC SCE8 when combined with 2 wt.% CDH and 0.1 wt.% TNF and having an applied electric field of $+0.3 \text{ V}/\mu\text{m}$.

generated at the interference fringes in conjunction with a phase shift. This grating was associated with Bragg diffraction, without any higher-order diffractions.

Figure 9a summarizes the effects of temperature on the gain coefficient of SCE8 containing 0.1 and 2 wt.% TNF and CDH, respectively. In this system, temperatures less than 46°C were required to realize asymmetric energy exchange. **Figure 9b** plots the effects of temperature on the spontaneous polarization of an equivalent specimen and demonstrates a loss of polarization at the same temperature. These data demonstrate that the sample had to be within the SmC^* phase temperature

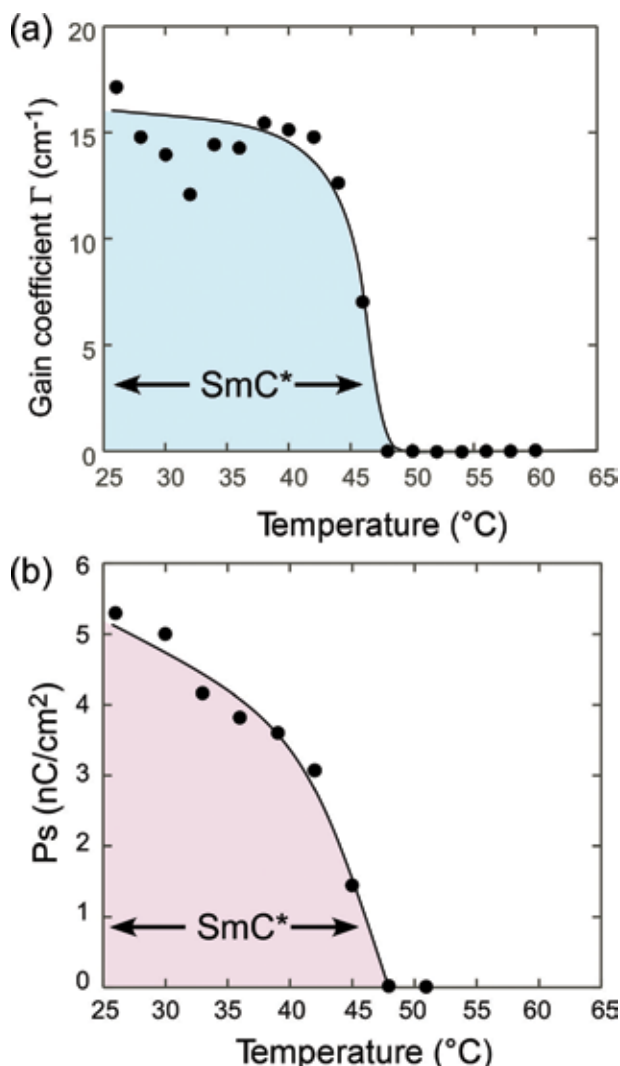


Figure 9. The effect of temperature on (a) the gain coefficient and (b) the spontaneous polarization of the FLC SCE8 when combined with 2 wt.% CDH and 0.1 wt.% TNF. During these dual-beam coupling trials, a 0.1 V/ μm electric field was applied.

range (that is, it had to exhibit ferroelectric properties) for the asymmetric energy exchange to appear. An FLC in the N* or SmA phase cannot undergo significant variations in molecular axis orientation in response to an internal electric field because the molecular dipole moments are perpendicular to the molecular axis and have small magnitudes. In contrast, an internal electric field can result in spontaneous polarization associated with dipole reorientation in the SmC* phase. The spontaneous polarization also causes the orientation of FLC molecules in the corresponding area to change accordingly. The data show that this specimen exhibited a maximum resolution of 0.8 μm [15].

2.2 Effect of the applied electric field strength on the gain coefficient

The external applied electric field strength has a significant effect on photorefractive polymers and acts to promote photorefractivity by enhancing the efficiency of charge separation. Several tens of volts per μm are necessary, and so a

typical film thickness of 100 μm requires several kilovolts. However, much weaker fields can induce photorefractivity in FLCs. As an example, an SCE8 film will exhibit its largest possible gain coefficient in conjunction with a field strength in the range of 0.2–0.4 $\text{V}/\mu\text{m}$. As such films are often 10- μm thick, a field of just several volts is sufficient. **Figure 10** plots the effect of the electric field strength on the gain coefficient for an FLC(SCE8)/CDH/TNF specimen. SCE8 containing 0.5–1 wt.% CDH exhibited a coefficient that increased along with the field strength, while the addition of 2 wt.% CDH resulted in a lower coefficient at field strengths above 0.4 $\text{V}/\mu\text{m}$. Increasing the field strength to 0.2 $\text{V}/\mu\text{m}$ promoted the generation of an oriented grating due to charge separation, but zigzag defects became evident in the SS state at higher field values, which would be expected to lower the gain coefficient due to light scattering. As of 2004, the gain coefficients reported for FLC-based specimens were significantly lower [15] than those obtained for certain polymers.

2.3 The effect of applied electric field strength on response time

Both charge separation and reorientation are associated with refractive index grating formation. Both of these processes help determine the time required to form the index grating, meaning the photorefractivity response time, and can potentially determine the rate of formation. A simple single-carrier photorefractivity model was employed to assess the time required for the formation of a refractive index grating in SCE8 [1, 2], incorporating an exponential gain transient. A single exponential function was used to fit the increases in the diffraction beam signal, written as:

$$\gamma(t)-1 = (\gamma-1)[1-\exp.(-t/\tau)]^2. \quad (3)$$

Here $\gamma(t)$ is the intensity of the transmitted beam at time t ratioed to the initial intensity (that is, $\gamma(t) = I(t)/I_0$), while τ is the time required for grating formation. **Figure 11** plots the effect of the external electric field strength on the formation

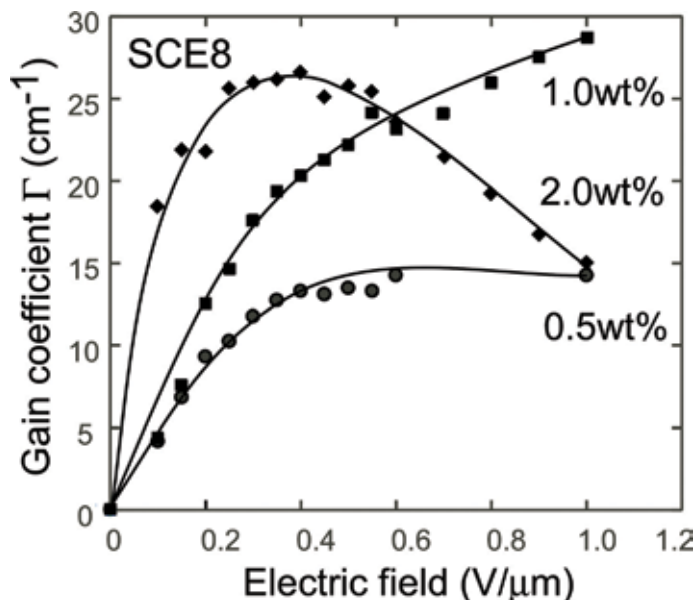


Figure 10. The effect of electric field strength on the gain coefficient of the FLC SCE8 when combined with CDH at various concentrations and 0.1 wt.% TNF at 30°C in a cell having a 10- μm gap.

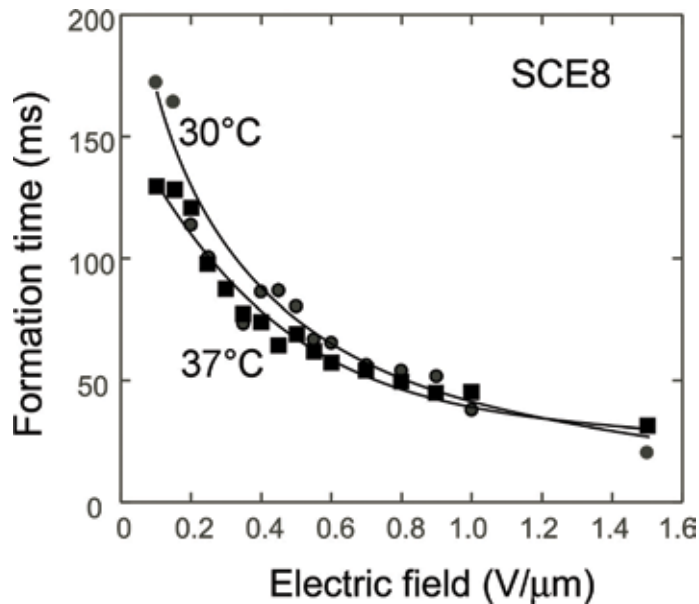


Figure 11.
The effect of electric field on the index grating formation time of the FLC SCE8 when combined with 2 wt.% CDH and 0.1 wt.% TNF in a dual-beam coupling trial. Legend: ● = data acquired at 30°C ($T/T_{SmC^} - SmA = 0.95$); ■ = data acquired at 36°C ($T/T_{SmC^*} - SmA = 0.97$).*

time for an SCE8/CDH/TNF sample and demonstrates that raising the field strength reduces the formation time, as a consequence of more efficient charge generation. Elevated temperatures also shorten the formation time, due to the lower viscosity of the material. At 30°C, the SCE8 exhibited a response time of 20 ms, which is much shorter than the typical 100 ms time span observed for polymers [7].

3. Photorefractive FLC blends

3.1 Pronounced photorefractivity of FLC blends doped with photoconductive chiral compounds

Prior to 2011, FLCs in the SS state tended to contain defects when combined with photoconductive materials. These defects reduced the photoreactivity of the mixtures due to scattering of the laser beam, and so new photorefractive FLC mixtures were researched, based on the synthesis of chiral photoconductive additives and subsequent mixing with SmC LCs. **Figure 12** shows one such blend based on an FLC [16]. In this case, the chiral photoconductive compound 3T-2 MB was added to an SmC LC together with TNF as a sensitizer, and the resulting dual-beam coupling signal acquired at 30°C is presented in **Figure 13**. Pronounced coupling was obtained in these trials, such that greater than 40% of the energy of the first laser beam was absorbed by the second beam when using a 10- μm -thick FLC film. **Figure 14a** summarizes the effect of the electric field strength on the gain coefficients. These data demonstrate that a low field strength of 1.9 $\text{V}/\mu\text{m}$ resulted in a gain coefficient in excess of 1200 cm^{-1} in the case of the 10 wt.% specimen. Relative to the values for FLCs in Section 2.2, this represents a 45-fold increase, and is ascribed to both the greater photoconductivity of this mixture and its improved transparency. In the case of photorefractive applications, the ability to induce photorefractivity in an FLC using only a low electric field is beneficial. **Figure 14b**

shows that increasing the field strength also reduced the response time, by providing more efficient charge separation, with a field strength of $1.9 \text{ V}/\mu\text{m}$ giving a formation time less than 1 ms. Both this rapid response and significant gain would assist in realizing applications such as distance measurement devices and real-time image amplifiers.

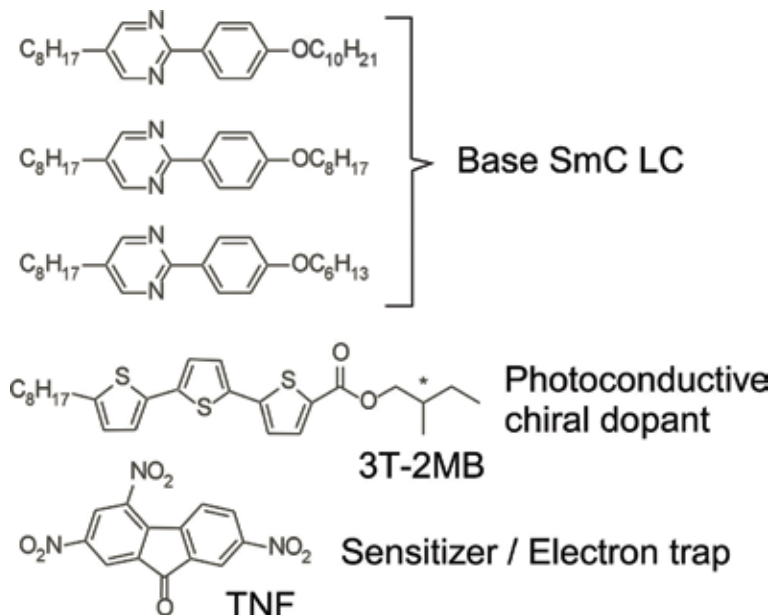


Figure 12.
A photorefractive FLC sample combined with a ternary mixture of smectic LCs.

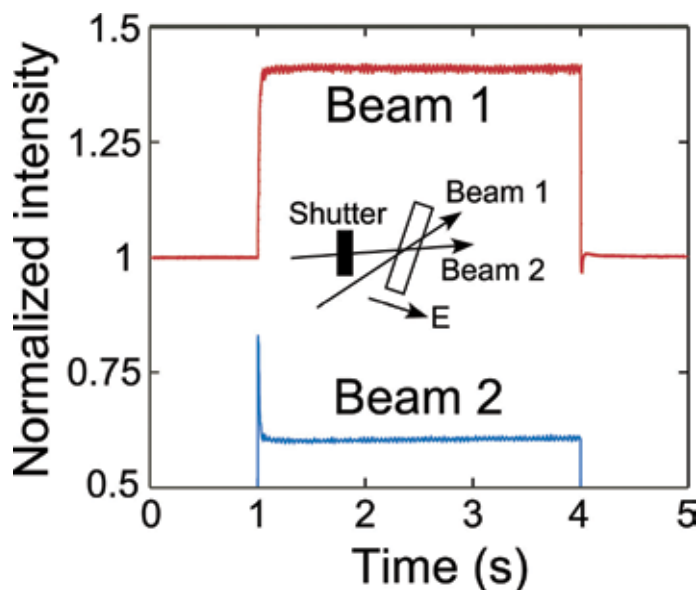


Figure 13.
Typical data obtained at 30°C from dual-beam coupling trials using a mixture of a base LC, 3T-2 MB, and TNF.

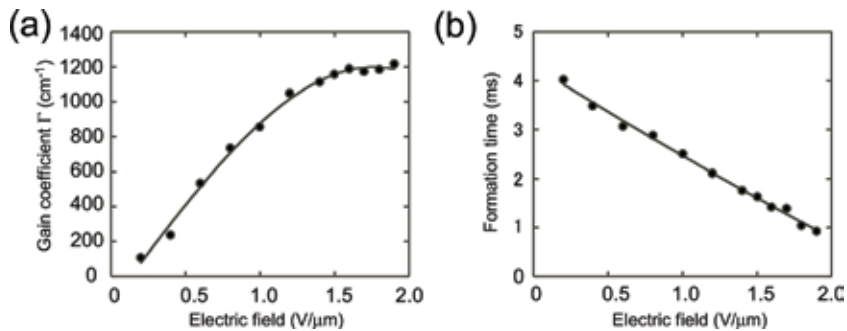


Figure 14. (a) The effect of electric field on the gain coefficients of mixtures of a base LC, 3T-2 MB (2–10 wt.%), and TNF (0.1 wt.%) at 30°C. (b) The formation times for refractive index gratings (that is, response times) for these same mixtures at 30°C.

3.2 Formation of dynamic holograms in FLC blends

A photorefractive FLC mixture has been demonstrated to form a dynamic hologram [17], such that a spatial light modulator (SLM) could be used to display a computer-generated animation. In this prior work, the SLM was exposed to a diode-pumped solid-state (DPSS) laser beam (at 488 nm) such that the FLC received the reflected beam. This beam underwent interference with a reference beam in the FLC and a refractive index grating based on Raman-Nath diffraction was generated. In other trials, a He-Ne laser beam (at 633 nm) was applied to the FLC to produce diffraction and a moving animation was generated in the diffraction (see **Figure 15**). Because image retention was not observed, the holographic image (that is, the refractive index grating) in the FLC was evidently rewritten at a rate sufficient to adequately reproduce the movie.

3.3 Dynamic amplification of optical images in photorefractive FLC blends

The photorefractive phenomenon has an obvious application in the amplification of optical signals, and this is a vital component of various optical techniques. This effect permits selective amplification, in contrast to the more well-known effects associated with lasers and nonlinear optics. Because photorefractivity results in the generation of a hologram in a material, a particular light signal can be distinguished from other signals on the basis of variations in phase, polarization, and wavelength. As an example, a photorefractive FLC mixture has demonstrated the ability to dynamically amplify a moving optical signal [16]. In this work, a rotating image (30 fps) was shown on an SLM via irradiation with a 473-nm beam such that the FLC was irradiated by the reflected beam, followed by interference with a pump beam. In these trials, amplification of the laser beam carrying the moving image was accomplished using the incident pump beam (**Figure 16**) and the signal beam intensity was increased by a factor of six. These data demonstrate that the speed of the photorefractive FLC response was such that the moving image could be amplified. It should be noted that this would not have been possible based on the average response time of a photorefractive polymer (about 100 ms). In such cases, the still image would be amplified, but not the moving image intensity.

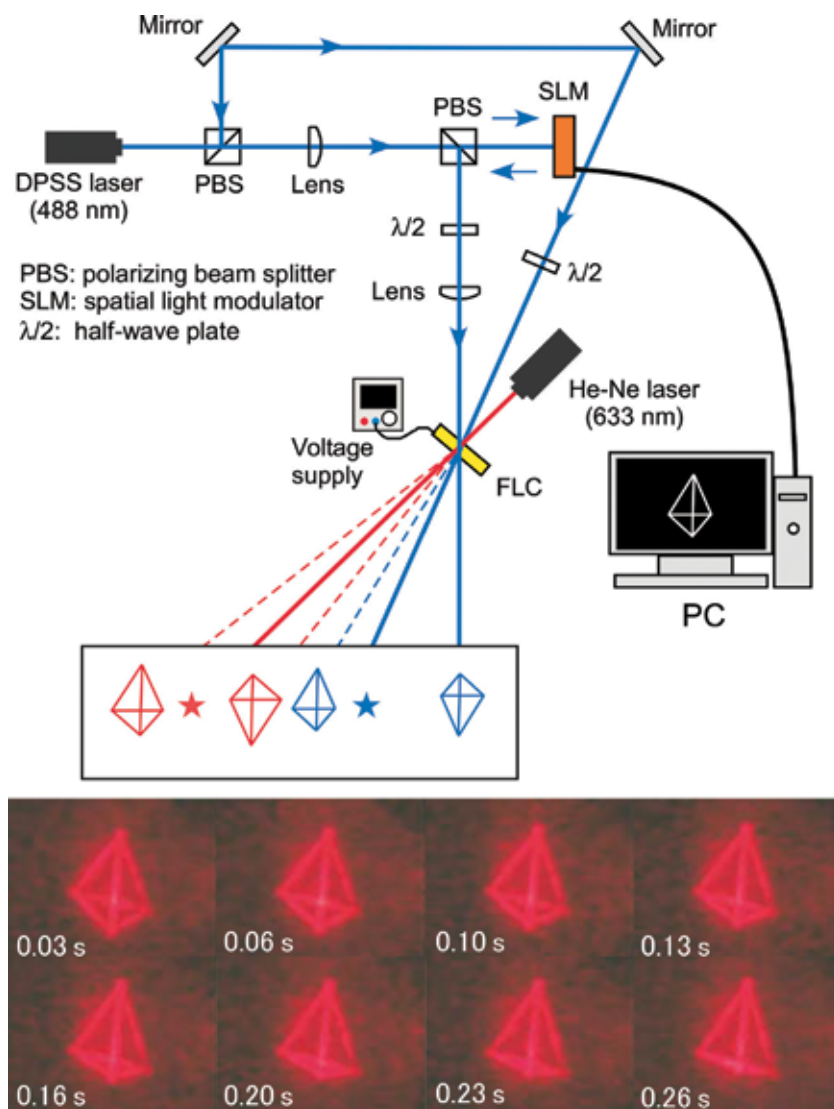


Figure 15. The formation of a dynamic hologram using an FLC, displaying a computer-generated animation on the SLM. Here, the SLM modulates the 488-nm object beam that irradiates the FLC and interferes with a reference beam. A 633 -nm readout beam irradiates the FLC to generate diffraction.

3.4 Photochemical durability of photorefractive ferroelectric liquid crystal blends with chiral terthiophene photoconductive dopants

There has been research regarding the robustness of photorefractive FLC mixtures with chiral terthiophene photoconductive additives [18], and **Figure 17** plots the gain coefficient of a blend with 3T-2 MB against irradiation time. These data demonstrate a rapid drop in the gain coefficient, to the extent that only 20% of the original value remains after 90 min. This decay can possibly be attributed to a photochemical reaction of the 3T-2 MB, based on dimerization or polymerization of the terthiophene chromophore in response to irradiation. The resulting products would be expected to be insoluble in the FLC, thus degrading the photorefractivity. Such reactions could potentially be inhibited based on steric hindrance effects, and so a series of analogs was prepared: 3T-2 MB, 3-Me-3T-2 MB, 3'-Me-3T-2 MB,

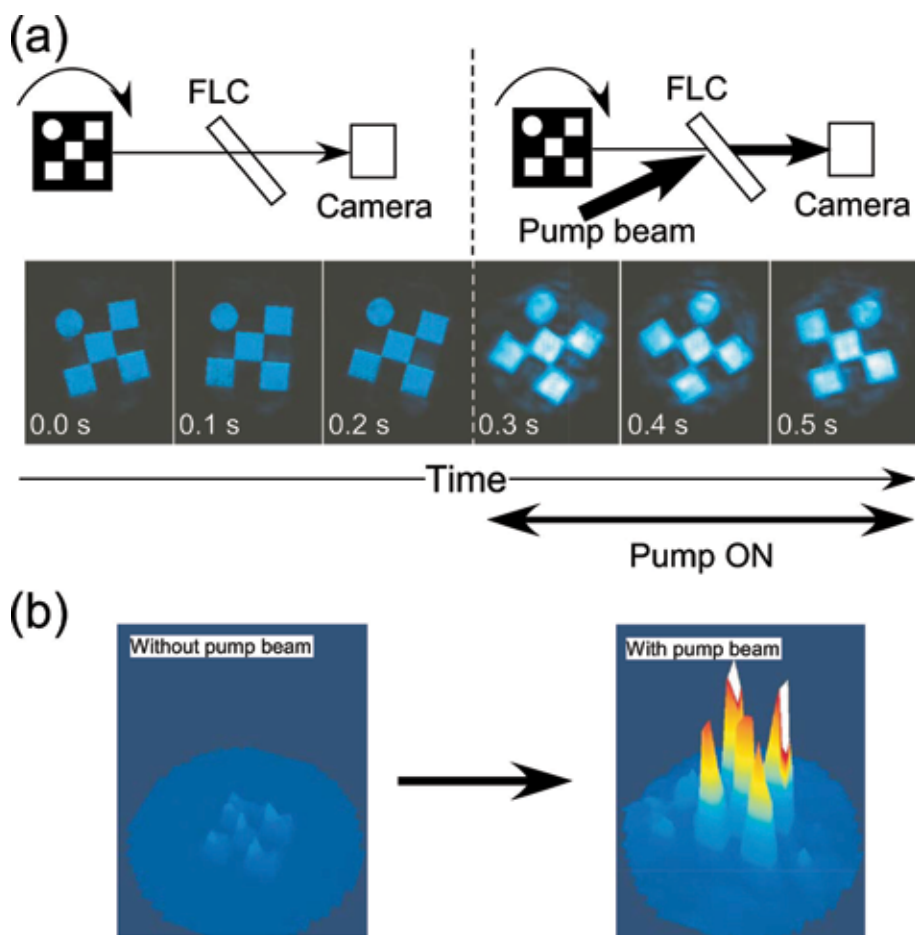


Figure 16. (a) A demonstration of optical image amplification, in which an SLM displays a computer-generated animation. The SLM modulates a 473 nm object beam that irradiates an FLC then interferes with a reference beam. A CCD camera monitors the image sent via the FLC sample containing 10 wt.% 3T-2MB. (b) Change in signal intensity.

3''-Me-3T-2 MB and 3',3''-Me-3T-2 MB (**Figure 18**). **Figure 19** summarizes variations in the gain coefficients of the resulting blends with irradiation time. Interestingly, the decay profiles were unchanged by varying the degree of steric hindrance in the dopant, despite expectations that methyl substituents would hinder access to the reaction site as well as the approach to the terthiophene moieties. Consequently, the loss of photorefractivity evidently was not due to dimerization or polymerization. Additional analyses of a 3T-2 MB specimen via ^1H NMR, infrared and UV-visible spectroscopy following exposure to 488-nm light found no reaction or degradation of the terthiophene moiety. Based on these results, it appears that the loss of photorefractivity resulted from factors other than those described above.

When a DC field is applied, the photorefractive gain has been shown to decay as the irradiation time is prolonged. This phenomenon was assessed by a dual-beam coupling trial employing a decayed sample stored under dark conditions. **Figure 20** presents the original gain signal following laser irradiation for 60 min, after which the specimen was maintained in darkness for 12 h in the absence of an electric field. In this trial, 85% of the initial signal was recovered, demonstrating that the loss of the photorefractive effect was due to changes in the material that were reversible. The observed recoverable loss in gain can possibly be attributed to the formation of

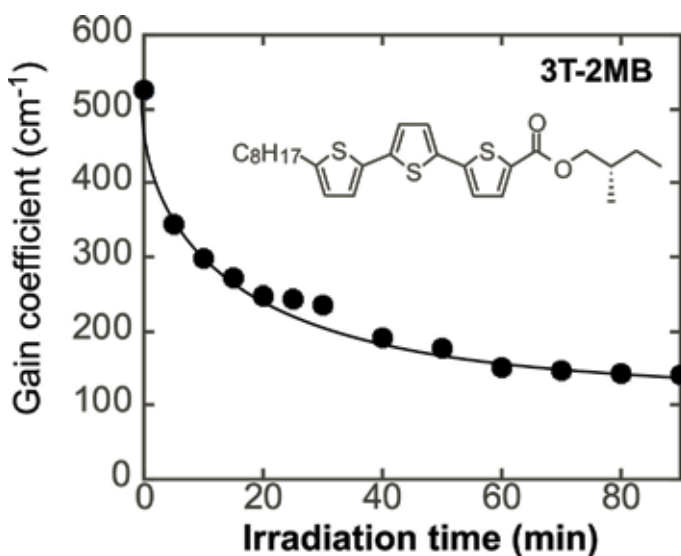


Figure 17. Molecular structures of the smectic LCs 8PP8 and 8PP10, chiral photoconductive dopants and TNF, an electron trap reagent.

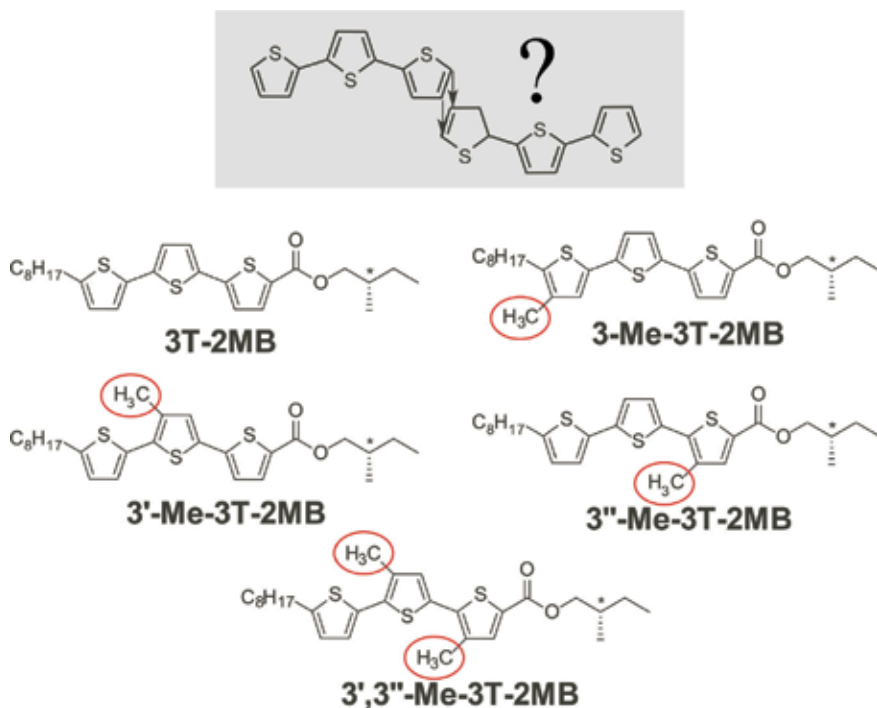


Figure 18. Variations in the gain coefficient of FLC with 6 wt.% 3T-2 MB and 0.1 wt.% TNF over time.

photogenerated ions that adhere to the indium tin oxide (ITO) electrode. It is known that charge transfer between the TNF and terthiophene occurs in response to 488-nm laser light to produce corresponding cations and anions, and these species may migrate to the electrode in response to the electric field. This process extracts ions from the LC phase, reducing its conductivity. Thus, the observed loss of photorefractivity could possibly be mitigated by employing a bipolar electric field, to reverse the direction of

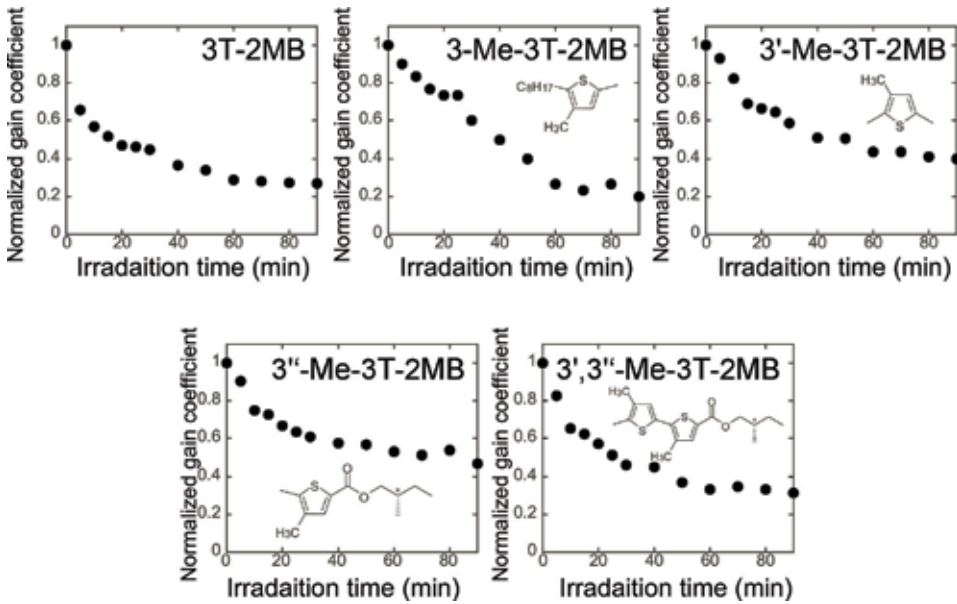


Figure 19. Variations in the gain coefficients of FLC mixed with 6 wt.% various photoconductive chiral additives and 0.1 wt.% TNF over time.

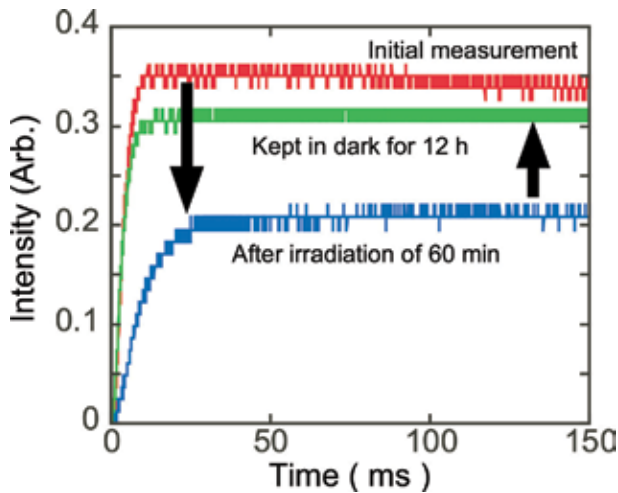


Figure 20. The dual-beam coupling signals generated by FLC doped with 3T-2 MB. The initial signal following 60 min of irradiation by laser beam (250 mW/cm^2) and the signal after storage in darkness for 12 h are shown.

migration of the photogenerated ions such that they move away from the electrode. Of course, it would be necessary to select an optimal frequency for this bipolar field based on ion mobilities, as well as to optimize the field strength. **Figure 21** presents decay profiles of the gain coefficients in conjunction with a bipolar field, and demonstrates that 80% of the original gain was retained under these conditions. These results help to confirm that the observed loss of photorefractivity in the FLC samples is due to ionic migration. The TNF anions and 3T-2 MB cations would be expected to migrate at different rates as a result of the difference in their sizes, and so the electric field strength and shape could be further tuned. In fact, the electric fields employed in present-day LC displays are somewhat complex bipolar fields rather than DC fields.

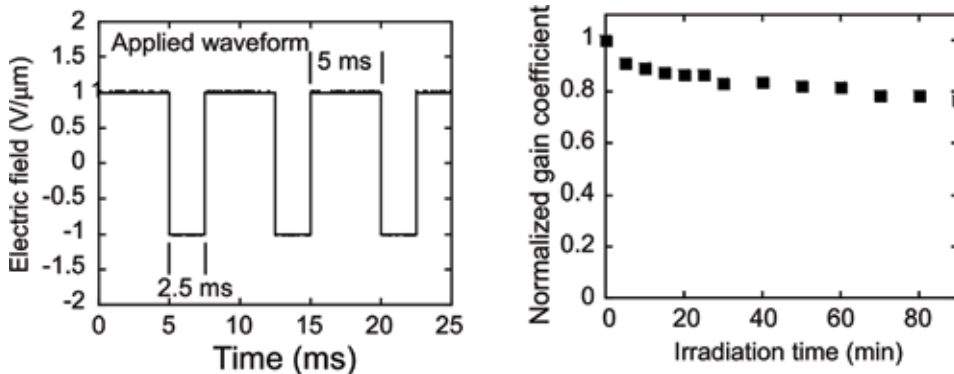


Figure 21. Variations in the gain coefficients of an FLC mixed with 6 wt.% 3 T-2 MB and 0.1 wt.% TNF over time in the presence of a bipolar electric field.

This is required in order to inhibit the adsorption of ions and the LC molecules themselves so as to prevent image sticking. Thus, the use of bipolar fields is already an important aspect of photorefractive LC devices.

3.5 Photorefractive effects in FLC blends containing extended π -conjugated compounds

The photorefractivities of terthiophene derivatives as chiral photoconductive additives have been examined at 488 nm. The practical application of FLCs in

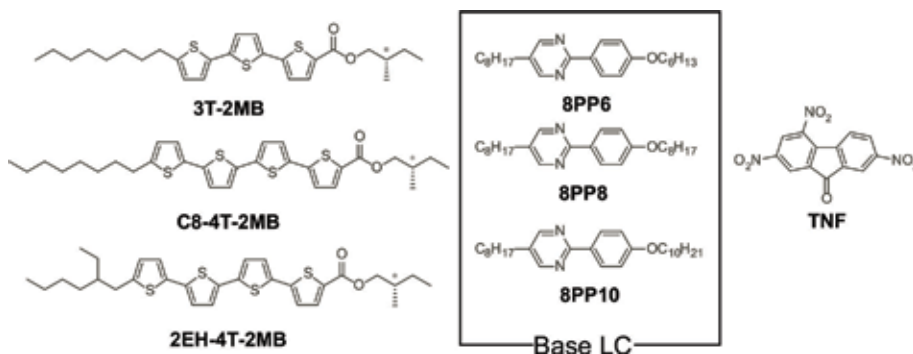


Figure 22. Molecular structures of the chiral photoconductive additives, smectic LCs, and TNF, an electron trap reagent.

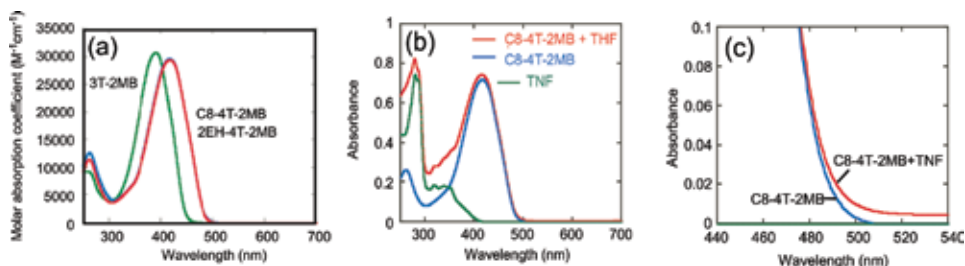


Figure 23. (a) The UV-vis absorption spectra generated by chloroform solutions of the chiral photoconductive additives C8-4T-2 MB, 2EH-4T-2 MB and 3 T-2 MB; (b) the UV-vis spectra of a chloroform solution of C8-4T-2 MB and TNF; (c) the UV-vis spectrum of C8-4T-2 MB compared to that of C8-4T-2 MB and TNF (all in chloroform solutions).

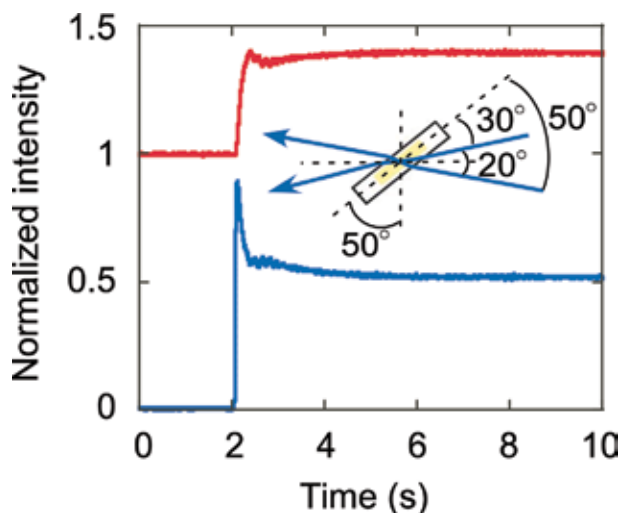


Figure 24.
 A typical asymmetric energy exchange obtained from a dual-beam coupling experiment at 30°C using a combination of a base-LC, 2EH-4T-2 MB, and TNF. Pump beam incidence occurred at the 2-s mark. The beam incidence parameters are given in the figure.

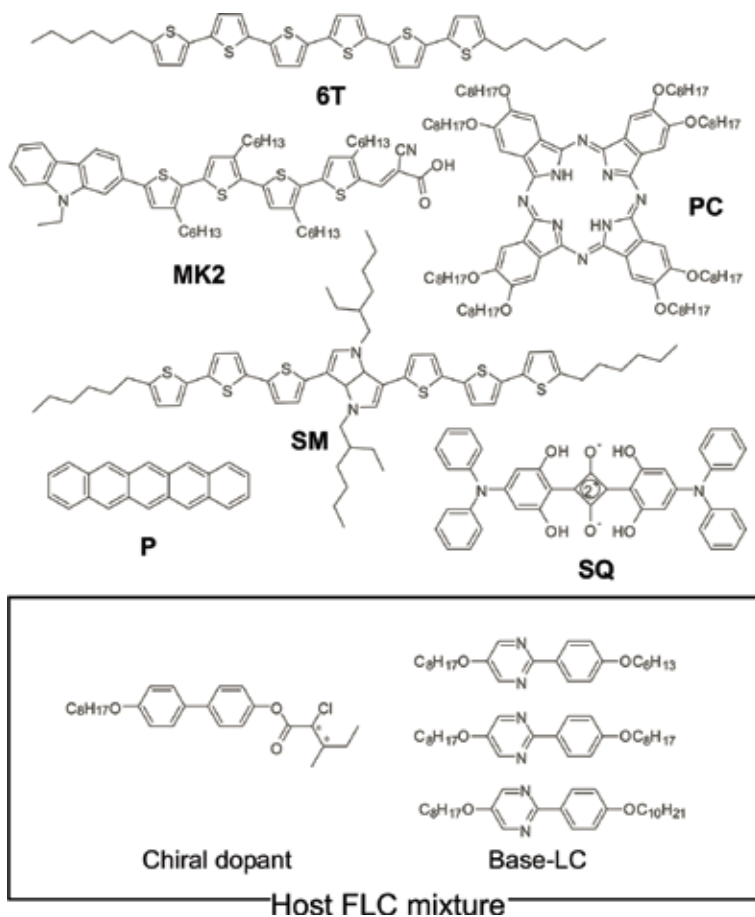


Figure 25.
 Molecular structures of the host FLC and the photoconductive compounds used in the work described herein. The chiral dopant was added at a concentration of 10 wt.% relative to the total mass of the 2:1:1 ternary mixture.

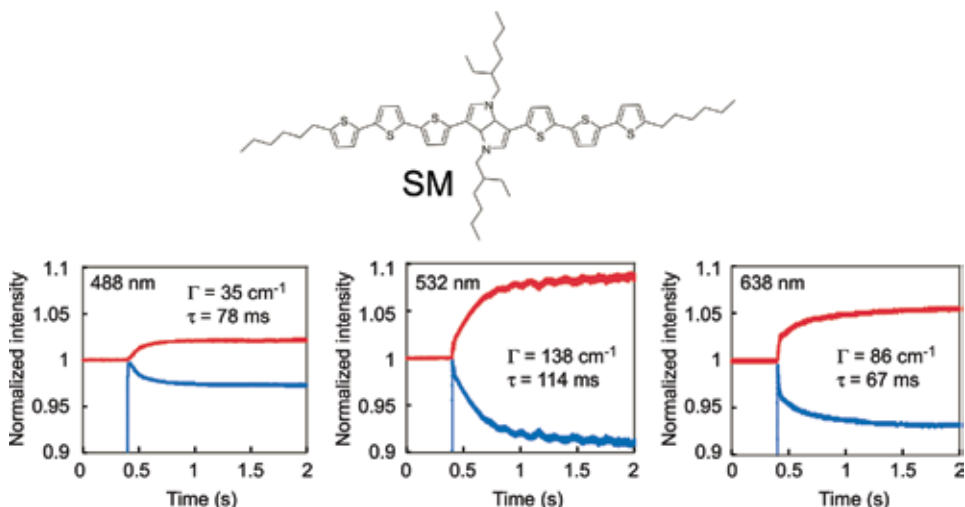


Figure 26. Asymmetric energy exchanges in an FLC mixture in which the photoconductive compound SM is present at less than 1 wt.%.

ultrasound imaging and photoacoustic interferometry requires sensitivity at longer wavelengths. Thus, chiral compounds such as those containing quarter-thiophene chromophores and sexithiophenes, as well as more complex molecular structures, have been synthesized (**Figure 22**). The photorefractivity of mixtures of FLCs with these dopants at longer wavelengths has also been assessed [19]. The addition of TNF to a quarter-thiophene was found to result in absorption at longer wavelengths (**Figure 23**) due to the formation of a charge transfer absorption band, allowing these materials to be employed in conjunction with a 532-nm writing beam. Dual-beam trials were subsequently employed to examine the photorefractivity of the resulting FLC blends. **Figure 24** shows typical data for the asymmetric energy exchange in a 2EH-4 T-2 MB specimen in conjunction with a 532-nm writing beam wavelength.

Photoconductive materials having longer absorption wavelengths were additionally investigated (**Figure 25**). In these trials, the photoconductive compounds were mixed with a base FLC and a chiral additive. Most of the materials listed in **Figure 25** could not be dissolved in the FLC, with the exception of the SM, which could be added at levels up to 1 wt.%. Thus, a blend containing 1 wt.% SM was employed for dual-beam coupling trials (**Figure 26**), in conjunction with continuous laser irradiation at 488, 532, and 638 nm. This sample exhibited asymmetric energy exchange even at the longest wavelength, albeit with a slow response and minimal gain. The generation of a space charge field at the interference fringes evidently involved ionic conduction, which was reflected in the slow response.

4. Conclusions

LCs are exceptionally birefringent and thus produce a significant photorefractive effect, although they suffer from light scattering due to heterogeneous molecular orientations. Smectic LCs show more pronounced photorefractivity, especially in the case of the bulk (or spontaneous) polarization of FLCs combined with photoconductive compounds. These mixtures exhibit photorefractivity solely in the ferroelectric phase and with reduced response times relative to those obtained from nematic

LCs. The various properties of FLCs, including spontaneous polarization, phase transition temperature, viscosity and SS-state homogeneity, all greatly affect photorefractivity. Both the time required for formation of a refractive index grating (that is, the response time) and the gain coefficient are significantly affected by the last factor, and so extreme homogeneity is required in a photorefractive device. Finally, FLC blends have exhibited sensitivity to wavelengths up to 638 nm following doping with photoconductive compounds.

Author details


Takeo Sasaki^{1*}, Khoa Van Le¹, Yumiko Naka¹ and Takafumi Sassa²

¹ Tokyo University of Science, Tokyo, Japan

² Photonics Control Technology Team, RIKEN Center for Advanced Photonics, RIKEN Laser Science Laboratory, Wako, Japan

*Address all correspondence to: sasaki@rs.kagu.tus.ac.jp

IntechOpen

© 2018 The Author(s). Licensee IntechOpen. This chapter is distributed under the terms of the Creative Commons Attribution License (<http://creativecommons.org/licenses/by/3.0>), which permits unrestricted use, distribution, and reproduction in any medium, provided the original work is properly cited. 

References

- [1] Solymar L, Webb JD, Grunnet-Jepsen A. *The Physics and Applications of Photorefractive Materials*. Oxford: New York; 1996
- [2] Yeh P. *Introduction to Photorefractive Nonlinear Optics*. New York: Wiley; 1993
- [3] Moerner WE, Silence SM. Polymeric photorefractive materials. *Chemical Reviews*. 1994;**94**:127-155
- [4] Ostroverkhova O, Moerner WE. Organic photorefractives: Mechanisms, materials, and applications. *Chemical Reviews*. 2004;**104**:3267-3314
- [5] Sasaki T. Photorefractive effect of liquid crystalline materials. *Polymer Journal*. 2005;**37**:797-812
- [6] Meerholz K, Volodin BL, Kippelen B, Peyghambarian N. A photorefractive polymer with high optical gain and diffraction efficiency near 100%. *Nature*. 1994;**371**:497-500
- [7] Blanche PA. *Springer Series in Materials Science 240, Photorefractive Organic Materials and Applications*. Switzerland: Springer International Publishing; 2016
- [8] Khoo C, Li H, Liang Y. Observation of orientational photorefractive effects in nematic liquid crystals. *Optics Letters*. 1994;**19**:1723-1725
- [9] Ono H, Kawatsuki N. High-performance photorefractivity in high- and low-molar-mass liquid crystal mixtures. *Journal of Applied Physics*. 1999;**85**:2482-2487
- [10] Wiederrecht GP, Yoon BA, Wasielewski MR. Photorefractivity in ferroelectric liquid crystal composites containing electron donor and acceptor molecules. *Advanced Materials*. 2000; **12**:1533-1536
- [11] Sasaki T, Kino T, Shibata M, Mizusaki N, Katsuragi A, Ishikawa Y, et al. Spontaneous polarization-vector-reorientation photorefractive effect in ferroelectric liquid crystals. *Applied Physics Letters*. 2001;**78**:4112-4114
- [12] Skarp K, Handschy MA. Ferroelectric liquid crystals. Material properties and applications. *Molecular Crystals and Liquid Crystals*. 1988;**165**: 439-509
- [13] Oswald P, Pieranski P. *Smectic and Columnar Liquid Crystals*. New York: Taylor & Francis; 2006
- [14] Sasaki T, Naka Y. Photorefractive effect in ferroelectric liquid crystals. *Optical Review*. 2014;**21**:99-104
- [15] Sasaki T, Mochizuki O, Noborio K, Nakazawa Y. Influence of the laser incidence conditions on the spontaneous polarization reorientation photorefractive effect of ferroelectric liquid crystals. *The Journal of Physical Chemistry. B*. 2004;**108**:17083-17088
- [16] Sasaki T, Kajikawa S, Naka Y. Dynamic amplification of light signals in photorefractive ferroelectric liquid crystalline mixtures. *Faraday Discussions*. 2014;**174**:203-218
- [17] Sasaki T, Ikegami M, Abe T, Miyazaki D, Kajikawa S, Naka Y. Real-time dynamic hologram in photorefractive ferroelectric liquid crystals with two-beam coupling gain coefficient of over 800 cm^{-1} and response time of 8 ms. *Applied Physics Letters*. 2013;**102**(1-6):063306
- [18] Sasaki T, Yoshino M, Naka Y, Le KV, Sassa T. Laser irradiation durability of photorefractive ferroelectric liquid

crystal blends containing terthiophene
photoconductive chiral dopants. RSC
Advances. 2016;**6**:70573-70580

[19] Sasaki T, Morino S, Sumiya A,
Yamamoto Y, Nakano M, Le KV, et al.
Enhancement of photosensitivity of
photorefractive ferroelectric liquid
crystal blends to green and red
wavelength regions using
oligothiophene photoconductive
dopants. Journal of Physical Chemistry
C. 2017;**121**:16951-16958



Edited by Irina Carlescu

Liquid Crystals—Self-Organized Soft Functional Materials for Advanced Applications is focused on both theoretical models and experimental results, pointing out the chemical and physical properties (thermodynamics, electro-optic switching behavior, and non-linear optic phenomena) of liquid crystals used in a wide range of devices. In this respect, the chapters cover the following topics: chemical structure and phase transitions in bent-core liquid crystals, phase and structural behavior of liquid crystals used to align carbon nanotubes, molecular alignment, and photorefractive effect in the ferroelectric phase, which has the potential to be used as transistors, for image storage, and in optical signal processing. It is expected that the book will be of interest to researchers in academia and industries, as well as advanced students.

Published in London, UK

© 2019 IntechOpen
© chotika_dong / iStock

IntechOpen

ISBN 978-1-83881-810-4



9 781838 818104

